NONDESTRUCTIVE REPAIR AND REHABILITATION OF STRUCTURAL ELEMENTS USING HIGH STRENGTH INORGANIC POLYMER COMPOSITES

By

MATTHEW J. KLEIN

A Dissertation submitted to the

Graduate School-New Brunswick

Rutgers, The State University of New Jersey

in partial fulfillment of the requirements

for the degree of

Doctor of Philosophy

Graduate Program in Civil and Environmental Engineering

written under the direction of

Professor P. N. Balaguru

and approved by

____

____

____

____

New Brunswick, New Jersey

May, 2013

ABSTRACT OF THE DISSERTATION

NONDESTRUCTIVE REPAIR AND REHABILITATION OF STRUCTURAL ELEMENTS USING HIGH STRENGTH INORGANIC POLYMER COMPOSITES

by MATTHEW J. KLEIN

Dissertation Director

Dr. P. N. Balaguru

Results reported in this dissertation focus on the development of an inorganic polymer composite for rapid, nondestructive repair and rehabilitation of physical infrastructure. The composite consisting of an alkali-aluminosilicate made of nano/micro size particles and high strength fibers was evaluated for repair and strengthening of concrete structural elements. In the area of repairs, the focus was to repair small width voids such as delaminations and cracks developed due to restrained shrinkage and long-term distress in concrete bridge decks and other similar structural elements. A strengthening study was done to increase the capacity of reinforced concrete beams with carbon fibers. Uniqueness of the strengthening system with inorganic matrix is its fire resistance.

For the repair system, the matrix composition was evaluated for flowability using plexiglass models and concrete slabs, bond strength using slant shear and bending specimens, and durability studies using wet/dry and freeze/thaw conditions. Delivery of the composite to cracks and delaminations was also investigated using equipment that is

currently used with organic polymers. The temperature resistant repair system with carbon fibers was evaluated using strengthened concrete beams heated to over 1,000°F at the maximum bending moment location.

The following are all the major findings of the investigation: The inorganic nano/micro composite flows well into cracks – even cracks that are between 0.03 and 0.04 inches wide. Commercially available equipment can be used for the inorganic matrix. The hardened matrix bonds well with concrete and provides a structurally integral repair. Strength tests showed that the strength at the repaired locations is higher than the strength of the parent material. In addition, since the modulus of elasticity of the inorganic system is comparable to concrete, the repaired structural components regain full structural integrity as compared to mere cosmetic repairs provided by organic polymers. The system is durable under wetting/drying and freezing/thawing conditions. For both, strength and durability increases with the nano-size material content and improves performance. The heat tests showed that the repaired beams can be heated up to 1,385°F repeatedly with minimum loss of strength.

ACKNOWLEDGEMENTS

"Blessed be the name of God for ever and ever: for wisdom and might are His:"

– Daniel 2:20

This work would have been so much more difficult without the assistance, support and suggestions of so many other people. First of all, I am grateful to have such a loyal and dedicated wife. Laura, you complete me. Thank you for your motivation, love and patience. This would not have been as much fun without you. Alyssa, my sweet baby girl, you were always such an adorable distraction.

Dr. P. Balaguru, you have been so much more than an advisor. Your wisdom was always well timed and your advice appreciated. Our meeting was not by chance. You are a prudent counselor and a true friend. I could not have done this without you.

I especially want to thank my friend, Dr. Giri Venkiteela for making this journey so much more attainable by sharing your advice, criticism, and experiences. The days were always shorter when you were around. Thank you for all of your help.

I also want to give special recognition to my "editors": Laura Klein, Sarah Jackson, and Jay Freeman. You heard the call and answered. My work is much more respectable due to your suggestions.

Special thanks to my committee members: Dr. H. Najm, Dr. J. Yi, and Dr. H. Wang. Also recognized are Dr. T. Williams for giving me something to be proud of and Dr. Y. Yong for assistance with the basics. Sincere appreciation to Dr. N. Gucunski for convincing me to work on this project and for giving me many opportunities.

Of special note are the civil engineering department and CAIT staff: Gina Cullari, sometimes I just needed to talk and you always listened. Ed Wass, you made working in the lab much more enjoyable. Tara Looie, many thanks for helping with all of those material and equipment orders.

I also want to note the help that I received from people who worked for me but also became friends and colleagues: Dan Grek, I could always count on you; Chris Mazotta, thanks for the extra hand; Anthony Casale, Johanna Doukakis, Abanda Abanda, and Justin Bewley, your long days and hard work are deeply appreciated. Jeremy Brownstein, your friendship is appreciated.

I received much support and encouragement from many dear friends: Gary Banks, you didn't have to but you did it anyways. I'm glad that time and distance didn't prevail. Dennis and Shellie Campbell, I would not be here without you. Allan Fisher, your positive attitude was infectious. Denise and the McKillop family, you are my family. Alistair Aylward, thanks for believing in me. Becca Carey, your cheering kept me going.

My family endured much because of my dreams and I am grateful to have such support and encouragement through all of these years. Mom, you taught me that I could be anything. Mom and Dad Jackson, thank you for always trusting me. Tim and Tami Little, you were always interested even though it really was boring, really. Nana, you make me proud. I always believed that if you could do the things you did, I could do this. Papa, I wish you were here. Alina Rice, thank you for the inspiration. Sarah Lowney, you are a true sister. Kate and Brett Aquilino, AJ and Nate Jackson, Dusty Cole, Katlyn, Megan, Devin, Nora, and William Culhane, thanks for your constant assurance and ready conversation.

TABLE OF CONTENTS

TITLE PAGE……………………………………………………………………………

ABSTRACT OF THE DISSERTATION ii

ACKNOWLEDGEMENTS iv

TABLE OF CONTENTS vi

LIST OF TABLES xi

LIST OF FIGURES xii

CHAPTER 1 - INTRODUCTION 1

CHAPTER 2 - STATE OF THE ART 4

2.1 Introduction 4

2.2 History of Epoxy Repaired Concrete 4

2.3 The Search for the Effective Epoxy 6

2.4 Equipment Development 8

2.5 Features of the Epoxy for Repairing Concrete Bridge Decks 14

2.6 Epoxy Repair of Cracks 15

2.7 Inorganic Systems 17

2.7.1 Introduction to Potassium Aluminosilicate 17

2.7.2 Chemistry and Molecular Structure 18

2.7.3 Synthesis 19

2.8 Inorganic Polymer Properties 21

2.9 Composite Properties 26

2.10 Durability 27

2.11 Strengthening Systems 31

2.12 Field Applications 33

2.13 Summary 39

CHAPTER 3 - PROCESSING VARIABLES AND PLASTIC PROPERTIES 44

3.1 Introduction 44

3.2 Part 1: Mix Design 44

3.2.1 Group A Mixes 45

3.2.2 Group B Mixes 46

3.2.3 Group C Mixes 49

3.2.4 Group D Mixes 52

3.2.5 Group E Mixes 55

3.3 Part 2: Flow Tests 59

3.3.1 Flow Tests in Narrow Channels 60

3.3.2 Sample Preparation 62

3.3.3 Results and Discussions 63

3.3.4 Injection Systems 66

3.3.5 Rapid Repair Paver Table 68

3.3.6 Repair Methodology/Theory 70

3.3.7 Results 71

3.4 Summary 73

CHAPTER 4 - MECHANICAL PROPERTIES OF THE COMPOSITE 77

4.1 Introduction 77

4.2 Splitting Tensile Repair Tests 78

4.3 Flexural Repair Tests 80

4.4 Direct Shear Tests 85

4.5 Slant Shear Tests 87

4.6 Summary 89

CHAPTER 5 - COMPARISON OF ORGANIC AND INORGANIC POLYMERS 90

5.1 Introduction 90

5.2 Slant Shear Compatibility 91

5.3 Compatibility Tests 92

5.4 Prototype Beam Tests 95

5.5 Full-Scale Compatibility Tests 100

5.5.1 Instrumentation 104

5.5.2 Results 106

5.6 Summary 110

CHAPTER 6 - DURABILITY 112

6.1 Introduction 112

6.2 Test Materials ... 113

6.3 Adhesion Testing ... 116

6.4 Freeze/Thaw Test Set-up ... 120

6.5 Wetting Test Set-up ... 121

6.6 Freeze/Thaw Durability Results ... 123

6.7 Freeze/Thaw Results Interpretation ... 133

6.8 Wetting Durability Results ... 134

6.9 Wetting Test Interpretation ... 144

6.10 Summary ... 145

CHAPTER 7 - HIGH TEMPERATURE APPLICATIONS ... 146

7.1 Introduction ... 146

7.2 Initial Tests ... 149

7.3 Confirmation Tests ... 151

7.4 Materials ... 151

7.5 Test Specimens ... 152

7.6 Testing Equipment ... 155

7.7 Testing Procedure ... 157

7.8 Initial Test Analysis ... 159

7.9 Initial Test Results ... 164

7.10 Confirmation Test Analysis ... 169

7.11 Confirmation Test Results 172

7.12 Summary 181

CHAPTER 8 - FIELD TRIALS 184

8.1 Introduction 184

8.2 Surface Crack Repair 184

8.2.1 Specimen Preparation 184

8.2.2 Test Set-up 186

8.2.3 Test Results 187

8.3 Delamination Repair 188

8.3.1 Specimen Preparation 188

8.3.2 Test Set-up 192

8.3.3 Test Results 192

8.4 Summary 195

CHAPTER 9 - CONCLUSIONS 197

REFERENCES 201

VITA 205

LIST OF TABLES

Table 3-1: Summary of Flow Test Mix Composition.. 60

Table 3-2: Summary of Slab/Plexiglass Results.. 66

Table 6-1: Durability Mix Summary 114

Table 6-2: Mix Notation 116

Table 7-1: Heat Beam Concrete Mix Proportions 152

Table 7-2: Heat Beam Design Summary 155

Table 7-3: Initial Test Summary.. 168

Table 7-4: Confirmation Test Summary.. 174

LIST OF FIGURES

Figure 2-1: Kansas DoT's Custom Chuck 9

Figure 2-2: Tip Designs 10

Figure 2-3: Insertable Gasket Type Injection Probe 11

Figure 2-4: Surface Mounted Injection Probe 12

Figure 2-5: Kansas DoT Custom Injection Cart 14

Figure 2-6: Example of Insertable Injection Probes 16

Figure 2-7: Chemical Structure of Potassium Polysialate 19

Figure 2-8: Aluminosilicate Reaction Time and Viscosity 20

Figure 2-9: Wetting Test Set-Up 28

Figure 2-10: Flexural Test Set-Up 29

Figure 2-11: Freeze/Thaw Test Set-Up 30

Figure 2-12: Scaling Test Set-Up 31

Figure 2-13: Strengthened I-Beam Test Set-Up 32

Figure 2-14: Inorganic Coating on I-280 Retaining Wall 34

Figure 2-15: Color Matching 34

Figure 2-16: Inorganic Coating in the George Redding Bridge House 35

Figure 2-17: Self-Cleaning Properties Discourages Algae Growth 36

Figure 2-18: Inorganic Coating on Woodbridge Mall Retaining Wall 37

Figure 2-19: Graffiti Removal Demonstration on the Inorganic Coating 38

Figure 3-1: Mix Group B Results 49

Figure 3-2: Mix Group B and C (Enhanced) Results 51

Figure 3-3: Mix Group C Results 52

Figure 3-4: Zinc Oxide Activator Results 54

Figure 3-5: Curing Temperature Results 54

Figure 3-6: Mix Group D Results 55

Figure 3-7: Mix Group E Results 57

Figure 3-8: Mixer Speed Results 58

Figure 3-9: Curing Temperature Results 58

Figure 3-10: Flow Test Setup 63

Figure 3-11: Filling the Channel by Gravity 64

Figure 3-12: Vacuum used to Fill Channel 64

Figure 3-13: Diaphragm Pump Injection 65

Figure 3-14: From left to right - Surface Mount with Zerk, Mechanical Packer, Polyethylene Packer 68

Figure 3-15: Rapid Paver Repair Table 69

Figure 3-16: Top and Bottom Results of a Paver Test 70

Figure 4-1: Splitting Tensile Test 78

Figure 4-2: Flexural Repair Test 81

Figure 4-3: Flexural Specimen Forms 84

Figure 4-4: Direct Shear Test 85

Figure 4-5: Slant Shear Test 87

Figure 5-1: Slant Shear Results 92

Figure 5-2: Typical Reinforcement Placement in Bridge Deck 93

Figure 5-3: Internal Stress Distribution in Third-Point Bending 94

Figure 5-4: Diagram of Compatibility Beam 95

Figure 5-5: Prototype Beams 96

Figure 5-6: Completed Prototype Beams... 97

Figure 5-7: Prototype Beam Test.. 97

Figure 5-8: Prototype Beam Results 98

Figure 5-9: Prototype Failures; Inorganic (left), Organic (right)..................................... 99

Figure 5-10: Full-Scale Beam Elevation Dimensions 101

Figure 5-11: Full-Scale Beam Cross-Section Dimensions 102

Figure 5-12: Notched Full-Scale Beams... 103

Figure 5-13: Instrumentation Set-Up 105

Figure 5-14: Full-Scale Beam Test Instrumentation... 106

Figure 5-15: Full-Scale Beam Curvature Comparison 107

Figure 5-16: Full-Scale Beam Comparison 108

Figure 5-17: Shear Movement Comparison; Inorganic (left), Organic (right).............. 109

Figure 5-18: Shear Crack in Epoxy Repaired Beam.. 110

Figure 6-1: Adhesion Test Set-Up 117

Figure 6-2: Coring the Specimens 118

Figure 6-3: Failure Modes A through C 119

Figure 6-4: Failure Modes D through F 120

Figure 6-5: Wetting Test Set-Up.. 122

Figure 6-6: Wetting Test Set-Up Schematic 123

Figure 6-7: Beam 451 Results.. 125

Figure 6-8: Beam 446 Results.. 125

Figure 6-9: Beam 427 Results.. 126

Figure 6-10: Beam 405 Results 126

Figure 6-11: Beam 449 Results 127

Figure 6-12: Beam 448 Results 127

Figure 6-13: Beam 458 Results 128

Figure 6-14: Beam 457 Results 128

Figure 6-15: Beam 454 Results 129

Figure 6-16: Beam 436 Results 129

Figure 6-17: Beam 437 Results 130

Figure 6-18: Beam 406 Results 130

Figure 6-19: Beam 416 Results 131

Figure 6-20: Beam 411 Results 131

Figure 6-21: Beam 412 Results 132

Figure 6-22: Beam 424 Results 132

Figure 6-23: Beam 459 Results 136

Figure 6-24: Beam 426 Results 136

Figure 6-25: Beam 408 Results 137

Figure 6-26: Beam 402 Results 137

Figure 6-27: Beam 425 Results 138

Figure 6-28: Beam 407 Results 138

Figure 6-29: Beam 410 Results 139

Figure 6-30: Beam 432 Results 139

Figure 6-31: Beam 423 Results 140

Figure 6-32: Beam 455 Results 140

Figure 6-33: Beam 422 Results 141
Figure 6-34: Beam 430 Results 141
Figure 6-35: Beam 453 Results 142
Figure 6-36: Beam 456 Results 142
Figure 6-37: Beam 414 Results 143
Figure 6-38: Beam 439 Results 143
Figure 7-1: Mid-Span Deflections (Kodur and Ahmed 2011) 148
Figure 7-2: Heat Distribution in Initial Heat Source 149
Figure 7-3: Third-Point Bending 152
Figure 7-4: Heat Beam Dimensions 153
Figure 7-5: Glass Bead/Cement Polymer Insulation 154
Figure 7-6: Screw Jack Loading Frame 156
Figure 7-7: Beam Notation 160
Figure 7-8: Finite Element Node Designation 163
Figure 7-9: Beam 1 Initial Test Results 165
Figure 7-10: Beam 2 Initial Test Results 166
Figure 7-11: Beam 6 Initial Test Results 167
Figure 7-12: Beam 6 Initial Retest Results 168
Figure 7-13: Beam 0 Confirmation Test 174
Figure 7-14: Beam 1 Confirmation Test 175
Figure 7-15: Beam 2 Confirmation Test 176
Figure 7-16: Beam 3 Confirmation Test 177
Figure 7-17: Beam 4 Confirmation Test 178

Figure 7-18: Beam 6 Confirmation Test 179

Figure 7-19: Real Light Image 180

Figure 7-20: Infrared Images; Beam 0 (top left), Beam 1 (top right), Beam 2 (middle left), Beam 3 (middle right), Beam 4 (bottom left), Beam 6 (bottom right) 181

Figure 8-1: Surface Crack Preparation 185

Figure 8-2: Surface Mount Port and Slide-On Zerk Fitting 186

Figure 8-3: Surface Crack Injection Test Set-Up 187

Figure 8-4: Artificial Delamination Inserts 189

Figure 8-5: Cross-Section of Artificial Delamination 190

Figure 8-6: Drilling Injection Holes using Dust Extraction Equipment 191

Figure 8-7: Delamination Injection Nozzle 192

Figure 8-8: Performing the Delamination Injection 194

CHAPTER 1 - INTRODUCTION

This dissertation contains an investigation focused on the development of an inorganic aluminosilicate polymer for nondestructive rehabilitation for cracked concrete structural elements. The alkali-aluminosilicate composite features nano- and micro-sized particles specially chosen for their refined properties and also includes high strength fibers to help provide strength. The mixture was designed to penetrate into small cracks with the use of commercially available injection equipment. Testing was performed to insure sufficient strength and concrete compatibility. Durability testing for wetting, freeze/thaw and fire was provided. The inorganic matrix was also used to strengthen concrete beams with carbon fibers in an effort to resist high temperatures.

Chapter 2 provides an overview of the history and the state-of-the-art of organic and inorganic systems. Injection equipment development and recommendations are summarized. The advantages and disadvantages of the organic epoxy are given. Mechanical properties of previous inorganic aluminosilicate mixes are shown along with the testing procedures. The chapter is closed with an outline of the current applications of the inorganic mixture.

Chapter 3 is divided into two parts. Part 1 follows the evolution of the inorganic system that was developed for injection into surface cracks and delaminations. The mix featured a total of five iterations with each iteration targeting a specific variable and applicable test methods. A final mix design is then recommended for use in the injections system based on its overall performance. The mix iterations include ingredient ratios and proportions as well as mixing and curing conditions. The second part gives an overview of how the flow characteristics affect the design of the material. Flow tests were designed specifically to emulate crack and delamination injection conditions in order to provide valuable feedback on the mix performance.

Mechanical properties related to injection systems are provided in Chapter 4. All tests performed were given even if the results did not ultimately yield relevant data. The tests performed are splitting tensile repair tests, flexural repair tests, direct shear tests, and slant shear tests. The discussion includes specimen preparation, test set-up and test results though the actual data is given in Chapter 3 to show the mix design development.

Chapter 5 is concerned with a direct comparison to existing organic epoxies. Both systems are tested in slant shear, prototype beam tests and full-scale beam repair tests. Slant shear tests show that the inorganic repair material can provide the same benefits as the organic version. The prototype and full-scale beams were designed to indicate which system is more compatible with concrete in allowing the transfer of stresses across the repaired plane.

Durability questions are answered in Chapter 6. The specimen preparation, test arrangement, and results are shown for wetting and freeze/thaw durability. The metric used to provide the comparison between the different mixtures are the adhesion pull-off test. Given the application of the material to fix concrete cracks, this test provides the most direct means of the inorganic material's resistance to cyclical deterioration conditions.

High temperature applications are presented in Chapter 7. The inorganic material is used in conjunction with carbon fibers to strengthen full size concrete beams. Then the beams are placed in static loading jigs where a load is applied and allowed to equalize. Then the carbon fiber face of the beam is exposed to extremely high temperatures to show that the inorganic matrix can provide carbon fiber strength during heat events. A method for determining deflection of beams subjected to point heat sources is derived using elastic-beam theory and moment-area theorems given third-point loading and simply supported conditions.

No discussion on crack and delamination injection systems would be complete without a demonstration of the repair. This is provided in Chapter 8. Several surface cracks and delaminations were constructed and then repaired with the inorganic system using commercially available equipment. The demonstration provided valuable data on the proper techniques and recommended preparation of the specimens for injection.

CHAPTER 2 - STATE OF THE ART

2.1 Introduction

The use of organic systems for the non-destructive repair of concrete bridge decks has been thoroughly tested and analyzed. The basic components of a 2-part epoxy have not changed since they were first formulated in the 1930's. The 2-part epoxy consists of a petroleum-based resin and hardener or curative. The reaction is usually rapid and highly exothermic meaning excessive heat is produced when the resin and hardener is mixed in large quantities.

2.2 History of Epoxy Repaired Concrete

The first epoxies were designed both in America by Dr. S. O. Greenlee and in Switzerland by Dr. Pierre Castan around 1935 (Epoxy Chemicals, Inc. 2013). The first applications for using epoxy as a concrete adhesive occurred in 1948. In 1957, the first concrete repair using epoxy was performed on a concrete girder in Kansas. By 1962, the practice of repairing cracked concrete by epoxy injection had become so popular that the American Concrete Institute (ACI) published a method for its use (ACI Committee 403 1962). The method consisted of a complex network of fittings and connections and has largely remained unchanged to this day despite attempts to improve the procedure.

In the late 1960's, the Kansas Department of Transportation began a series of research studies aimed at outlining the feasibility and effectiveness of repairing concrete bridge decks using organic epoxy (Pattengill, Crumpton and McCaskill 1969).

Epoxy injection was considered to have so many benefits that the Texas Department of Highways and Public Transportation, in partnership with the Federal Highway

Administration, investigated impregnation of the entire concrete bridge deck surface prior to any developed deterioration in order to prevent salt water infiltration and to enhance shear and tensile properties of the concrete (Webster, Fowler and Paul 1978). The innovation, however, was only partially successful as it proved to be costly and only provided limited depth of penetration and a slightly improved water resistance.

In the 1980's, after the technique of epoxy injection had become well documented and widely accepted, the question of its cost effectiveness came under scrutiny. Iowa Department of Transportation investigated how long the repair actually lasted before the deck would have to be replaced (Stratton and Smith 1988). It was concluded that due to the organic nature of the resin, and its susceptibility to breakdown by solvents and because the resin grows increasingly brittle over time, the injection repair only extended the bridge deck life on average about 5 years' time before additional repairs would be required.

Through the 1990's until the present, the evolution of the epoxy injection system has largely been by the development of advanced epoxy formulations designed specifically to overcome the deficiencies of the earlier formulations. This led to the compilation of minimum requirements for acceptable epoxies and how to test their suitability for field application (Krauss, et al. 1995) (Iowa DOT, Office of Materials 1998).

Despite the disadvantages of organic epoxy injection systems, it is currently the most popular method for repairing delaminated and cracked concrete bridge decks compared to the alternative of removing the affected areas and replacing the concrete. This is usually only done if the damage to the reinforcement is severe enough to warrant replacement of the bars. Reinforcement replacement can only be done after the concrete has been removed. If the deck is badly deteriorated and damaged, the entire deck is demolished and replaced.

2.3 The Search for the Effective Epoxy

Early epoxy choices were arbitrary and subject to locality availability. Initial epoxies featured a higher viscosity, meaning pressures were greater during injection. Once an analytical survey had been completed, it was found that a lower viscosity epoxy was necessary to allow an effective repair solution. The Kansas DoT studied types of epoxy and gave an outline of the suitable feature set required for successful epoxy injection (Stratton and McCollom 1974) (Connor 1979). Six epoxy systems were targeted to determine acceptable features. The following distributers were used: Kimmel Engineering Company (KR52-2 resin and KH-78 hardener), Sinmast of America, INC. (Sinmast Injection Resin), Adhesive Engineering Company (Concresive 1050-15), and the other three available from Sika Chemical Corporation (Colma Fix LV, Sikastix 37, and Sikadur Hi-Mod). However, the epoxy available from Adhesive Engineering Company was not tested since the manufacturer limited usage to company trained and licensed technicians. In addition, early on it was discovered that the Kimmel Engineering Company supplied epoxy could be diluted in contact with moist conditions. Researchers had noted that water could be displaced from the delaminations during injection, thus recommending the epoxy be water-resistant.

The analytical research indicated that the maximum room temperature viscosity should be about 30 poise. The range of the tested epoxies was between 3 and 17 poise. The manufacturer low temperature curing requirements varied but the lowest was the epoxy manufactured by Sinmast at 33°F and Sikadur Hi-Mod at 40°F. All other systems minimum temperature was at about 60°F. It was noted that the average low temperature in Kansas often dipped below 60°F at night.

The remaining epoxies were tested for bond and durability against wetting and saline solutions by the use of repaired flexural tests. These tests involved gluing concrete together to form beams and testing in flexure. In the durability tests, the specimens were soaked in water during the epoxy curing. In all the dry bond cases the break location was located in the concrete except for the Sika Colma Fix LV which failed in the bond between the concrete and the epoxy. In the wetting tests, none of the epoxies survived the test. The Sikadur Hi Mod had the best performance with 75% concrete failure and the Sinmast followed with 66% concrete failure. The rest of the failure was in epoxy debonding. The Sinmast manufactured epoxy was recommended because of its overall performance including low application temperature and viscosity.

Durability tests on the field applied epoxy systems were conducted by the Kansas DoT by utilizing a detailed method for determining the length of time that the epoxy remained effective in comparison to structures that were not repaired (Stratton and Smith 1988). The tests occurred over a five year period beginning in 1979. A total of four bridges were divided into four sections for epoxy injection and the results of the injection were observed over the time period of the tests. All sections were given an initial injection to the delaminated areas and then checked annually for increased delamination. For each section, additional injections were given in different frequencies. For example, Section 1 received additional injections every year, Section 2 would only receive the injection for additional delaminations every second year and so on to the fourth zone. This was done to find the optimal reinjection schedule and to determine if it was cost effective to continue repairing the deck or to provide a PCC overlay. It was already noted that subsequent observations for epoxy injection repairs indicated that the repair was only temporary due to the increased brittleness of the organic compound over time. Different types of epoxies were used over the course of the testing due to competitive bid rules but the same epoxy was used at the same time.

The conclusion of the study found that the optimal injection schedule is between 3 and 4 years frequency to keep spalling to a minimum and to reduce maintenance costs. It was also noted that the frequency of repairs may increase or decrease based on weather factors. Above average occurring events such as freeze/thaw accompanied by a wind-chill factor, thunderstorms, precipitation, and overcast conditions during the day appeared to have a direct relationship on the growth of the delamination over the year as measured in percent of the total bridge deck area. The other events that were tracked and that did not appear to have an effect on increasing the delamination sizes were sunny daytime conditions, windchill, temperature differences of 28°F or more, and snow, ice or glaze occurrences.

2.4 Equipment Development

Drilling: One of the initial problems encountered during the early days of epoxy injection was how to deliver the material to the delaminated plane. Initially, an unmodified drill and carbide tipped masonry bits were used in order to provide a passage for the epoxy to travel. However, once the drill bit tip reached the open area of the delamination, the dust created by drilling was forced outward from the drill bit into the narrow thickness of the hollow plane. This created significant blockage and prevented the epoxy from fully penetrating the area.

The first innovation was to design a proprietary chuck and drill bits for use in a modified drill as shown in Figure 2-1. No commercially available alternatives were available in the 1970’s nor have any other attempts to improve on the original design been as effective. The chuck was designed to have a vacuum hose attached to it from an externally supplied shop vacuum machine. The chuck was hollow and featured a rotating collar that was sealed against air leakage against the main shaft. In essence, the shaft was free to rotate and the collar would stay in place around the rotating shaft.

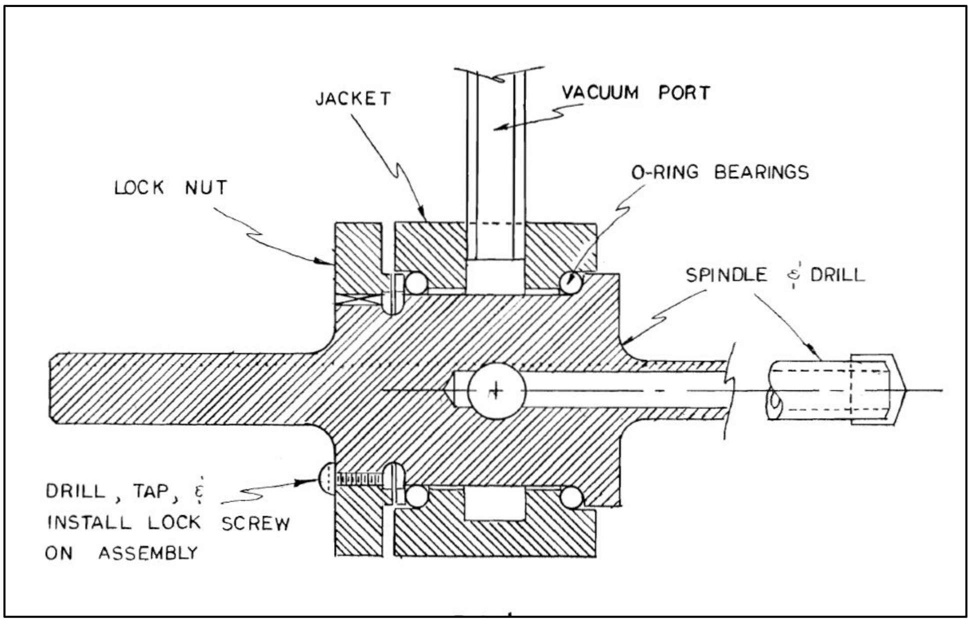

Figure 2-1: Kansas DoT’s Custom Chuck

The drill bits were designed from small diameter pipes and were fitted with a carbide tip slightly larger than the diameter of the shaft. The carbide tip provided longer wear against the concrete. The drill bit could then be fixed to the chuck and while the system was in operation, the debris from the removed concrete would be vacuumed up the carbide tip, through the drill shaft, into the hollow portion of the chuck, and out the ports in the collar into the vacuum container.

Tip designs were also investigated to provide feedback on the type of tip that would allow for the straightest penetration and to produce the fastest time to reach the maximum depth (see Figure 2-2). Additional developments and improvements came from the determination of the most effective rotational speed and the design of a drill press that positioned the drill at a fixed angle to the concrete deck without movement.

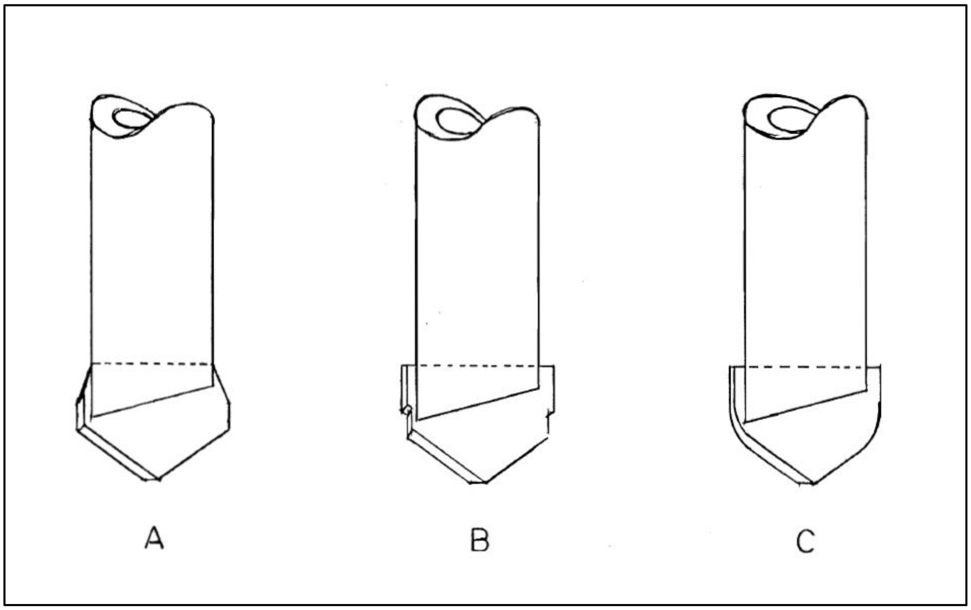

Figure 2-2: Tip Designs

Injection Probe: Once a clear path free of blockage is made to the hollow plane, a connection had to be made between the epoxy injection equipment and the concrete deck. The first types of epoxies used to repair the bridge defects were those that featured a high viscosity. These viscosities required increased pressure to convey the epoxy to the narrow thickness of the delamination.

The pressure that the connection had to withstand initially was up to 600 psi. It was difficult to find a configuration to accommodate those pressures. However, as the epoxy types were investigated, other lower viscosity epoxies were identified that reduced the pressure to a maximum of 200 psi with a working pressure around 50 psi.

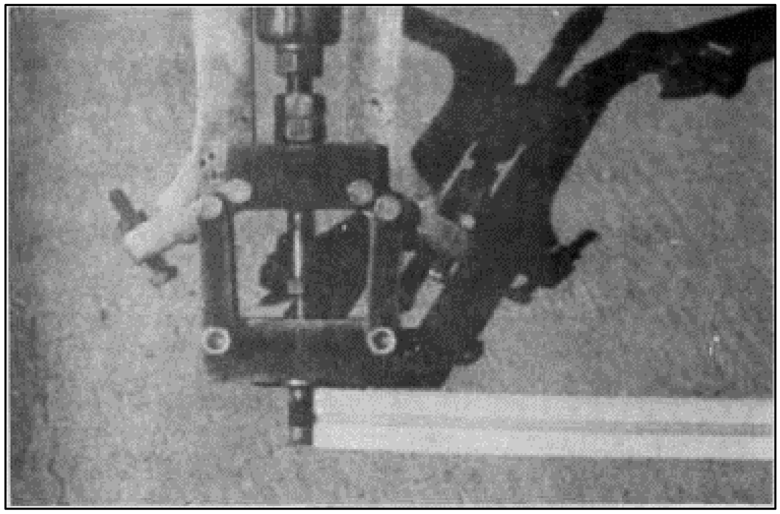

Figure 2-3: Insertable Gasket Type Injection Probe

The first type of injection probe investigated was an insertable gasket type as shown in Figure 2-3. This type featured a tip that could be inserted into the hole leading to the delamination. A rubber gasket was assembled on the outside of the tip next to a movable collar. The collar was attached to a lever on the probe handle which, when rotated, pressed the collar against the gasket, expanding it radially and forming a seal against the inside wall of the drilled hole. The second type of injection probe still featured an insertable probe, but this time the gasket was surface-mounted and held in place by the downward force of the technician who is operating the probe (see Figure 2-4).

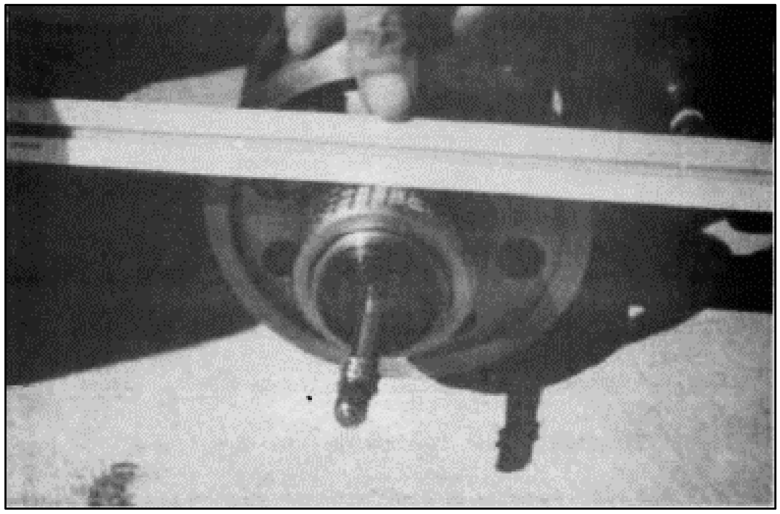

Figure 2-4: Surface Mounted Injection Probe

While the internal gasket type could withstand greater pressure and could remain in position without assistance during injection, it required a minimum depth of insertion to form an effective seal. In addition, the gasket took more time to replace since it involved removing the injection tip. The surface gasket type could resist leakage as long as the operator is using the equipment properly and a lower viscosity epoxy is used. However, if the surface was uneven, the seal could leak. The surface gasket type is prone to cause operator fatigue though it allowed for quick gasket replacements and quick injection set-up times.

Injection Pumps: The first equipment used for epoxy injection was high maintenance and required extensive set-up and clean-up times. Parts could only be used once due to plugging of the equipment by the epoxy. Proprietary design and specialized equipment was specified to deal with delivery and injection of the epoxy.

The first pumps used for epoxy injection were hand operated grease gun pumps. These pumps could produce satisfactory injection pressures but required the epoxy to be mixed prior to loading in the pump and were very messy. Also pumping the lever for injection produced significant wobble in the tip interfering with a proper seal. Later a mechanically driven positive displacement pump and mixing system were developed to reduce the human variable and improve clean-up. This system could meter the two parts of the epoxy for precision mixing and quality control more effectively. Based on an analytical study, the pressure was found to be too high for the given flow rate. So by using the lower viscosity epoxy, lower pressures could be achieved for the same flow rate. At the specified viscosities between 3 and 50 poise based on the temperature, the pump was outfitted with a variable speed controller. The minimum temperature for injection was set based on the setting requirements for the epoxy and the pump had to be able to work through the range of temperature dependent viscosities.

Mixer: Four in-line mixer types were tested. The first was a brush type mixer constructed originally from several test tube cleaners. The second was a metal reverse spiral mixer that was available from only one supplier. Third was a type of scouring pad that could be inserted into the hose. The fourth type of mixer tested was a reverse flow mixer.

The scouring pad and reverse flow mixer did not work at all. The best mixer was the in-line reverse spiral mixer. Since the cost was high, additional mixers could not be procured, which required cleaning of the existing mixer. The cleaning was time consuming, therefore the disposable brush mixer was recommended.

Miscellaneous Equipment: Other equipment was tested and specified including the delivery hoses, pressure gauges and a custom steel framed cart. The delivery hoses needed to be able to withstand deterioration from the solvents used in the clean-up of the injection system. While other combinations and types of solvents worked well, the solvent of choice was xylene because it was able to be used without special training and did not pose any special hazardous conditions. The hoses and gauges should be selected for solvent resistance and inspected periodically, replacing defective components when necessary. Current practices utilize biodegradable citrus based cleaners that are water-soluble and environmentally friendly.

The custom cart allowed for the material hoppers, pumps, and motors to be mounted in one portable location (see Figure 2-5). The hoppers were outfitted with a funnel type bottom which aided in the delivery of the epoxy components. The piping was routed with valves for versatility. Hangers were provided for storage of the hoses and the injection probe. Finally, the cart was fitted with wheels and handles for easy transport and maneuverability.

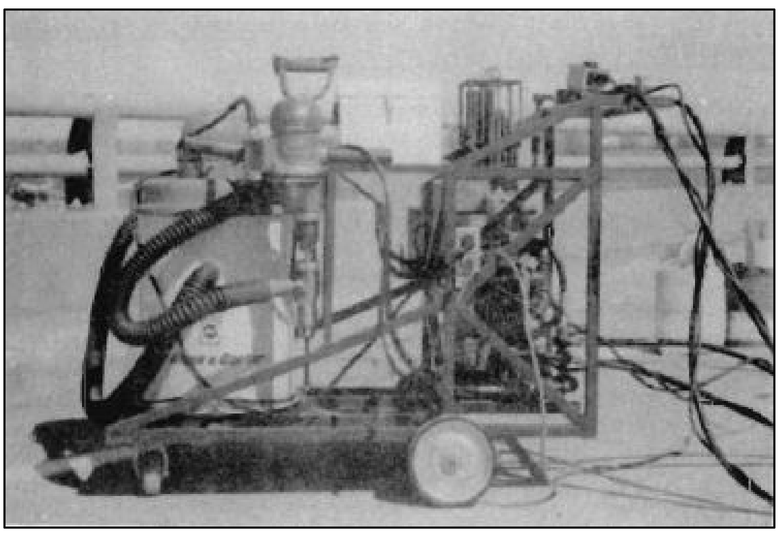

Figure 2-5: Kansas DoT Custom Injection Cart

2.5 Features of the Epoxy for Repairing Concrete Bridge Decks

Cheaper Alternative: Epoxy injection is so widely used because it can seal off delaminations and cracks using relatively inexpensive equipment and does not require a large labor force. Thus epoxy injection has become the cheaper repair alternative over jack-hammering out the affected area and replacing with fresh concrete. This allows for less cost in man-hours and reduced lane closures since the areas repaired do not have to be closed during the curing of the new concrete.

Reduction in Delamination Rate: While epoxy injection is used to fill delaminations and cracks, it has not been proven to eliminate the growth of new delaminations or cracks. During a two year period, it was determined that 15% of the areas rebonded formed delaminations again. This was in contrast to the 130% per year rate if the area is left untreated.

2.6 Epoxy Repair of Cracks

Up to this point, the equipment and methods for using epoxy have been with respect to delaminated concrete, that is, concrete that has a crack not intersecting with any other concrete surface. A vertical crack occurs when the crack in the concrete reaches the surface or originates at the surface (Smoak 1996). Additionally the force mechanism controlling the crack is different from that causing delaminations. Delamination cracks are usually caused by the corrosion of the steel reinforcement or by excessive voids allowing water penetration and internal freeze/thaw deterioration surface. Cracks can be caused by many mechanisms including external damage, alkali-silica reaction (ASR), reinforcement corrosion, poor quality concrete, freeze/thaw cycles, etc. (Darwin, et al. 1998).

When using epoxy to repair vertical or surface cracking in concrete, there are several similarities shared with the methods used for delaminations. First, the epoxy type and requirements remain the same. In fact, the first concrete repairs made using epoxy were to repair surface cracking and that knowledge was later applied to delamination repairs. The equipment for the epoxy mixing and pressure head is also the same – two chambers for each component and positive displacement piston type pumps for each chamber. The mixing element is also the same, either a disposable brush mixer or reverse spiral are commonly used. The differences occur at the delivery interface. The delamination repair method does not utilize either the insertable injection probe or the surface mounted injection probe.

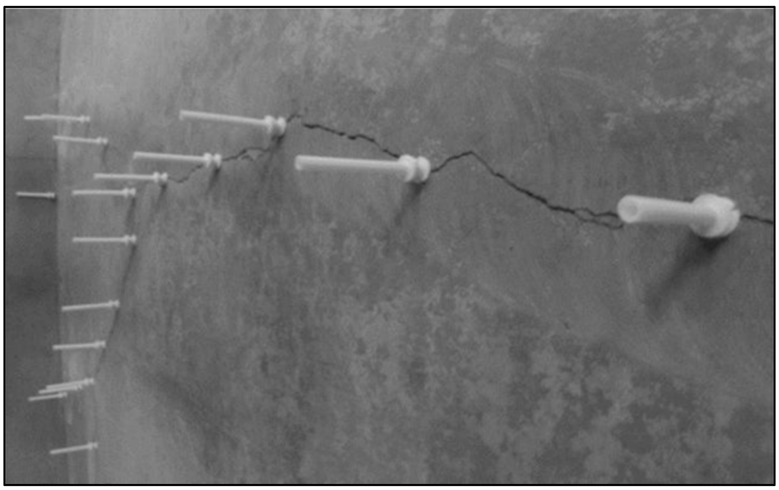

Figure 2-6: Example of Insertable Injection Probes

Instead, special injection ports are mounted at regular intervals directly over the crack or drilled into the crack if obstructions or calcium deposits exist (see Figure 2-6). If the injection ports are drilled in, the same vacuum drill that was used for delamination injection should be used to ensure that concrete dust or debris does not block the path of the epoxy. Several different types of injection ports are available depending on the application crack width and depth and these are discussed in chapter 3 in connection with the inorganic crack repair system. Once the injection ports have been properly installed and care has been taken to confirm that the port will intersect with the crack properly, the surface of the crack in between the ports must be sealed to contain the injected epoxy. This is either done with epoxy or a special quick setting mortar so the sealer can cure before injection. The injection probe is then connected to the ports and injection occurs until the maximum pressure is reached or the epoxy reaches the next port. When injection is completed and sufficient curing time has passed, the injection ports can be removed by scrapping or grinding to leave the epoxy flush with the surface of the concrete. If aesthetics are not an issue, the ports and sealer can be left in place.

2.7 Inorganic Systems

Though organic epoxy systems have suitable benefits and have been used successfully for decades, some of the most detrimental features include the high modulus of elasticity and the increasing brittleness and deterioration that occur naturally as a result of the breakdown of the organic system over relatively small periods (< 5 – 10 years).

There have been several inorganic systems identified for use in concrete repair procedures. The greatest benefit being that the properties of the inorganic repair material match very closely to the properties of the concrete. These include dry-pack mortar, proprietary repair mortars, fiber-reinforced mortar, grouts, low-slump dense concrete, magnesium-phosphate concrete and mortar, preplaced-aggregate concrete, rapid-setting cements, shotcrete, shrinkage-compensating concrete, silica-fume concrete and, the highlight of this thesis, aluminosilicate polymer (ACI Committee 503 and 548 2007).

2.7.1 Introduction to Potassium Aluminosilicate

In the 1970's a French scientist, Joseph Davidovits, developed a new class of inorganic "plastics" in response to several fire outbreaks in France (Davidovits, Synthesis of New

High-Temperature Geo-Polymers for Reinforced Plastics/Composites 1979). The material that he found was a group of inorganic mineral compositions that shared similar hydrothermal conditions that control the synthesis of organic phenolic plastics such as high pH values, concentrated alkali, thinset at atmospheric pressure and temperatures below 300°F.

The new family of materials was given the name Geopolymer because of the geologic origin of the main components and how the materials share properties with other naturally occurring minerals such as feldspathoids, feldspars, and zeolites. These properties include thermal stability, smooth surfaces, hardness, weather resistance and high temperature resistance up to over 2,000°F. Unlike the naturally occurring minerals, the so-called Geopolymers are polymers meaning they can be transformed, tooled, and molded. They are created in a similar manner to thermosetting organic resins and cement by polycondensation. The inorganic polymer can be formulated with or without the use of additional performance enhancing fillers or reinforcement. Applications of the material are found in automobile and aerospace industries, civil engineering and plastics/ceramics.

2.7.2 Chemistry and Molecular Structure

The terminology for the division of Geopolymers based on aluminosilicates is polysialate. Sialate is the acronym for silicon-oxo-aluminate of Na, K, Ca, Li. The structure of the sialate is composed of SiO_4 and AlO_4 tetrahedrals linked by the shared oxygen. In the case of potassium aluminosilicates, the positive ion K+ is present to balance the negative charge of the Al^{3+} in the IV-fold coordination. The chemical formula of the potassium polysialate is:

$$K_n\{-(SiO_2)_z - AlO_2\}_n \cdot H_2O \tag{2.1}$$

where n is the degree of polycondensation and z is 1, 2, or 3. Polysialates are characterized as chain or ring polymers and in the case of the potassium aluminosilicate the resin hardens to an amorphous solid. The empirical formula of the potassium polysialate is $Si_{32}O_{99}H_{24}K_7Al$. Elemental composition, x-ray diffraction, and Si magic angle spinning nuclear magnetic resonance spectroscopy (Si MAS-NMR) have been used to create a representative structure of the cured inorganic material shown in Figure 2-7 (Davidovits 1991).

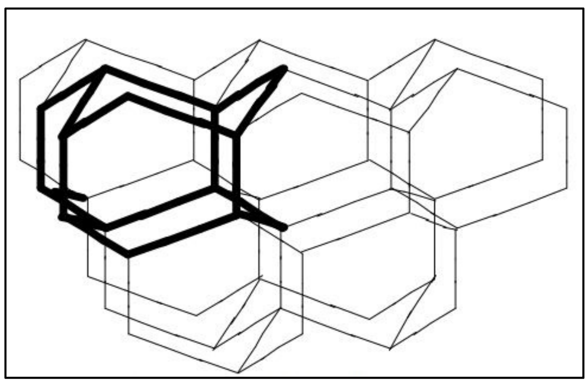

Figure 2-7: Chemical Structure of Potassium Polysialate

2.7.3 Synthesis

There are two basic components to the inorganic system – a liquid and a powder. Other ingredients are added as fillers and to enhance the properties of the matrix such as adding water to increase workability. Some of the other materials that can be added are fibers, wetting agents, retarders, etc. The ingredients are mixed in a high shear mixer for 60 seconds, then given a 30 second rest before finishing the mixing with another 30 seconds. The matrix can be applied using common painting and plastering tools such as brushes and trowels depending on the application surface. Optimal curing was initially set as 12 hours at no less than 175°F but different applications may call for different curing regimes. For example, in some cases it may be impractical to cure the specimen at any other temperature but room temperature. It has since been found that the properties are not significantly impacted by curing temperature.

Some of the fluid properties of the mixed aluminosilicate have been measured. Figure 2-8 shows that as the component cures over time, the viscosity of the mix will increase. Workability of the mixture remains for up to 4 or 5 hours though in reality, it is much less for injection systems. The initial mix viscosity has been measured at room temperature with a dynamic rheometer using parallel plate mode with 1 inch diameter steel plates and was found to be 20 poise (Lyon, et al. 1997).

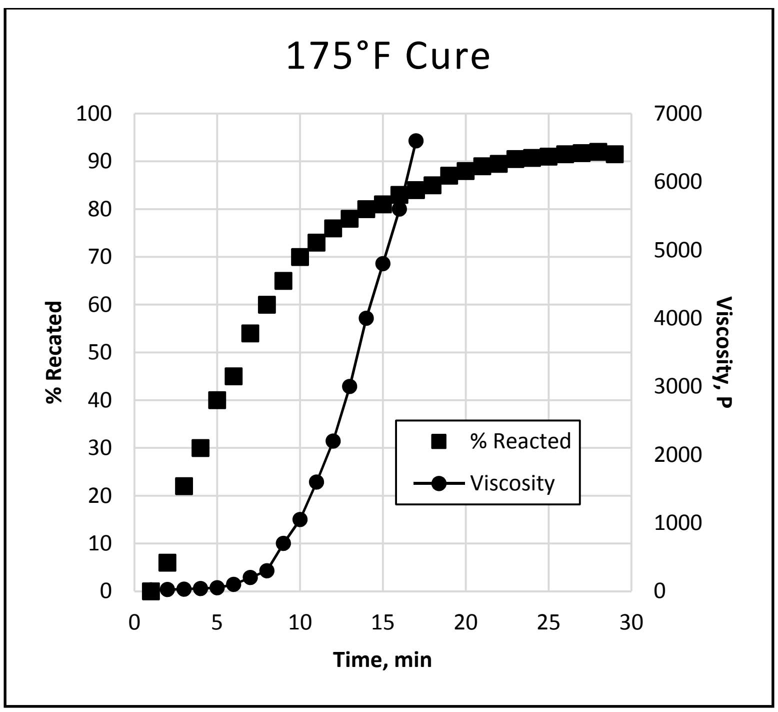

Figure 2-8: Aluminosilicate Reaction Time and Viscosity

2.8 Inorganic Polymer Properties

Each of the results shown below have been previously tested as a part of a long standing research regime performed at Rutgers University under the guidance of Dr. P. N. Balaguru and in partnership with the Federal Aviation Administration and the Connecticut Department of Transportation. The results came largely from the PhD dissertations of Andrew J. Foden and Ronald J. Garon (Foden 1999) (Garon 2000). Under each test section is a description of the test and the test result. In all tests, the same basic potassium aluminosilicate material composition was used. The curing regime was also same for all mixes and included heating at 100°F for 6 hours, 140°F for 6 hours and 175°F for 24 hours after mixing.

Tension: Tensile strength was determined based on ASTM C496 Standard Test Method for Splitting Tensile Strength of Cylindrical Concrete Specimens (ASTM C496 2011). The tests were performed using 5 – 1 inch diameter by 1-1/2 inch long cylinders comprised of pure potassium aluminosilicate using a Sintech 10GL test frame with a 10 kip capacity at 0.05 inches per minute rate. The results show that the average splitting tensile test strength is 530 psi.

Compression, Strain, and Modulus of Elasticity: Compression strength was performed using ASTM D695 Standard Test Method for Compressive Properties of Rigid Plastics (ASTM D695 2010). In addition, the stress-strain relationship was determined. The tests were performed using 5 – 1 inch diameter by 3 inch long cylinders of pure potassium aluminosilicate using a Sintech 10GL test frame with a 10 kip capacity at 0.05 inches per minute rate. Strains were monitored using an Instron extensometer and the loads, displacement and strain were stored using a computer controlled data acquisition system.

The results show that the stress-strain behavior was linear to failure indicating a brittle linearly elastic material with no post-peak residual strength. The average compressive strength, strain capacity and elastic modulus were found to be 5,665 psi, 0.49% and 1.4 x 10^6 psi.

Strain Capacity and Surface Energy: The strain capacity and surface energy tests were performed using a technique by Deteresa et al, developed for determination of Kevler™ fiber properties (Deteresa et al 1984). The test involves coating one side of an elastic rectangular beam and loading it in a cantilever configuration. By observing the time of the first crack and noting the load responsible for inducing the crack, Bernouli-Euler beam theory can be used to find the tensile and compressive strains using the following equation:

$$\varepsilon_u = \frac{My}{EI} \tag{2.2}$$

Where:

ε_u is the ultimate strain capacity

M is the bending moment when the first crack is observed (L_c * P)

L_c is the distance from the load point to the first crack

P is the load at which the first crack is observed

y is 1/2 t

t is the thickness of the rectangular beam

E is the elastic modulus of the rectangular beam

I is the moment of inertia of the rectangular beam

The surface energy of the inorganic matrix can also be determined from this test. The concept is the result of using fracture mechanics and conservation of energy principles in the following equation:

$$\gamma = \frac{1}{4}\varepsilon^2 Ea \qquad (2.3)$$

Where:

γ is the surface energy in joules per unit area

ε is the strain

E is the elastic modulus of the matrix

a is the debonded distance perpendicular to the crack in the inorganic matrix

Three steel beams having the dimensions 0.06 inches thick by 1 inch wide and 8 inches long were tested after coating with the potassium aluminosilicate. The beam was held in place with two closely spaced clamps to ensure zero slope. For the tension tests, loads were applied directly to the end of the beam. For the compression tests, a pulley was used to provide the opposite force.

The average tensile strain capacity was found to be 743 x 10^{-6} in/in and the average compressive strain capacity was found to be 5,173 x 10^{-6} in/in. This corresponds well with the compressive strain found in the compression tests mentioned earlier (4,900 x 10^{-6} in/in). Finally the average surface energy was found to be 0.994 x 10^{-6} Btu/in^2.

Dynamic Elastic Modulus: The dynamic modulus test was performed by measuring the compressive wave velocity in a sample. A 1 inch diameter by 12 inch long specimen was fixed to a large steel cylinder. An accelerometer was attached to the free end of the specimen and connected to a Krenz PO 5050 Dynamic Signal Analyzer to capture the acceleration and time history. The test specimens were impacted with six different spherical strikers of different sizes, three of which were made out of steel and the remaining three made out of copper. A total of twelve specimens were used – two for each striker. The collected data was transformed using a Fast Fourier Transform and graphed to identify the frequency at which the peak value was located. The modulus is then calculated using the frequency of the first three modes and averaging the result using the following formula:

$$E^* = \left(4f_n\frac{L}{n}\right)^2 \rho \qquad (2.4)$$

Where:

f_n is the natural frequency of the n^{th} mode of vibration

n is equal to 1, 3, 5,…

L is the length of the specimen

ρ is the density of the material

The average elastic modulus was found to be 1.57 x 10^6 psi which is close to the value found in the compression test (1.4 x 10^6 psi).

Dynamic Shear Modulus: The dynamic shear modulus was found using the methods given by ASTM D4015 Standard Test Methods for Modulus and Damping of Soils by Resonant-Column Method (ASTM D4015 2007). This test method offers procedures to determine shear modulus, Young's modulus and shear damping for solid cylindrical samples. A quasi-static torsional simple shear and resonant column apparatus supplied by Soil Dynamics Instruments, INC. was used in conjunction with an oscilloscope to find the resonant frequency of the sample. Once the frequency is determined, the shear modulus is found using a formula that incorporates calibration data from the apparatus. This result can then be used along with the dynamic modulus of elasticity to find Poisson's ratio using the following equation:

$$v = \frac{E^*}{2G^*} - 1 \tag{2.5}$$

Where:

E^* is the dynamic Young's modulus

G^* is the dynamic shear modulus

The two specimens used in the test were 1 inch in diameter and 12 inches long. The average dynamic shear modulus was found to be 0.706 ksi and the resulting Poisson's ratio was 0.244. Note that Poisson's ratio for common glass is 0.245.

Flexural Strength: The tests for flexural strength, flexural modulus and failure strain were conducted in accordance with ASTM D790 Standard Test Methods for Flexural Properties of Unreinforced and Reinforced Plastics and Electrical Insulating Materials

(ASTM D790 2010). The four specimens were 1 inch in diameter and 7 inches in length. The loading machine was an MTS Teststar system with center-point loading and a deflection rate of 0.11 inches per minute. Deflections were measured using a spring-loaded LVDT. The MTS system collected the data.

The average flexural strength was calculated using the moment at which the specimen failed and was found to be 1.17 x 10^6 psi. The average flexural modulus was found to be 1.36 x 10^6 psi which is similar to the elastic modulus found from the compression tests (1.4 x 10^6 psi) and the dynamic elastic modulus value of 1.57 x 10^6 psi. The failure strain obtained was 860 x 10^{-6} in/in and correlates with the tensile strain capacity of 743 x 10^{-6} in/in shown earlier.

2.9 Composite Properties

Other tests have been performed on composites of the matrix and fiber reinforcements such as steel, carbon and fiberglass. The tests on these specimens were performed to find if the inorganic matrix can be used as a suitable alternative to the two-part epoxy bonding systems typically used in such applications. The tests performed included flexure, tension, compression, shear, fatigue, and heat durability. The use of additional reinforcement fibers was not studied in this report, thus the description and results from the composites tests are not given in detail. However the test conclusions are summarized below:

- Flexural, tensile and shear strength of inorganic matrix composites are comparable to those obtained by organic matrix composites.

- Compressive strengths are reported to be lower than that of similar organic based composites due to the premature tensile splitting failure mode. It should be noted that fiber reinforcements are seldom used in pure compression type elements and configurations.
- The performance of the carbon/alumino-silcate composite under fatigue loading is similar to that of other structural materials and is reported to sustain about 10 million cycles at a stress range of 40%, minimum stress of 10%, giving a mean stress value of 30%.
- The flexural strength of the composite decreases by approximately 40% when exposed to temperatures around 1500°F. Interlaminar shear strength decreases by about 70% when exposed to temperature up to 1800°F. At 400°F, the loss in strength is only 10%. Note that organic epoxies begin to melt at around 250°F.

2.10 Durability

The question of durability is common for new materials. Basic durability tests were performed on the composite of the fiber reinforced inorganic matrix. All tests featured 32 - 2 inch square by 13 inch long coated concrete specimens and 16 - 2 inch square by 13 inch long flexural specimens with various types of tensile fiber reinforcement. The coated specimens were used to determine the matrix's effectiveness as a protective coating. Here the dynamic modulus was measured by determining the harmonic frequency of the specimen. The flexural specimens gave information related to the durability of the system in terms of deterioration of flexural strength. The load for the flexural test was applied using an MTS testing machine with 10 kip capacity. The deflections were recorded with a LVDT and recorded using a computer.

Wetting and Drying: The wetting and drying conditions were performed using a fiber reinforced aluminosilicate coating in saline water conditions. The testing was to show whether the coating could protect the concrete during the test. Dynamic modulus test data was gathered to show the integrity of the concrete using equipment specifically designed for the electronic measurement of the natural frequency and accompanying calculation of the dynamic modulus. The test continued to 200 cycles of three hours of wetting in 3% saline solution at 100°F and three hours of fan-aided drying as shown in Figure 2-9. Throughout the testing the modulus did not change more than 2%.

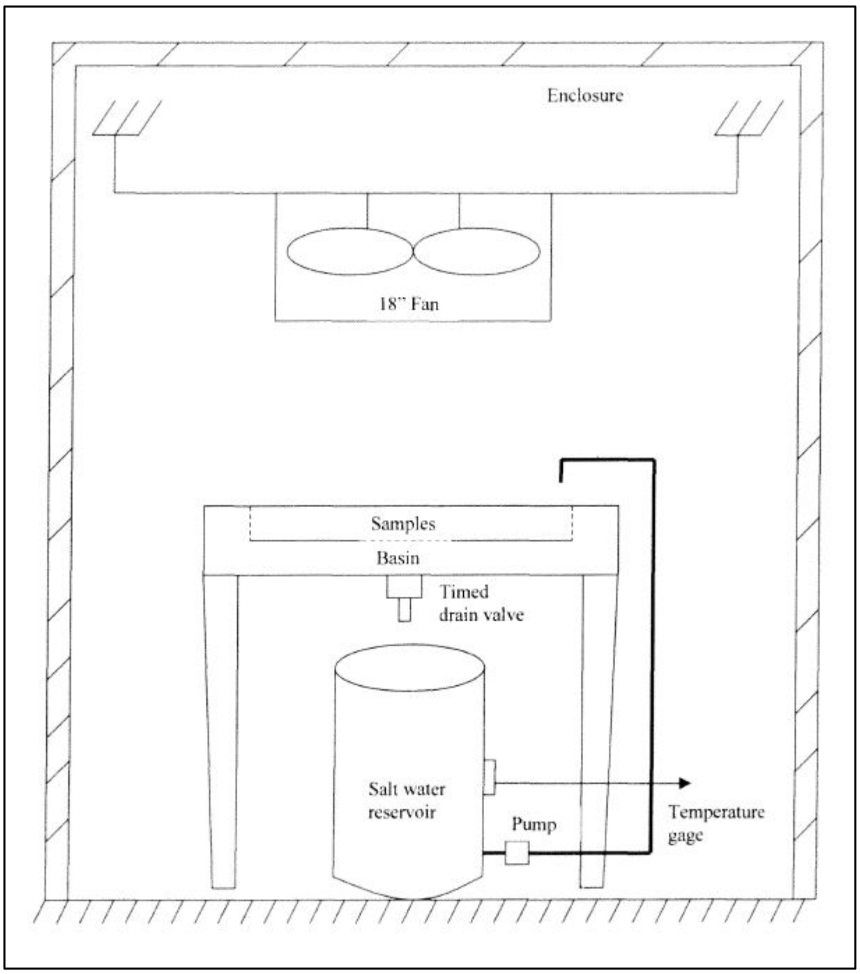

Figure 2-9: Wetting Test Set-Up

The flexural tests specimens were prepared by fixing continuous fiber tows or layers of fiber fabric using the inorganic matrix (see Figure 2-10). Flexural tests were performed with the same set-up as the dynamic modulus but were tested at 50 and 100 cycles. It was determined that wetting and drying cycles on the strength specimens do not noticeably affect the strength.

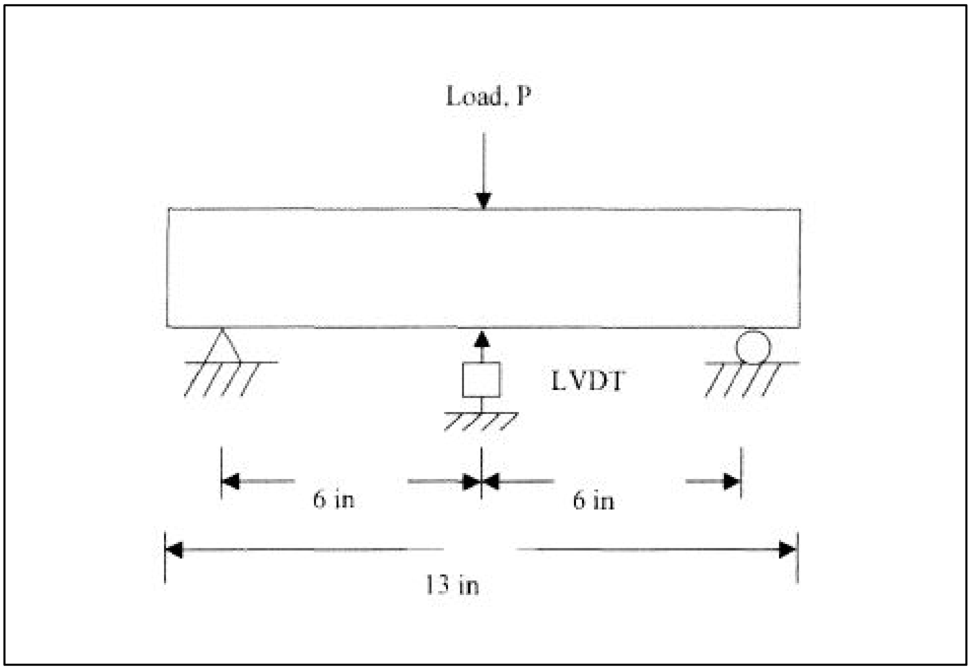

Figure 2-10: Flexural Test Set-Up

Freeze/Thaw Durability: Freeze/thaw tests were performed on the same number and size of samples as in the wetting durability tests (see Figure 2-11). The tests were also used to show the ability of the coating to protect against deterioration of the underlying concrete substrate. ASTM C666 Standard Test Method for Resistance of Concrete to Rapid Freezing and Thawing was used for the testing method and included 200 cycles of 0°F to 40°F temperature changes in a saline solution (ASTM C666 2008). The dynamic modulus was used to determine the integrity of the concrete. While it was noted that the coating maintained its bond with the concrete throughout the testing, it was not able to sufficiently protect the concrete substrate from significant deterioration. Flexural tests were not performed on these specimens.

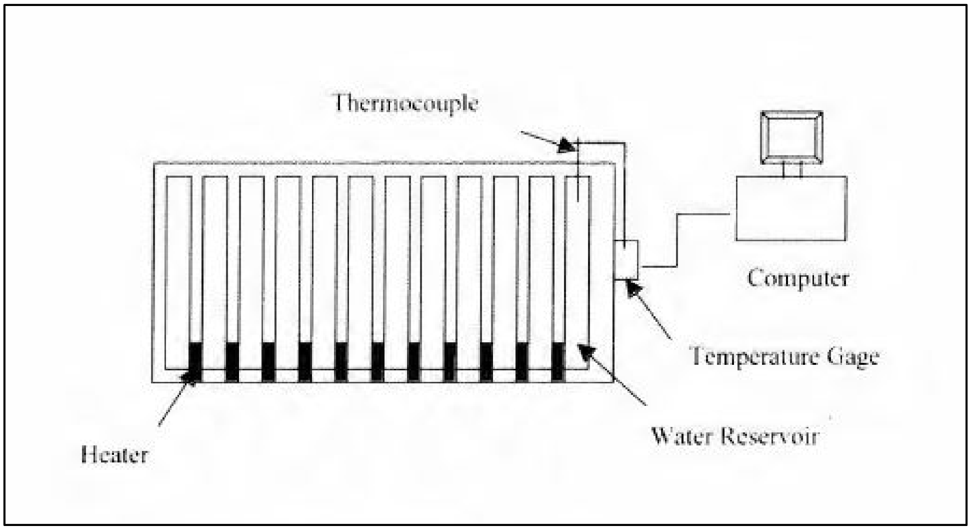

Figure 2-11: Freeze/Thaw Test Set-Up

Scaling: Scaling tests were performed on the same number and size of samples as in the two previous durability tests. Rectangular dams were constructed on the top surface of the beams and contained saline solution (see Figure 2-12). ASTM C672 Standard Test Method for Scaling Resistance of Concrete Surfaces Exposed to Deicing Chemicals was used as the testing method where the samples were kept at 20°F for 16 hours and at 72°F for 8 hours for a total of 50 cycles (ASTM C672 2012). The ASTM method gave a rating system for visually inspecting the specimen to determine the severity of scaling. Compared to control specimens, the coating either slowed or prevented scaling.

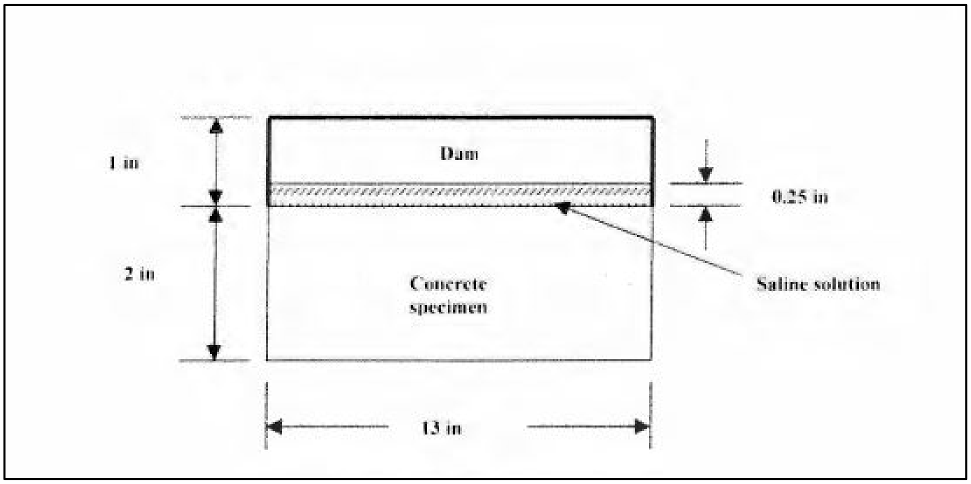

Figure 2-12: Scaling Test Set-Up

The flexural specimens adapted for this test featured the rectangular dam placement on the tensile face of the beams. The beams were then tested in center-point loading after 50 cycles of testing. Here, as in the wetting and drying tests, scaling conditions did not appear to have an effect on flexural strength.

2.11 Strengthening Systems

The inorganic epoxy was used to strengthen both steel and concrete beams for increased flexural capacity. The steel beams that were strengthened were S3X7.5 and 19 inches in length. Continuous and mat carbon fibers were added to the tension face of the beam to increase capacity. The fibers were varied from 1 to 3 tows of continuous fibers and 1 to 2 layers of carbon fabric. The beams were tested in a custom designed single-load point stainless steel jig at a loading rate of 500 lb per minute as shown in Figure 2-13. Deflections were measured using an Ames 282 dial gauge at the midpoint of the beam. The added fibers increased the stiffness and delamination of the carbon fibers only occurred after the beam yielded, indicating that the inorganic matrix is suitable for bonding fibers to steel.

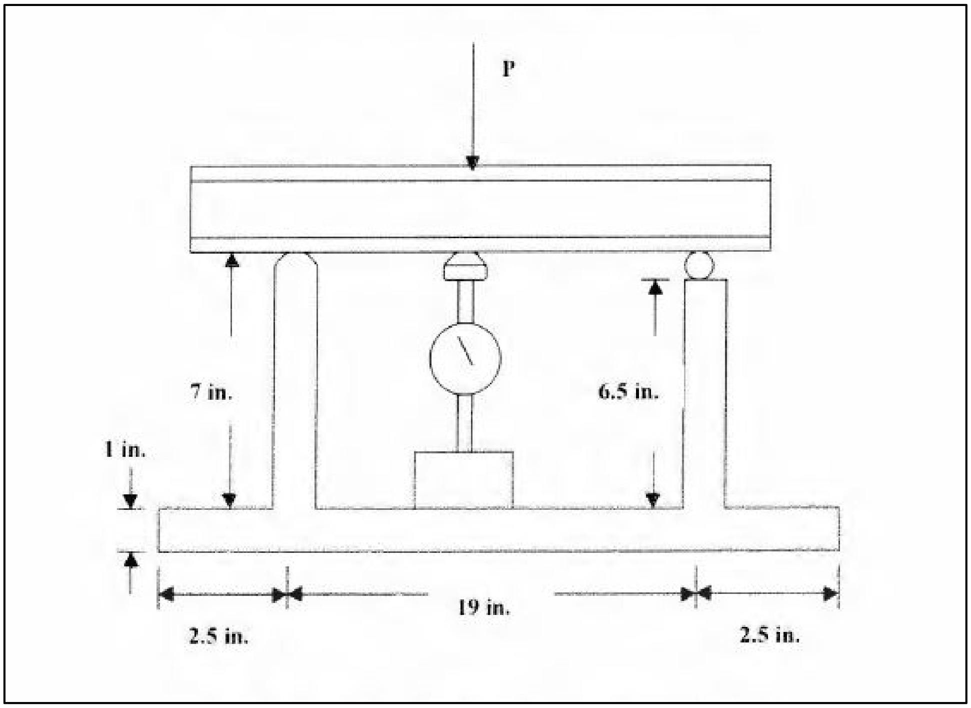

Figure 2-13: Strengthened I-Beam Test Set-Up

The inorganic matrix was also successfully used to strengthen concrete beams. In a head-to-head comparison of organic and inorganic epoxy for bonding carbon fibers to concrete test, four beams were cast 126 inches long, 11.8 inches deep and 7.875 inches wide. The span was 118 inches and the beam featured 2 - #4 bars for tensile reinforcement. Compressive strength of the concrete was 6,800 psi. The load was applied in third-point loading located at one-third points over the span. Loads were measured using MTS data logging systems. Flexural capacity was increased by up to 50% over the non-strengthened control beam. The inorganic matrix beams failed by rupture of the fiber in contrast to the epoxy bonded beams which failed by delamination of the fibers. It has long been understood that the desired failure mode is rupture of the fibers because the full capacity of the fibers can be utilized. This demonstrated that the inorganic aluminosilicate matrix can be used for bonding fibers to beams to increase flexural capacity.

2.12 Field Applications

In addition to the use of the inorganic aluminosilicate compound being used to bond carbon fibers to structural elements for strengthening and to create fiber reinforced composites, the epoxy has also been used as a coating for civil structures because of the some of the following benefits: salt-water protection, depollution properties and self-cleaning and anti-graffiti abilities (Brownstein 2010).

Color matching: The inorganic epoxy shows excellent versatility in terms of acting as a base where other additives and colors can be combined to enhance the feature set of the original composition. The mix has been successfully treated with different metal oxides to create over two dozen color schemes including phosphorescent blends.

In a large-scale coating project chosen to demonstrate the feasibility of covering large areas and color matching, a special inorganic coating was designed. The project located at the Exit 12A entrance ramp to I-280 EB highway in South Orange, New Jersey. A varying-height architectural retaining wall was built on the right-hand side of the ramp in 2008 and featured a random cut stone pattern with faux mortar joints in counter-relief (Figure 2-14). Only the raised part of the design was coated to give a contrast between the “stone” and “mortar” components. The retaining wall varied in height from 3 feet to 12 feet and extended for over 900 feet for a total of about 7,200 square feet.

Figure 2-14: Inorganic Coating on I-280 Retaining Wall

The mix utilized amounts of red and green oxide pigments and the use of a retarder. The color was designed to match a nearby outcropping of a dark reddish-brown shale formation as seen in Figure 2-15. An isopropyl alcohol retarder was added to the mix during the hotter portions of the day to increase workability during application.

Figure 2-15: Color Matching

Application of the coating was accomplished best using regular nylon bristle painting brushes. Since the coating is inorganic, clean-up was done with water and allowed the equipment to be reused. The application rate was about 200 square feet per person per day. Mixing was performed on-site to give the maximum application time. The coating has been in place for over four years and no deterioration or adverse effects have been observed.

Field durability: The inorganic compound has already been lab tested for durability against salt water and has shown satisfactory resistance. A salt water durability field test was conducted at the George Redding Bridge on Route 47 in Wildwood, New Jersey. A bridge house is located on both the upstream and downstream side of the single-leaf Chicago or fixed-trunnion bascule bridge for monitoring waterway and automobile traffic and to house the equipment for operating the lift bridge. Both towers displayed deterioration due to salt water intrusion from window and roof leakage. After repairs were made to prevent water leakage, the interior sheet-rock and concrete walls were coated with the inorganic coating to protect the structural components against further deterioration as shown in Figure 2-16. The coating and its performance were then monitored for three years. During the time of the research observation, no deterioration was detected on the surfaces of the coating.

Figure 2-16: Inorganic Coating in the George Redding Bridge House

Self-cleaning and depollution: The self-cleaning properties were demonstrated at a retaining wall located at the south-bound I-295 scenic overlook at milepost 58 near Trenton, New Jersey. Self-cleaning is defined as the ability of the coating to prevent specific soiling agents to adhere to or form on the surface of the coating. This is accomplished by the addition of zinc oxide (ZnO) to the coating. The major advantage of this ability is that the coating does not show the effects of age and dust and mold will not collect on the surface, reducing the need for cleaning and improving the overall appearance. In the tests performed, a section of the wall was coated for comparison to an uncoated section. After several months, a layer of algae had formed on the untreated section but was not present on the directly adjacent coated section as shown in Figure 2-17. In addition, no dust had collected on the coating which was detected on the panels that were not treated.

Figure 2-17: Self-Cleaning Properties Discourages Algae Growth

In the field test for depollution, a dye, Rhodamine B, is used to demonstrate the special ability of the coating. Since the concentration of the dye is directly related to its color, a colorimeter can be used to measure the effect of the self-cleaning properties of the inorganic coating. Ultra-violet light has been identified as the activator for the photocatalysis of the pollutant. The location of the test was at the US Route 1, Woodbridge Mall west entrance ramp retaining wall on the right side of the roadway (see Figure 2-18). This wall also featured a raised panel random stone pattern similar to the one featured in the I-280 project. Here the entire surface was coated with a white color to match the existing new concrete construction. When the dye was initially added to the surface, it was difficult to get the liquid to remain on the vertical surface. After just a week, the dye had been reduced by nearly 90% and after a month, the dye had been reduced to only 2%. This demonstrated that the self-cleaning properties are satisfactory.

Figure 2-18: Inorganic Coating on Woodbridge Mall Retaining Wall

In separate lab tests, the coating, with a titanium dioxide (TiO_2) admixture was able to scrub nitric oxide (NO) and nitrogen dioxide (NO_2) from the air in closed container environments. Since this ability is difficult if not impossible to measure in an open environment, field testing results were not performed. When the coating is activated by

UV light from the sun, the resultant photocatalytic reaction is able to reduce the concentration of the harmful pollutants by nearly 95% in a matter of hours (Amer 2008).

Anti-graffiti: Given the self-cleaning properties of the inorganic aluminosilicate coating, it would not be much farther to conclude that the coating could also be graffiti resistant. In fact, lab tests confirmed that the coating is resilient to a large number of organic substances including various dyes, tinted resins, and solvents found in permanent markers and paints. When the foreign substance is added to the coating, it is easily removed with water, mechanical scrubbing, biodegradable solvents or a combination of these.

The coating was applied to the wing walls on the south side of the Milltown Road overpass located on US Route 1 in Milltown, New Jersey. This location was chosen because of the frequent application of graffiti on the structure. The application of the coating made removal of the graffiti easier. Shortly after applying the protection, graffiti was sprayed on the abutment. DOT maintenance crews responded by applying a layer of paint over the entire abutment. So when the coating was tested for easy removal, there was both a layer of graffiti and paint. The paint and graffiti were easily removed using a mechanical scrubber and pressure washer as shown in Figure 2-19.

Figure 2-19: Graffiti Removal Demonstration on the Inorganic Coating

2.13 Summary

The following points are noted in regard to the history of organic epoxy systems:

- Epoxy has been used for concrete repair since 1948.
- Research to determine the best practice for epoxy repair began in 1968 and included equipment development, injection techniques and comparison of epoxy brands.
- Systematic tests to determine the effectiveness of epoxy to repair concrete began in 1978 using durability tests.
- Inorganic systems for concrete repair were outlined in the mid-1990's.

The following topics were covered with respect to epoxy injection systems development:

- The use of organic epoxies to bond concrete surfaces including cracks, delaminations and structural elements (with reinforcement) is widely documented, accepted and a common repair technique.
- Low viscosity epoxy no greater than 20 poise must be used to repair delaminations in concrete bridge decks and vertical/surface cracks. Higher viscosity epoxy is approved for large width cracks only.
- Epoxy with the ability to cure at low temperatures, resistance to dilution in water and deterioration by salt solutions are preferred.
- Preparation for repairing delaminations include vacuum drilling to the depth of the hollow plane. Preparation for crack repair includes mounting the injection

ports and sealing the external surface of the crack to prevent leakage during injection.

- Injection systems include a pump, mixer and injection probe. The specified pump is a positive displacement pump. Recommended mixers are either a brush type or reverse spiral inline mixer. For delamination injection, suggested injection probes should feature a surface seal to eliminate minimum injection depths and to make the process faster for multiple injections. For crack repair, the injection probe should be compatible with the injection ports to form a non-leaking seal during injection.

- Epoxy systems are part of a continuous repair scheme. It is not intended for one-time use but should be evaluated periodically to determine the repair effectiveness. Most repairs should be re-injected every 3 to 4 years.

- Above average occurring events such as freeze/thaw accompanied by a windchill factor, thunderstorms, precipitation, and overcast conditions during the day appear to have a direct relationship on delamination growth.

- Organic epoxy systems are susceptible to natural breakdown and experience increased brittleness over time.

The following conclusions can be made about inorganic epoxy systems:

- Inorganic epoxy systems are more suitable for concrete repair due to the similarities in chemical make-up, stress distribution and stiffness.

- Some of most well-known inorganic systems include dry-pack mortar, proprietary repair mortars, fiber-reinforced mortar, grouts, low-slump dense concrete, magnesium-phosphate concrete and mortar, preplaced-aggregate concrete, rapid-setting cements, shotcrete, shrinkage-compensating concrete, silica-fume concrete and aluminosilicate polymer.
- Aluminosilicate epoxy was originally developed for fire protection.
- Applications of the aluminosilicate material are found in automobile and aerospace industries, civil engineering and plastics/ceramics.
- The inorganic system components are a liquid part and a powder (solid) part and must be mixed in a high shear mixer to adequately disperse the reactants. It is recommended to cure the system in low heat between 100°F and 175°F.
- The viscosity increases from 20 to 50 poise after 0.5 hours. At about 4 to 5 hours after mixing, 90% of the reagents had reacted.
- Advanced mix design has led to the development of room-temperature cured polymers.
- Additional properties include thermal stability, smooth surfaces, hardness, weather resistance and high temperature resistance up to over 2000°F.

Mechanical properties of the Rutgers University inorganic epoxy system include:

- Tensile stress: 530 psi
- Compression stress: 5,665 psi

- Tensile strain capacity: 0.07%
- Compressive strain capacity: 0.49%
- Modulus of Elasticity: 1,400 ksi
- Surface energy: 0.994 x 10^{-6} Btu/in^2
- Dynamic modulus of elasticity: 1,570 ksi
- Dynamic shear modulus: 0.706 ksi
- Poisson's ratio: 0.244
- Flexural strength: 1,170 ksi
- Flexural modulus: 1,360 ksi
- Flexural strain: 0.86%

The durability of the inorganic epoxy system by itself has not been tested. It has been tested as both a coating and the bonding component or matrix of a fiber composite system and the following conclusions can be made:

- The coating and matrix capacity of the inorganic epoxy can withstand repeated cycles of wetting and scaling in contact with salt water.
- The use of the inorganic matrix as a protective coating for freeze/thaw cycles is not recommended for non-air entrained concrete as it cannot provide additional protection against freezing and thawing.

The use of the inorganic matrix to bond fiber reinforcement to steel and concrete tensile faces to increase strength capacity has been successfully tested. In addition, the use of the inorganic epoxy as a protective coating has the following advantages demonstrated by several field applied projects:

- Adaptive mix designs including the use of pigmentation for color matching and admixtures for set retarding in South Orange, NJ.
- Protection against salt water deterioration in Wildwood, NJ.
- Self-cleaning and depollution properties in Trenton and Woodbridge, NJ.
- Anti-graffiti applications in Milltown, NJ.

CHAPTER 3 - PROCESSING VARIABLES AND PLASTIC PROPERTIES

3.1 Introduction

One of the aims of this thesis is to formulate a variation of the previously described inorganic polysialate specifically for use in concrete injection systems. Since the basic mechanical and fluid properties are already known and documented, the mix can be optimized to increase those properties with respect to injection systems. Specifically, those optimization items are flowability, shear strength and bond strength or adhesion. This chapter will be divided into two parts. In the first part, the mix designs formulated for this study will be introduced as well as the processing variables that were adjusted for concrete crack repair. The second part of this chapter will include tests to determine flowability of certain mix designs and their contribution to a final mix.

3.2 Part 1: Mix Design

As noted through the research of Dr. Hammell in 2000, the silica/alumina ratio has an effect on the properties of the inorganic matrix (Hammell 2000). The research showed that a lower silica/alumina ratio provided better durability. In addition, the thermomechanical properties and tensile strain capacity were unaffected, though in the case of flexural strength, a small increase was detected.

The main purpose in varying the mix design in this research is to find the silica/alumina ratio that provides the optimal durability and strength as well as the effect of the mineral oxide activator type on the strength and durability of the inorganic material. Finally, the use of different inert fillers and admixtures are also studied to investigate the possible enhancements they may provide. Water has also been added to matrix to increase workability but if more water is used, increased cracking occurs.

In the search for the optimal injection matrix, a total of twenty-four mixes were developed and tested. These twenty-four mixes were developed over the course of five different testing regimes and represented an evolution of the mix with respect to injection requirements. While different mixes performed well in response to the specific test regime, the poor-performing mix was not entirely discarded from future testing in order to provide details on what component could be altered to increase the mix properties. Also, additional details would be discovered about the test itself which would point to the use of another type of test in an effort to tease more information about the mix. The details about each test and their effectiveness are left for Chapter 4 in the interest of brevity and to keep the focus on the mix evolution.

Mix design was organized in the five groups and given a letter to designate each group. For instance, the first iteration consisted of two mixes which are assigned A1 and A2 mix respectively. The five groups are A, B, C, D, and E. As mentioned, there were 2 mixes in Group A, 4 mixes in Group B, 4 mixes in Group C, 10 mixes in Group D and 4 mixes in Group E for a total of 24 mixes.

3.2.1 Group A Mixes

Group A mixes were referred to as the preliminary mixes. The first tests were in the interest of concrete applicability and to determine whether the current mix design used for coating systems could be a potential candidate for injection systems. Only two tests were performed and included a normal silica/alumina ratio, filler, activator and coloring (to highlight the repair). Excess water was used to increase workability for injection systems. The test that was used was the repaired splitting tensile test. The result from the first repaired splitting tensile test was lower strength than expected and attributed to the use of the fillers. Also the voids were not filled very well indicating that too much water was used. The second repaired splitting tensile test used less water and was able to fill the voids better, though it was noted that the water amount could be reduced further. The second test involved a rudimentary injection system and showed that the mix could be injected and fill the voids as expected. Here as in the first test, the strength was lower than expected and was attributed to the higher water content.

Compatibility tests were conducted after the optimal mix design had been formulated. These tests were to prove that the mix design allowed the repaired concrete to distribute the internal forces across the repair plane. These tests did not contribute to the mix design but rather verified them and the entire test discussion is given in Chapter 5.

3.2.2 Group B Mixes

Strength Tests: Strength tests were conducted in three stages. Each stage was used to isolate specific variables as the mix design evolved. Also, in each stage a different mix iteration is specified. That is, Group B mixes were used in stage 1, Group C mixes in stage 2 and Group D mixes in stage 3. The logic behind the mix development was to determine the most relevant oxide activator first, then test whether the oxide activator can be enhanced before completely ruling one or the other out. Additional admixtures and fillers were used in the second stage to determine if enhancing the oxide activator would improve its performance. The third stage was to use the successful oxide activator in conjunction with the silica/alumina ratio to find the optimal proportion for strength. The strength tests used were flexural repair tests, direct shear tests and slant shear tests.

In the first stage of the tests, the variables of the mix were the mineral activators required for curing. The standard alumino-silica reaction features activators that are naturally present in the liquid hydroxide of the alumino-silica mixture. These natural activators do not vary in the typical mix concentrations available so additional activators can be added. There were three types of activator added to the standard mix: additional aluminum oxide, phosphate binder, and nano-aluminosilicate. All mixes were mixed in a high shear mixer. The components were added at one time and mixed for sixty seconds, followed by a sixty second rest to allow the system to activate. A brush was used to apply the matrix and the test specimens were cured at room temperature for four weeks.

Aluminum oxide (Al_2O_3) was used to increase the silica/alumina ratio. Since it was known that a reduction in the ratio increased durability, it was thought that by decreasing the ratio the strength would increase.

The use of a phosphate binder to increase the strength would come by keeping the silica/alumina ratio the same and increasing the alumino-phosphate presence. The advantage of this mix design is that it lowers the setting temperature, allowing an increase in the maximum water content limits for workability (Wagh, Singh and Jeong 1997).

The use of nano-particulate aluminosilicate is relatively new and expensive. However, in the case of an injected repair material, is worth investigating because of the strength requirements in the repaired plane (Leivo, et al. 2006). The repaired delamination must be able to withstand shear and tensile forces that would cause the repair to delaminate a second time. In addition, the repair boundary should transfer stresses across the plane to utilize the full compressive and shear strength of the concrete compression zone. The use of the nano-aluminosilicate addition to the inorganic matrix has not been studied before and was expected to bring increased strength to the repair mix.

The results of the initial Group B strength tests are shown in Figure 3-1. The standard mix is Mix B1, Mix B2 includes additional Al_2O_3, Mix B3 features the phosphate binder, and Mix B4 utilizes the nano-aluminosilicate. It can be seen that the standard mix has the best results, followed by the mix with the reduced silica/alumina ratio, followed again by a close tie with the phosphate and nano-systems. Note that the reduced silica/alumina ratio did not increase strength as was expected. This usually happens unless the decrease in the ratio occurs at much lower values. The use of the phosphate binder gave only mediocre results. This was expected since alumino-phosphate mixtures only provide general strength. The nano-content added to the mixture was expected to yield higher than normal strengths. The reason that the strength was not achieved was due to a lack of exposure to additional activator.

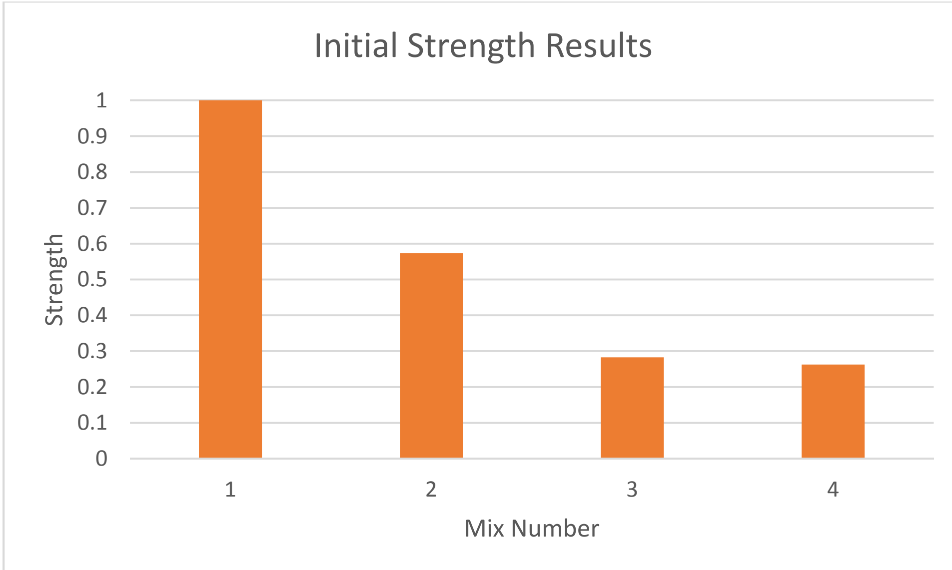

Figure 3-1: Mix Group B Results

3.2.3 Group C Mixes

The second stage of the strength tests involved enhancing the original Group B mix activators. Since none of the mineral activators contributed to the strength, additional ingredients or mix procedures were added to counteract the effect of adding the activators. The second stage of the tests also involved a change in the curing temperature. All test samples were cured in a custom-designed heat chamber at 150°F (65°C).

For the standard Mix B1, an additional 5% activator was added to create Mix C1. Even though Mix B1 performed the best, the percent recovered in the repair of the test specimen was below the specifications for the injected matrix strength. The activator was added to see if more was required to increase the strength output. That is, if the effect of added activator increases the strength, then there wasn't enough reagent to cure the reaction. However, if the effect reduces the strength, then the optimal amount was already achieved.

Mix B2 stayed the same with silica/alumina ratio but included the same 5% additional activator that was added to Mix C1 to create Mix C2. It was known already that if the silica/alumina ratio was further reduced, the strength would also be reduced. Of course, for very low ratios, some strength recovery is gained but not to exceed the currently reached values. The expected effect is to increase the strength in a similar manner to Mix C1.

For the phosphate activated system, Mix C3, the proportions stayed the same as in the initial trial, Mix B3. The part changed was the mixing procedure. Instead of using the traditional liquid and powder components, the mix was made in two liquid components. The water that would have been added in the beginning was dispersed equally through both the liquid and powder components before adding the two together. In the initial Group B mix procedure, the mixed compound was observed to cure rapidly. In the second Group C attempt, water is added to reduce the mixing time and allow for rapid application to the repair surfaces by dispersing the particles in the water first and then adding the two parts.

When the Mix B4 data was analyzed, the observation that the aluminosilicate amount was increased with the added nano-content but the amount of activator was not increased. The decision was made to add more activator in proportion to the added nano-aluminosilicate in an effort to unlock the nano-properties to produce Mix C4. In this case, zinc oxide (ZnO) was used for the activator.

The results for the stage two Group C strength tests are shown in Figure 3-2. While the enhanced properties are displayed, the initial Group B results are also shown for comparison. Additionally, the results of the direct shear tests are also given in combination with the flexural results. The following trends are noticed: the increased activator in Mixes 1 and 2 fail to give increased strength meaning that the optimal proportion of the activator is already being used, the modified mix procedure for Mix 3 was not effective. In fact, this was predicted during the application of the repair matrix since the mix nearly hardened instantaneously after mixing the two parts together. The most surprising result came from the addition of the ZnO in Mix 4. The use of the activator gave nearly an 80% increase from the initial mix design. Another trend to point out is that the curing temperature did not seem to provide a positive effect on the strength overall. Recall that one of the goals of the mix design is to provide a mix that can cure at room temperatures or less.

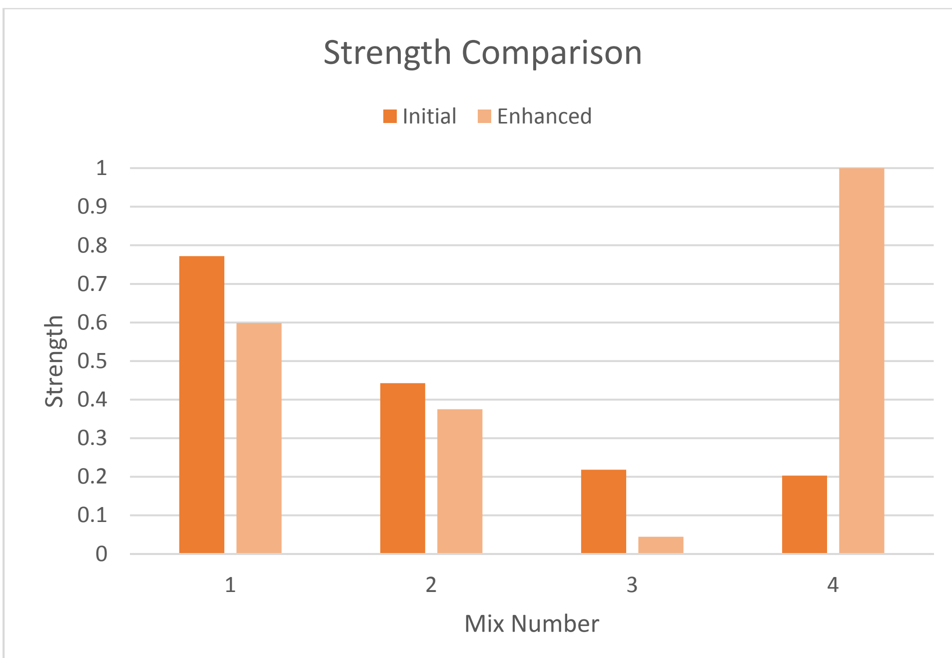

Figure 3-2: Mix Group B and C (Enhanced) Results

When the results from the flexural tests are combined with the shear tests, the evidence lies strongly in behalf of Mix 4 even though Mix 1 had better shear resistance (see Figure

3-3). Note that the nominal shear strength of the inorganic matrix has not been tabulated previously, so the results cannot be compared to expected results.

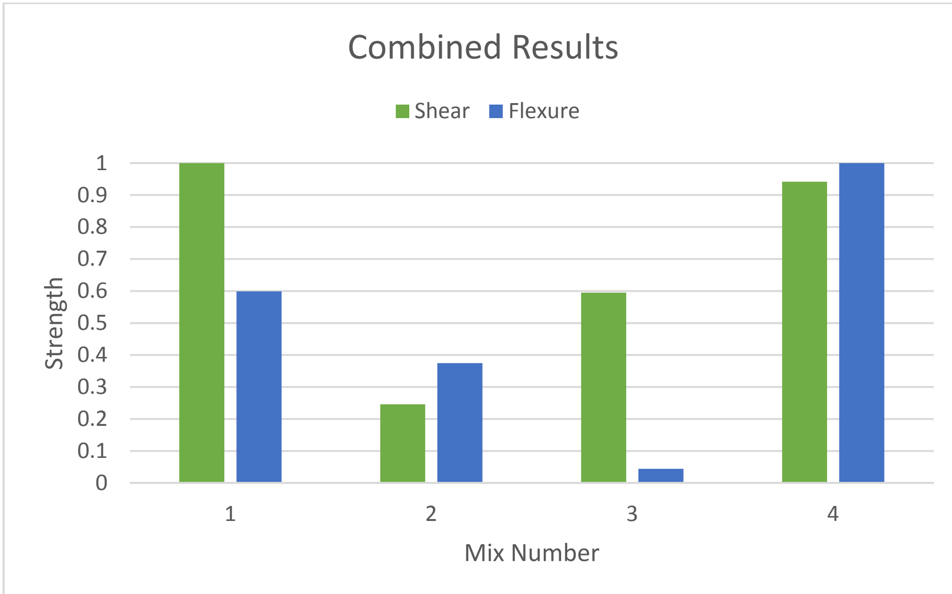

Figure 3-3: Mix Group C Results

3.2.4 <u>Group D Mixes</u>

The third stage of the strength tests (Group D Mixes) occurred in two parts. The first part consisted of incrementally varying the mix design variables and the second repeated the extreme variations of the design proportions except at room temperature curing. All of the specimens in the first part are cured at a lower temperature than before (120°F) but still utilize higher than normal curing temperatures. The second part specimens are all cured at room temperature and adds a new test sample is added: the slant shear test. Slant shear tests replaces the direct shear test because it can be compared directly to the results from existing epoxy repair systems.

For the first part of the third stage, a total of ten mixes were developed from the first two stages of the strength test influence on the mix evolution. The decision was also made that it was not in the interest of a practical injection alternative to use nano-aluminosilicate material due to the increase in cost. But since the addition of the zinc oxide gave such a significant jump in strength, the ingredient was varied across the five mixes to identify an optimal amount. And, instead of using additional nano-aluminosilicate, a purer source of the aluminosilicate was investigated by omitting it from the first five mixes and including it on the second five mixes.

The results for the effect of varying the amount zinc oxide on the strength, the effect of curing temperature and the combined results of slant shear and flexural strength from the second part of the tests are shown in Figure 3-4, Figure 3-5 and Figure 3-6. The following conclusions can be made: increasing ZnO without nano-aluminosilicate does not increase strength. This is because the ZnO is an activator and needs a reagent to cure. Surprisingly, the same is true for the additional aluminosilicate in the mixture. Since the aluminosilicate is not nano-sized, the ZnO has difficulty reacting with the aluminosilicates. The first time around (the enhanced tests), the increased curing temperature was detrimental, however, this time, the increased curing temperature, though slight, has a small to moderate effect. Finally, opposite trends are noticed in the combined results when curing at room temperature. Thus the optimal mix design should fall somewhere in the middle of the two extremes.

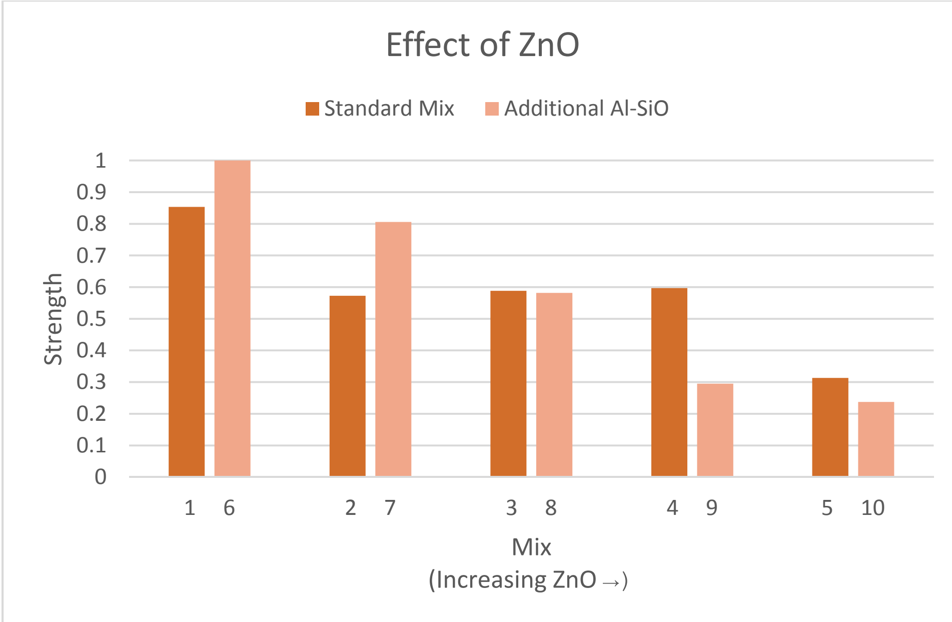

Figure 3-4: Zinc Oxide Activator Results

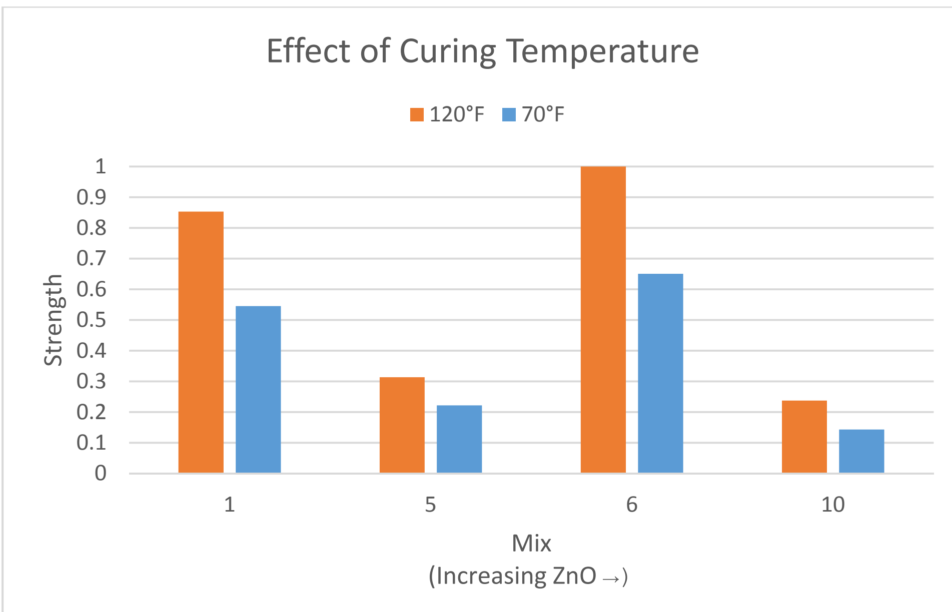

Figure 3-5: Curing Temperature Results

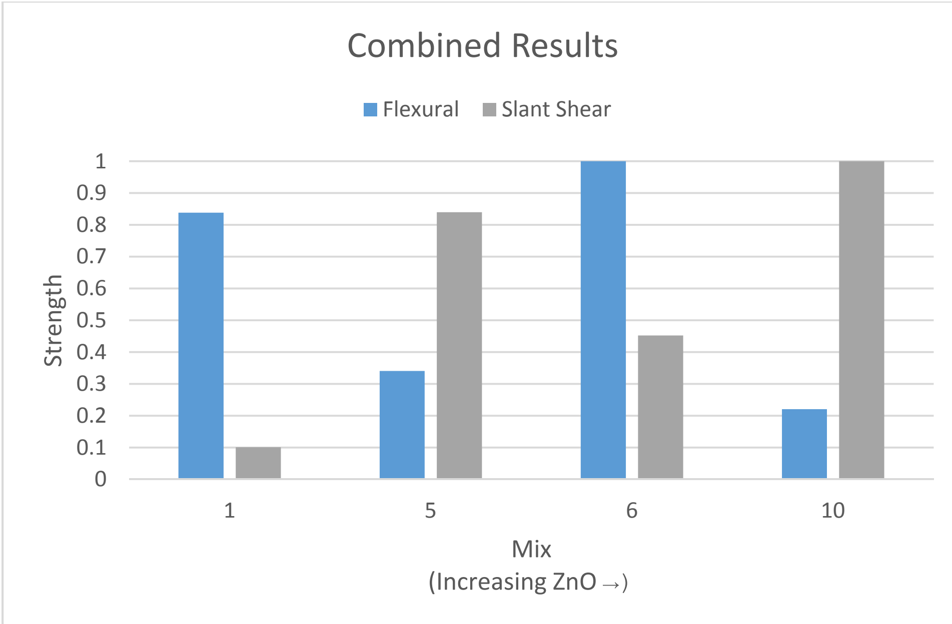

Figure 3-6: Mix Group D Results

3.2.5 Group E Mixes

The last iteration of the mix design included a total of four mixes designated Group E. These mixes were based on Mix D6 which held the overall best performance in the Group D mixes. Here the use of the ZnO activator was exploited again but the amount was kept constant for all of the Group E mixes. The objective of the Group E mixes was to test the durability of Mix D6 by varying the silica/alumina ratio. The mixes were used in flexural and slant shear tests to test the effect of mixing speed and curing temperature on the strength of the mix. Mixes E2 and E4 were essentially the same except that Mix E4 included nano-aluminosilicate material. Mix E3 had the lowest silica/alumina ratio while Mix E1 had the highest.

This iteration of this mix design required the use of many tests and as many variables. It is out of the scope of this chapter to deal with all of them. However, the measured mechanical properties of the material and all their related details are found in Chapter 4.

The details of the slant shear tests comparing inorganic and organic alternatives are shown in Chapter 5. Durability testing including test setup, procedure and results are given in Chapter 6.

The results of the mix designs are shown in Figure 3-7. This chart combines the results of the flexural tests, slant shear tests, freeze/thaw durability and wetting durability tests. As can be seen, Mix E1 performs the best overall. In flexure, Mix E1 was the best and Mix E2 was the lowest. This supports the theory that decreased silica/alumina ratio means decreased strength. Some of the strength was regained in Mix E3. E3 had the lowest silica/alumina ratio. This also concurs with observations made that the decrease in strength may be asymptotic. However, in slant shear, the lowest strength was found in Mix E3. An interesting observation is made with respect to freeze/thaw durability. First, a brief description is given about the duration of the freeze/thaw cycles. One freeze/thaw cycle was completed every 24 hours with five such cycles occurring in a week. The freeze/thaw adhesion tests were performed after every five cycles and continued for a total of 30 cycles or 6 weeks. During this time, the data suggests that no distinct advantage or disadvantage could be inferred to any mix or other variable. Looking closely, slight differences were detectible such as the fact that the lower silica/alumina ratio mixes were outpacing the higher ratio mixes by a fraction. The wetting durability tests again favored Mix E4 and the worst performing mix was E3. Mix E1 was the second best followed by E2. In both the durability tests, the mix with the nano-aluminosilicate material appeared to give an advantage over the other mixes. However, since Mix E1 performed well in all categories, it is favored over all the rest and is the recommended mix for the full scale and injection testing.

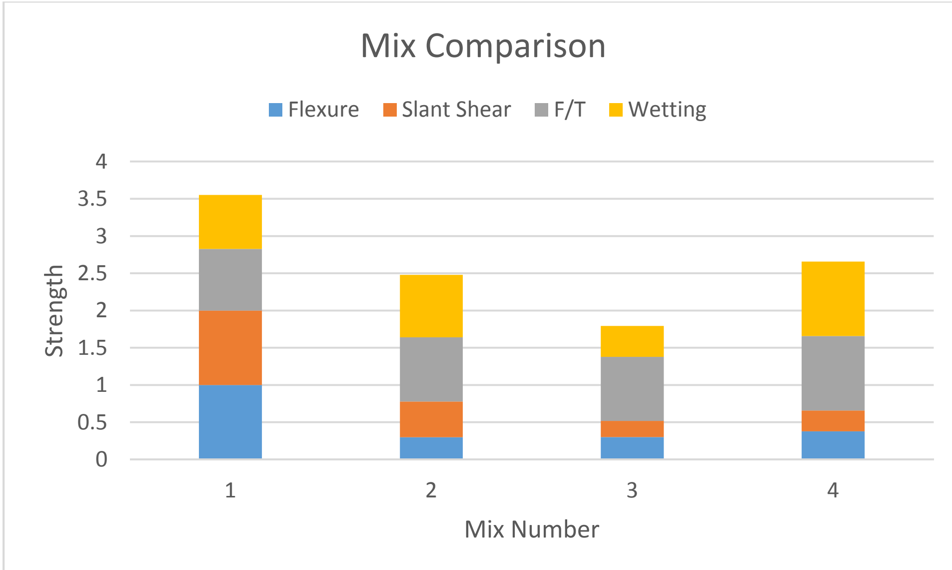

Figure 3-7: Mix Group E Results

In the comparison of mixer speed and curing temperature on the strength and durability of the coating, no distinct advantage is given by either alternative. It was hoped that the higher speed mixer would allow for more surface area reactant by breaking the weak molecular bonds that form as a result of clumping. In addition, past research showed that curing the inorganic matrix at higher temperatures resulted in stronger mixes. Nonetheless, the addition of the zinc activator allowed for true room temperature curing. The results of both processing variables are shown in Figure 3-8 and Figure 3-9.

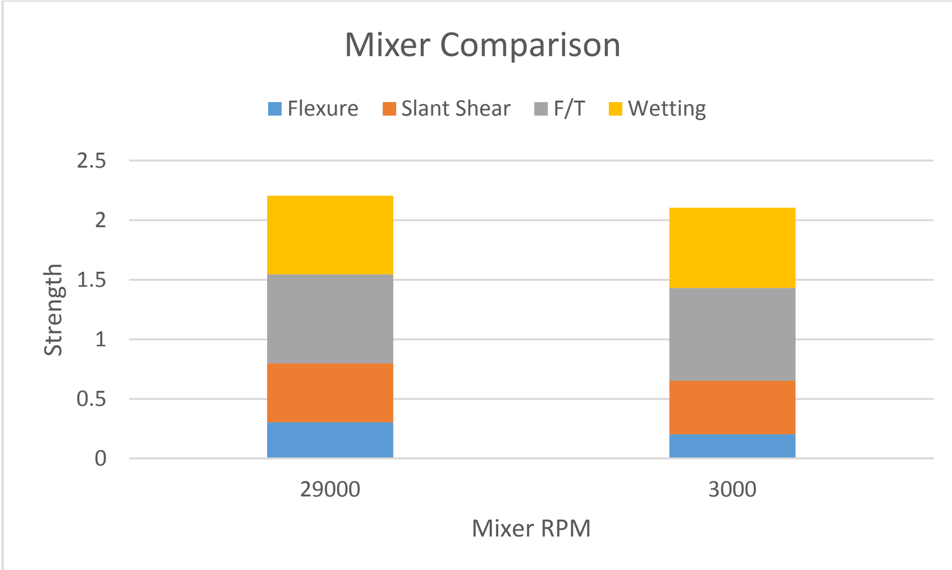

Figure 3-8: Mixer Speed Results

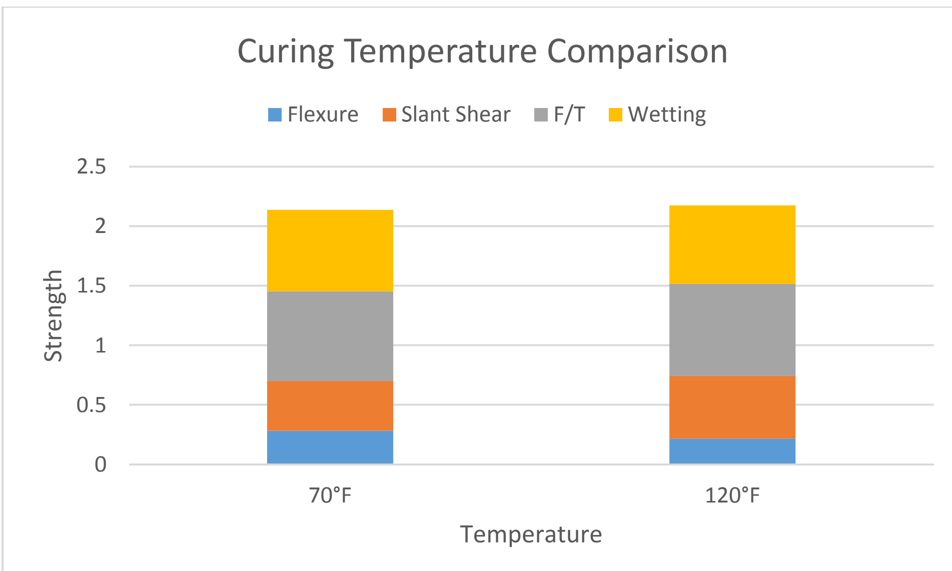

Figure 3-9: Curing Temperature Results

Since neither processing variable provides a major advantage over the other, it is recommended to use the 3000 RPM mixer and room temperature curing in the use of Mix E1. In observing the 29000 RPM mixer, it was noted that the mix pot life of the inorganic material was greatly reduced due to the high temperature caused by the rotating blades. In addition, since the mix is to be eventually injected into concrete structural elements where it would be impossible to raise the temperature for curing, the conclusion that sufficient strengths and durabilities can be obtained by curing at room or ambient summer temperatures.

3.3 Part 2: Flow Tests

The flow tests that contributed to mix design were a part of the early development of the injection mix. The mixes used for the first flow tests were modified from the basic inorganic coating mix (Group B) with normal silica/alumina ratio yet without the use of any filler. The tests were conducted to determine if the mix would flow over concrete surfaces and to observe the effect of increasing or decreasing water requirements. Additionally, the use of an admixture to increase flow was investigated. The results of the tests lead to the confirmation of the initial applicability tests – that the coating mix can be adapted for use as in injection mix.

The second set of flowability tests were used to verify compatibility with existing crack injection systems. Instead of specifying new equipment that would have to be built or modified, an investigation was undertaken to test the material for compatibility with the most commonly used injection pumps and interface equipment. In addition, the study would allow the comparison of the equipment and selection of the most effective alternative. Since these tests were conducted at the end of the mixture proportion selection, only one mix was used: Group E1 mix. Recall that this mix is the one that was shown to be the most applicable for concrete repair.

For the flow tests, a total of three mix designs were presented and summarized in Table 3-1. These mixes varied in terms of liquid content and special flowability admixtures to decrease viscosity. Mix 1 featured a plasticizing-type admixture. Mix 2 was the same as Mix 1, except without the admixture. Mix 3 featured a decrease in liquid content. Additional mixes were not required since the powder material ratios do not affect the viscosity of the repair material.

Mix #	Composition
Mix 1	Viscosity Admixture
Mix 2	Normal Mix
Mix 3	Lower Liquid Content

Table 3-1: Summary of Flow Test Mix Composition

3.3.1 Flow Tests in Narrow Channels

The flow test designed for this research was developed exclusively for the repair material though the concept is simple. Since the repair material is designed to repair concrete, the flowability or the ability of the repair material to infiltrate very small cracks should be verified. At room temperature and during the application phase of curing, the repair material is known to have a viscosity of about 400 to 500 cP. Since the diameters of the particles involved in the inorganic repair material are on the nano-scale, the crack size is not the limiting factor in checking flow through small cracks. In an effort to quantify some of the fluid properties of the repair material such as the flow rate, a series of tests were developed to observe and assess the behavior of the material through a small, crack-like channel.

The channel is constructed out of a concrete plate, capped with a cast acrylic sheet and sealed with silicone caulk. The dimensions of the concrete plate are twelve inches square by ¼ inch thick. The concrete plate was cast using a mortar mix and then the surface was cleaned and roughened using muriatic acid. The cast acrylic sheet featured the same dimensions as the concrete plate. The width of the channels were delimited using the silicone sealer at three inch intervals to create four channels per plate. The plate and sheet combination was mechanically fastened using screws in each corner after the sealant was placed to form a water-tight seal against the two surfaces. At the end of each channel, a hole was drilled through the acrylic for the introduction of the repair material and to allow air to escape.

Several methods were used to drive the repair material into the crack. This included allowing the material to flow under its own head, using a simple hand-driven piston displacement system, and a powered diaphragm pump. The method using the weight of the material to flow through the channel involved a funnel that rested in the input opening and then filling the funnel with the repair material. The hand-driven system utilized the same funnel for flowing under its own head, but with a rod that was the same diameter as the conduit on the bottom of the funnel, where the rod was passed through the material in the cone and then forced it into the channel by way of the conduit affixed to the bottom of the cone portion of the funnel. The last method involved a pump connected to the specimen using friction-fit piping and a NPT thread fitted into the hole on the acrylic sheet. The pump would vacuum the material from a container and pump it into the channel.

A high-definition video camera was mounted over the test panel to video the movement of the liquid through the channel. The frame rate is 30 fps at 720p resolution and a scale is given next to each channel. Since the width and depth of the channel is fixed, the flow rate can be found as the material moves from one side to the other.

In addition, a pressure gauge installed on the diaphragm pump system provides real-time measurement of the pressure required to move the material through the channel. Finally, the hand-driven piston arrangement gives qualitative feedback on the behavior of the material as it flows over the concrete plate.

3.3.2 Sample Preparation

In order to investigate the properties of repair matrix, three different test specimens were prepared and tested. Figure 3-10 shows the flow test setup that was developed in this study. A narrow gap between acrylic and slab was designed to be adjustable from 1/32 inch to 1/4 inch, so that the repair material flow can be easily observed at different thicknesses and provide better understanding the material flow pattern in narrow cracks.

Figure 3-10: Flow Test Setup

3.3.3 Results and Discussions

The flow capabilities and the ease of application of repair materials were studied using flow test setup discussed above. The matrix is placed in a funnel, which assists in flowing of the matrix between the narrow gap of slab and plexiglass. If the material is pure workable, it should flow by it’s self-weight as shown in Figure 3-11. It was observed that among the three mixtures that were prepared, only mix 2 demonstrated this type of flowing behavior.

Figure 3-11: Filling the Channel by Gravity

The other two mixtures (Mix 1 and Mix 3) required external pressure to fill the narrow gap between the plate and acrylic. In the first case, a vacuum was applied to the opposite end to fill the space as shown in Figure 3-12. It was observed that vacuum generated voids in the repair material. Using a vacuum to fill the void is important because some cracks in concrete are so delicate that if any pressure were applied to the two surfaces, the concrete would be in danger of further degradation by spalling.

Figure 3-12: Vacuum used to Fill Channel

As an alternative to vacuuming, a positive displacement pump as shown in Figure 3-13 was employed to fill the channel with repair material. It was noticed that pressure pumping also generated voids in the matrix during the injection. From the understanding of material flow from these experiments, an alternative and promising procedure was identified that can displace the matrix without any integrity issues. A simple piston mechanism was introduced to the system and was found to have the properties required for suitable injection pumping. It is recommended that future injection systems utilize a piston pump with an overhead hopper to eliminate air voids created when priming the pump.

Figure 3-13: Diaphragm Pump Injection

When each test was performed with the inorganic matrix, a control test was initiated using only water. That way the test apparatus could be tested for leaks and also provide a baseline with which to compare the flow of the repair matrix. The table below shows the comparison of the water control tests with respect to the flow rate. In addition, the table summarizes which mixtures were used with which test.

Test #	Mix #	Type of Test	Flow Rate Ratio[1]
1	Mix 1	Vacuum	5.00%
2	Mix 2	Gravity	7.60%
3	Mix 3	Gravity	3.90%
4	Mix 2	Pump	48.00%

Table 3-2: Summary of Slab/Plexiglass Results

As can be seen in Table 3-2, Mix 2 provided better flowability when acting under its own head. The best results obviously came when the material was injected using a pump. The tests proved that the material is well suited to injection due to the proper liquid content and application of a positive displacement piston-type pump.

3.3.4 Injection Systems

The second flowability tests dealt with compatibility with injections systems. In order to test the injection systems, cracked concrete was required. Commercially available 12 inch by 12 inch square by 2 inch thick concrete pavers were used. The pavers were broken into two pieces creating the crack. By constraining the physical borders at set distances, the width of the crack could be controlled and the injection interface can be installed. In addition, with visual access to the top and the bottom of the paver during the injection

[1]This is the ratio comparing the flow rate of the water control test and the test rates for the repair material. For Tests 1 through 3, the water flowed under its own head and for Test 4, the water was pumped through a diaphragm pump.

process, the procedure can be monitored to give a sense of the quality of the injection repair. For this purpose, a special repair paver repair table was constructed.

To test the pavers two injection systems were used; the Seal Boss Concrete Solutions P3003 and the UMETA Lever Grease Gun. The P3003 is a lightweight two-component pump powered by a Bosch drill capable of pressures up to 5000 psi. The advantage of using the P3003 is the ability to have the injection material gravity feed into the piston pump. While the machine features two component chambers, by closing a valve, only one component chamber is required. The Lever Grease Gun is a hand pump with an extension delivering 0.06 ounces per stroke. Another advantage of the Lever Grease Gun is that control of the pumping rate and pressure is controlled by the operator.

Packers, zerks, and couplers provide the interface between the pumps and pavers. The types of packers that were tested were the plastic hammer-in type, the aluminum-rubber 13-100AL, the brass-rubber 10-60-3B, and the steel-rubber 13-60S. The plastic hammer-in packer is 3/8" in diameter. The 13-100AL packer is ½ inch wide and 4 inches long. The 10-60-3B Packer is 3/8 inch wide and 2-3/8 inches long. The 13-60S packer is ½ inch wide and 2-3/4 inch long. The rubber type packers are considered mechanical packers because they feature a rubber gasket that can be expanded against the concrete hole to provide a seal against repair material leakage. The hammer-in type packers seal against leakage by the tapered shaft which friction fits against the concrete hole. Each mechanical packer featured zerk fittings which are spring loaded ball bearings built-in for one direction injection. Also tested was a plastic injection surface port which had four holes for mounting to the surface of the paver straddling the crack with masonry screws. However, the typical and faster procedure is to use a clear epoxy to adhere it to the concrete. The plastic fittings allowed for two types of coupling systems: a slide zerk coupler and a snap-in zerk coupler that could be screwed into the plastic heads on the surface mounted port and the hammer-in packer. Examples of each fitting are shown in Figure 3-14.

Figure 3-14: From left to right - Surface Mount with Zerk, Mechanical Packer, Polyethylene Packer

3.3.5 Rapid Repair Paver Table

An injection jig was designed to hold three pavers for repairs, be easily accessible and feature a clear table and side for viewing the paver during the repair from all angles (see Figure 3-15). The frame of the jig was made out of extruded aluminum T-channel bars. The four legs of the table were 30 inches long as a standard working height. Braces were added at each corner to provide rigidity for the slender legs. The top of the table was made of 1 inch thick cast acrylic sheeting for clear viewing. The average dimensions of the pavers were measured to be 2-3/8 inches tall and 11-7/8 inches square. The cast acrylic paver side holders have the same heights but different lengths at a minimum of 12 inches. The length was chosen so that the paver could be inserted without binding and then shimmed into position. The spacing of the holders are 12-1/32 inches, 12-1/16 inches, and 12-3/16 inches to accommodate the different size cracks and room for shims. Under each paver a notched 8 inch square opening was created to mate with a reverse notched insert. The disposable insert allows for easy exchange of the paver before and after testing by pressing the paver out from below.

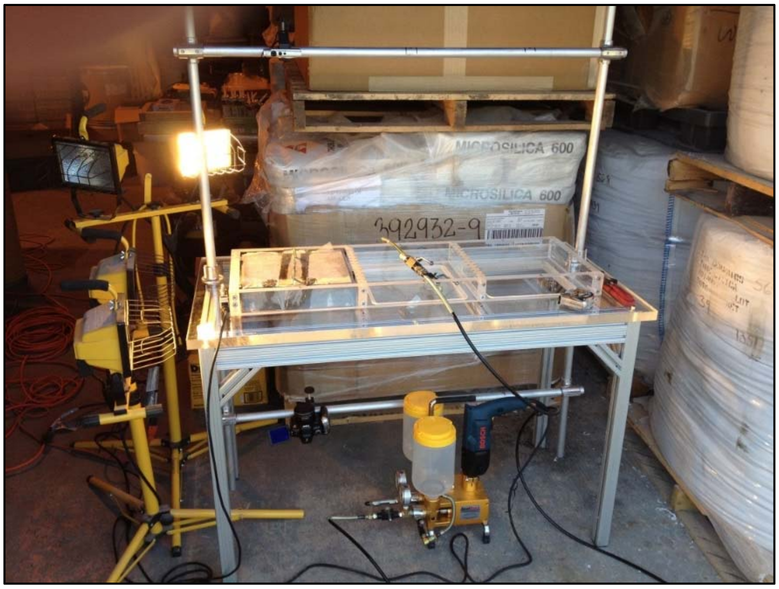

Figure 3-15: Rapid Paver Repair Table

Because the tests were performed each day and time was not allowed for data collection, the table was outfitted with mounts for video recording above and below the paver. The permanent record would then be available for review and analysis. The mounts were fastened to a horizontal aluminum bar above and below the table with vertical aluminum side bars bolted to the top and bottom of the table. The rails were adjustable to allow for optimal placement of the digital camera as shown in Figure 3-16.

Figure 3-16: Top and Bottom Results of a Paver Test

3.3.6 Repair Methodology/Theory

The function of the rapid paver repair table was to provide rapid and repeatable repairs for testing multiple scenarios of the injection systems. After the pavers were broken in half, they would be fitted with holes for the packer if required. If the paver was to be tested with a packer, they would be placed into a specially sized wooden jig based on the tested crack size. Then the paver would be wrapped on the sides and bottom with clear polyethylene sheeting to contain the liquid repair material. Next they would be placed on acrylic inserts that fit into the surface of the table and lowered into place in one of the three different sized paver holders. The paver holders are sized to 3/16 inch, 1/16 inch and 1/32 inch cracks. Once in place, acrylic covers featuring holes for the injection port placement were installed to seal the top of the crack. Two fittings for each paver were provided, placed two inches from the edge of the paver and centered on the crack. The injection testing is performed after a minimum of 24 hours to allow the sealant to cure.

The pumps are prepared by attaching the proper injection probe for the type of zerk coupling. Once the repair material was mixed it would be loaded into the appropriate injection pumping system. Then the pump is operated according to its individual operating instruction until the crack is filled halfway across. The injection probe is then switched to the other fitting and the procedure repeated until the crack is completely filled. After filling all three sized cracks and recording the results, the pavers would be discarded, the repair table would be cleaned from any spilled or leaked repair material and the pavers would be prepared for the next day's test.

A successful repair was based on flow, leakage, and injection removal. Test variables recorded were whether the pressure based injector pumps exceeded pressure specifications, whether the probe, coupler, packer or injector leaked, whether there was a solid and consistent flow of material, whether the injector probe easily connected and disconnected from the zerk coupling, and whether the crack was completely filled.

3.3.7 Results

In total, 42 tests were performed; 21 with the hand pump and 21 with the gravity-fed piston pump. Each of three packers were tested with each pump as well as the two plastic hammer-in packer and the surface mounted injection port. The plastic version were tested with both the slide-on zerk fitting and the snap-in zerk fitting. The results are designated as passed, semi-passed, or failed. A "passed" test meant all parameters were satisfied for injection, “semi-passed” was defined as passing one or more criteria and failing one or more criteria, and “failed” meant that all criteria were not reached. Out of the 42 paver tests, 19 scenarios passed the injection test while 13 semi-passed, and 10 failed completely. Since the mix design evolution had identified Mix E1 as a suitable mix, it was the only mix tested.

The P3003 injection system had no complete failures in any of its 21 injection tests. The hand pump had issues in 6 of its 21 injection tests. The reason for these issues was due to the fact that the pump was difficult to maintain in its optimal orientation during operation of the pumping lever. The P3003 injection system was more effective and efficient because once the connections were made, the injection probe would not move.

The fitting type was the issue for 19 of the 23 injection tests that did not pass. Each fitting type had three tests with the Hand Pump and three tests with the P3003 Pump. The snap-in zerk, when used with the hammer-in packer, failed to release from the hand pump during one injection test and leaked during the another one. The hammer-in packer leaked twice, once with the hand pump and once with the P3003 pump. The slip-on fitting failed to release from the hand pump during one injection test with the hand pump and leaked during a test with the P3003 pump. The 1/2 inch by 4 inch packer would not allow any mix to enter the cracks during three injections tests with the hand pump but worked perfectly with the P3003 pump. The 1/2 inch by 2-3/4 inch packer clogged immediately with the P3003 pump but flowed decently with the hand pump. The 3/8 inch packer worked well with the hand pump but built up too high of a pressure with the P3003 pump. The surface mount only had an issue with the slide-on zerk while tested with the hand pump.

In summary, the inorganic repair mix worked well for injection without any special admixture, filler or additive just as the tests in narrow channels showed. The mix flowed without difficulty in the smallest cracks (1/32 inch) and completely filled the void. Pressures were within specifications for keeping the surrounding concrete from being damaged further. The leakage problems were most likely caused by operator error and inexperience including difficulty engaging and disengaging the probe from the coupler. It is recommended that the P3003 injection pump be used for large volumes but the hand pump would be sufficient for smaller cracks provided the operator was experienced enough to manage the task with steadily. The surface mounted port paired with the slide-on zerk fitting provides the quickest and most direct way to introduce the repair mix to shallow vertical cracks. The 4 inch 13-100AL or equivalent is recommended for deeper cracks. While crack blockage was not a problem with these particular tests, a drill with vacuum should be used to provide the necessary clearances for the hammer-in or friction-fit packers so that the dust created by drilling will not block the crack cavity or dilute the mix. Finally, the rapid paver repair table performed well by providing a means to efficiently repair several size cracked concrete pavers simultaneously while providing 360° monitoring feedback and video recording to test the multiple combinations of injector equipment.

3.4 Summary

The mix design evolution to give the final recommended mix is summarized by the following:

- Group A mixes (preliminary) demonstrated that the inorganic coating/adhesive previously designed at Rutgers University could be used for injection and repair through the use of repaired splitting tensile tests. Mix A2 demonstrated the amount of liquid can be reduced to increase strength and still meet flowability requirements.

- Group B mixes were considered the first official iteration of the repair mix where several systems were compared including Mix A2. Using repaired flexural tests and direct shear tests, the best performing mix was identified as Mix B1. Mix B3 (magnesium phosphate) performed the worst.
- Group C mixes featured enhancements to the Group B mixes and by the use of zinc oxide activators and Mix C4 provided the best overall strength results in repaired flexural tests and direct shear tests.
- Group D mixes represented the effort to optimize the amount of the zinc oxide activator in Mix C4. Mix D6 was identified as the best performing mix in terms of both repaired flexural tests and slant shear tests. The use of a more pure source for an aluminosilicate component provided notable results.
- Group E mixes signaled the final effort in the mix design evolution. The main purpose was to vary the silica/alumina ratio to optimize the Mix D6 for both durability and strength. The tests included repaired flexural tests, slant shear tests, freeze/thaw durability and wetting durability tests. The final recommended mix was identified as Mix E1 with standard silica/alumina ratio and optimized zinc oxide activator.

The following general observations were made with respect to the mix design:

- Nano-materials can enhance the properties of the mix but at increased cost. The small gain in benefits was not necessarily worth the added expense.

- The speed of the mixer has little influence on the strength and durability of the repair mix. The 29000 rpm mixer is not recommended due to the increase in heat during the mixing process.
- In the final Group E mixes with the zinc oxide activator and more pure aluminosilicate source, sufficient strengths and durabilities are reached when the mix is cured at room temperature.

Flow tests in narrow channels resulted in the following comments:

- The use of alcohol based admixtures for decreased viscosity is not recommended due to the segregation of the mix.
- The use of regular amounts of liquid provide enough workability for the mix to flow in a horizontal channel under its own hydraulic head.
- The mix is well suited for use in positive displacement type pumps.

The injection tests used to repair concrete pavers produced the following remarks:

- The repair mix can sufficiently infiltrate cracks to 1/32 inch.
- Commercially available injection systems are compatible with the inorganic repair mix. The use of a gravity fed piston pump such as the SealBoss P3003 is recommended.
- The use of a rapid paver repair table allowed for controlled repair results for dozens of injection equipment combinations to identify the uses and most relevant systems.

- The surface mounted injection port paired with a slide-on zerk fitting is recommended for shallow vertical or surface cracks. A deeper penetrating (up to 4 inches) is recommended for deeper cracks or cracks with surface obstructions.

CHAPTER 4 - MECHANICAL PROPERTIES OF THE COMPOSITE

4.1 Introduction

The mechanical properties of the inorganic repair material are important because the concept is to provide a homogeneous repair to the concrete. The mechanical properties of the repair material were used extensively to determine the final mix design. While many of the mechanical properties have been previously studied, the properties with respect to concrete repair have not (Foden 1999). It is the purpose of this chapter to explore the relevant tests and provide a guideline for testing future materials for concrete repair. In addition, the values for the properties will be discussed and presented.

The properties that have already been tested are tensile and compressive stress, tensile and strain capacity, static and dynamic modulus of elasticity, shear modulus, Poisson's ratio and the flexural parameters. While these are important for understanding the stand-alone material, they tell us relatively little about the ability of the epoxy to function as a concrete repair material. In order to test the repair of the concrete, the repair material must be tested in the condition where the concrete has been repaired. All of the tests presented involve adhering concrete pieces together and investigating the integrity of the crack. To provide uniform material preparation, ASTM standards were consulted and used when possible. From the results of these tests, a baseline of the original concrete conditions were documented. Then the parts were used to create a new test to compare to the initial conditions by affixing them together using the repair material.

Since the results of the repaired tests were discussed in Chapter 3 with respect to the development of the aluminosilicate epoxy, they will not be covered again in this chapter.

Rather, a discussion of the relevance of each test, the initial and repaired preparation of the samples and the mechanical properties of the final mix design are summarized. Four tests were utilized throughout the study which are the splitting tensile repair test, flexural repair tests, direct shear tests and slant shear tests.

4.2 Splitting Tensile Repair Tests

The splitting tensile test was adapted from ASTM C496, Standard Test Method for Splitting Tensile Strength of Cylindrical Concrete Specimens. The procedure consists of performing the standardized test to split a concrete test specimen in half and then repair the fracture using the repair material. The test is performed a second time to find the integrity of the repair (Figure 4-1).

Figure 4-1: Splitting Tensile Test

The splitting tensile test was used initially to find whether the initial aluminosilicate formulation could be a good candidate for concrete repair. Group A mixes were tested by this method. The mixes featured a moderate silica to alumina ratio for strength. The mixtures included several fillers and iron oxide added for color distinction. One mix (A1) included a higher than normal water proportion to aid in crack filling.

The specimen required for the splitting tensile test was a 6 inch by 12 inch concrete cylinder. The specified strength for the concrete mix was 4,000 psi and the 28-day strength of the compression cylinders was 3,500 psi. Since the specimens had to be tested destructively in order to be repaired, 3/8 inch stone was used to ensure that the repair planes would fit back together again with minimal roughness. The concrete for the specimens was provided by Accurate Concrete Incorporated of South Amboy. The concrete was mixed on site in a special volumetric concrete mixer which batched the concrete on the truck. The cylinders were cast according to ASTM C31 Standard Practice for Making and Curing Concrete Test Specimens in the Field. The specimens were field cured. The original splitting tension tests were performed at 28-day strength using a 400 kip Tinius Olsen compression machine. The average splitting tensile strength of the specimens was 475 psi. This is slightly higher than the expected $7.5\sqrt{f'_c}$ of 445 psi. The splitting tensile specimens did not break in a clean, 2-piece, single plane but rather broke into four main pieces. At the top and the bottom, the specimen separated into two v-shaped portions after which the remaining segment separated into two halves.

The splitting tensile test repair was performed using a mix from Group A Mix 1. The matrix was applied to all sides of the four main pieces and loaded into the splitting tensile test repair jig. Since the mix flows and has low viscosity, all surfaces had to be as horizontal as possible. The repair jig consisted of a bottom and two sides to allow the specimen to be transported and stay in the correct orientation for repair. The specimens were loaded into the jig with the long axis horizontal as well. The sides of the jig prevent rolling and are taller than the diameter of the cylinder to allow a second cylinder to be placed on top and hold the repaired sections in place. The repaired specimen was cured for a minimum of 7 days.

The repair was tested using the same 400 kip Tinius Olsen compression machine with all the same procedures followed for the splitting tensile test including keeping the specimen in the same orientation as it was when it was originally tested. The repaired tensile strength was 20 psi. This is about 5% of the original strength of the specimen and only about 4% of the specified tensile strength of the aluminosilicate material.

There were several problems with the splitting tensile test so it was omitted from further testing. The first was the original failure mode. The specimen split into several pieces instead of forming a single failure plane. The material viscosity was low enough that the repair material was difficult to keep collected in the failure plane. It would spill out of the edges and not fill 100% of the voids so that after the test, only about 3 to 5% of the repaired surfaces were rebonded. If the tensile stress is adjusted for this fact, the estimated splitting tensile strength would be about 400 to 667 psi which is well in the ranges found by previous testing. The final objection to the splitting tensile repair test is that the tensile properties of the aluminosilicate material are already known and documented, therefore splitting tensile repair tests are considered unnecessary and do not yield data relevant to bridge deck delamination repair.

4.3 Flexural Repair Tests

The bulk of the repair material formulation adjustment came from three tests: flexural repair tests, direct shear tests and slant shear tests. The flexural repair tests were used to find the repair value of the inorganic matrix and also to test the compatibility of the matrix with the concrete. Flexural repair tests were conducted by creating concrete flexural repair specimens using ASTM standards and testing them to failure (Figure 4-2). Then the separated flexural test specimens were reattached using the repair material. Once the specified curing had been accomplished, the specimens are retested for the percentage of the original strength retained during the repair.

Figure 4-2: Flexural Repair Test

Two sets of flexural repair specimens were fabricated for this test. The first had 4 inch by 4 inch by 14 inch dimensions while the other set was scaled down to 3 inch by 3 inch by 11 inch dimensions. The second set of dimensions allowed more specimens to be cast at one time and were appropriate for use because the same results were obtained for either size.

The first set of flexural test specimens (4 inch) were made using self-compacting concrete so that a vibrator would not have to be used to consolidate the concrete during casting**Invalid source specified.**. The mix proportions were 816.75 lb/yd^3 Type 1 cement, 227.61 lb/yd^3 fly ash, 1647 lb/yd^3 sand, 945 lb/yd^3 3/8 stone, 424.71 lb/yd^3 water and 1.14% superplastisizer. The cement was provided by Lafarge North America's cement manufacturing plant in Whitehall, PA. The aggregates were provided by Weldon Material's Watchung Quarry in Watchung, NJ. The formwork was custom built from #2 Ponderosa 3/4 inch thick material to allow for simultaneous casting of 42 specimens at one time. The materials for the formwork were supplied by Tulnoy Lumber in Carteret, NJ. After 24 hours of the initial curing, the specimens were removed from their formwork and standard cured in a fog room.

The tests for flexure were executed by following the ASTM C78 Standard Test Method for Flexural Strength of Concrete (Using Simple Beam with Third-Point Loading). The initial tests were performed using the Forney 1,000 kip compression machine, a custom third-point bending jig and a 10 kip USB LoadStar load cell. The average modulus of rupture for the specimens was 840 psi and the compression strength of the concrete was 5,500 psi.

The mixes tested using the 4 inch flexural repair tests were Group B and Group C mixes. The discussion of these mixes and their results can be found in Chapter 3. The results from these tests not only established the basic modulus of rupture of the inorganic material but also helped to identify suitable mix designs for concrete repair.

Once the flexural tests were prepared for repair by the initial destructive test, they were rejoined together using the inorganic material. The material was mixed in a high shear mixer and applied to each face of the flexural repair sample using a brush. Each sample was cured according to the mix design and requirements. The cured flexural specimens were tested using the same set-up as the initial flexural tests.

The only mix that is discussed here is the mix that resulted in the final design. Mix C4 had an average modulus of rupture of 475 psi. The Group B Mix 4 had a modulus of rupture of 114 psi but when the zinc oxide activator was added, the strength increased by nearly 400%. The magnesium phosphate systems performed the worst with an average modulus of rupture of 97 psi for the Group B mix and 24 psi for the Group C mix.

Since there were 10 Group D mixes, many more flexural samples were required for testing. This lead to the change in cross-section and length for use in the computer controlled MTS Sintech 10/GL. Note that the ASTM C78 and referenced ASTM C31 allow those dimensions for flexural specimens as long as the width and depth is three times greater than the nominal maximum size coarse aggregate. Since the aggregate used in these tests are 3/8 inch, the specification is satisfied and applicable. The change in dimension allowed for over two times as many flexural specimens to be cast from the same volume of concrete.

The second set of flexural test specimens (3 inch) were made using normal strength concrete. The mix proportions were 802 lb/yd^3 Type 1 cement, 1,408 lb/yd^3 sand, 1,312 lb/yd^3 3/8 inch stone, and 318 lb/yd^3 water. The materials were all provided by the same suppliers as the 4 inch beams. The formwork was custom built from #2 SPF 3/4 inch thick material to allow for simultaneous casting of 80 specimens at one time as shown in Figure 4-3. After a minimum of 24 hours of the initial curing, the specimens were removed from their formwork, identified and standard cured in a fog room.


Figure 4-3: Flexural Specimen Forms

The tests were also performed using ASTM C78. Both initial and repaired flexural tests were performed on the MTS Sintech 10/GL at a loading rate of 0.02 inches per minute and using a custom built third-point bending jig. The average modulus of rupture for the initial tests were 1,060 psi. This is higher than the 4 inch beams but the compression strength of the 3 inch beams were also higher (6,660 psi).

Again, since the only relevant value is the one that relates to the final mix, only the modulus of rupture for Mix D6 is given. The modulus of rupture was 760 psi which is almost double the value found in the previous iteration (Group C Mix 4). In several of the tests, the beam broke in a different location than the initial break. This indicated that the repair material at least as strong as the concrete. Given that flexural failures do not account for the entire strength of the specimen but rather fail based on defects in the concrete, the concrete was probably weakened during the initial failure loading of the beam.

4.4 Direct Shear Tests

Direct shear tests provided a first look at the shear capacity of the repair material. They were used in both Group B and Group C mix testing. The procedure is not standardized by the American Society for Standards and Materials though it was published in the American Concrete Institute Materials Journal as a new method for evaluating the shear strength in the interface between existing and new concrete (Momayez, et al. 2004).

Figure 4-4: Direct Shear Test

The procedure requires three concrete blocks to be adhered to each other with the center block offset as shown in Figure 4-4. Once the repair material has cured, the specimen can be tested in a compression machine inducing shear stresses along the two interfaces. The shear stress can be calculated using the failure load and dimensions of the shear plane. The specimens were tested in a 1,000 kip Forney compression testing machine with a 10 kip LoadStar load cell for computer data acquisition.

Materials for the direct shear tests consisted of cutting commercially available standard concrete brick into 3-5/8 inch by 2-1/4 inch by 1-1/2 inch blocks using a wet tile saw. A 3/4 inch by 4 inch wooden block was used to create the offset under the middle block during assembly. The repair material was mixed and immediately applied to just over half of the shear plane at the overlapping edge on each side. This prevented the repair material from running down the exposed face which would affect the results. After the ends were aligned and the offset established, a C-clamp held the specimen together during the specified curing.

Group C Mix 4 values are used for the nominal shear strength of the repair material. The samples all failed when one side of the bi-surface specimen failed. The average shear value for the repair material was found to be 575 psi. Note that the concrete brick shear strength, at a compressive strength of 3000 psi, is 595 psi. In fact, several of the direct shear tests included large portions of the concrete from the adjacent block embedded to the repair material after the test. This indicates that the actual shear strength may be larger for the repair material.

The direct shear test was discontinued after the formulation of the Group C mixes. This was due to the difficulty in quality control of the specimen since a standard procedure is not available. In addition, it is widely accepted that the failure is a combination of flexural and shear behavior especially in the outside blocks. The bending forces cause tension on the repair material. These forces are difficult to resolve in pure shear because the top and bottom loading planes are nearly impossible to align properly during the specimen construction. In addition, research led to the discovery of the more popular slant shear test during the interpretation of these results.

In order to improve the results of the bi-surface direct shear test, a special confining jig should be designed to counteract the bending forces. Additionally, a capping mechanism should be developed to ensure that the compression load is parallel to the shear plane.

4.5 Slant Shear Tests

Slant shear tests, ASTM C882, are the most widely used test for determining the bond strength of epoxy repaired concrete specimens (ASTM C882 2012). The bond strength is found by using the specified repair system to adhere two sections of a concrete cylinder. The dimensions of the cylinder are 6 inches tall and 3 inches in diameter. The cylinder is cut diagonally into two pieces at a 30° angle from the long axis of the cylinder. After the repair material has cured according to the specific requirements, the test is performed by compression of the repaired cylinder (see Figure 4-5).

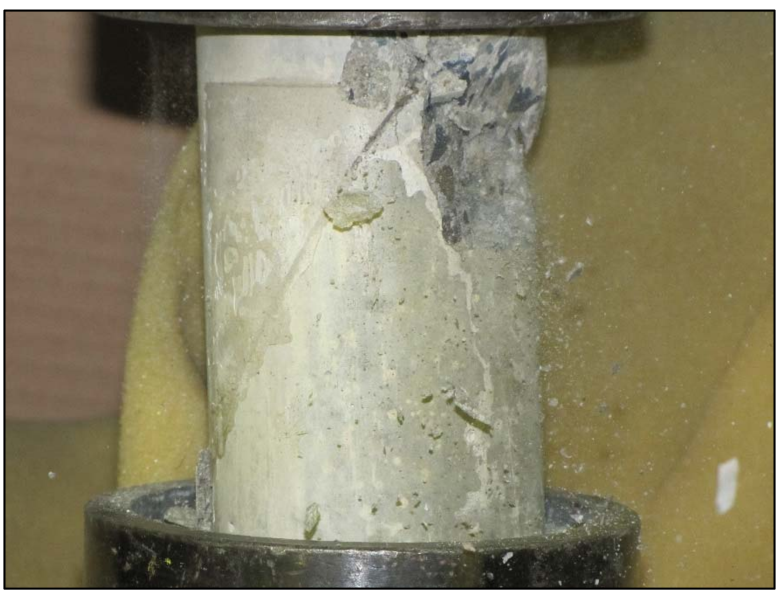

Figure 4-5: Slant Shear Test

The compressive strength of the concrete used for the slant shear specimens was found to be 6,740 psi. The mix design included 347.73 lb/yd^3 Type 1 portland cement, 167.27 lb/yd^3 water, 920.94 lb/yd^3 3/8 inch stone, and 603.63 lb/yd^3 of sand. Cylinders were removed from the molds after a minimum of 24 hours and standard cured in a fog room for a minimum of 28 days. Then the cylinders were cut using a custom 30° jig in a wet tile saw. The repair material was prepared using the standard procedure and both sides of the elliptical surface coated before mating the two halves. The freshly repaired cylinder was then placed back into the plastic cylinder mold to hold the two halves together in alignment. The cylinder molds were placed in a stand that kept the repaired surface horizontal for curing.

Once the repair material had cured sufficiently, the specimens were tested in a 1,000 kip Forney compression machine. The slant shear strength is given as the load at failure divided by the elliptical area of the repair plane. The maximum slant shear given for the Group D mixes were from Mix 10 at an average of 2,385 psi. Recall that the mix that was used in Group E formulations was the Mix 6 which had an average slant shear of about 1,100 psi. However, when the formula included the combination of zinc oxide and the pure aluminosilicate component, the slant shear jumped to 3,565 psi. Slant shear tests were also performed on commercially available structural 2-part organic epoxies (SealBoss 4040LV Epoxy Resin) and the result was very similar at 3,500 psi. This demonstrated that the inorganic epoxy compares well with commercially available alternatives.

4.6 Summary

The mechanical properties studied in this chapter are summarized as follows:

- The repaired splitting tensile test is not a very good indicator of the tensile strength of the repaired material because the original concrete cylinder does not split into two distinct halves. This makes it difficult to thoroughly repair each crack and void. The repaired splitting tensile test results, when adjusted for voids, came within the measured tensile range for inorganic aluminosilicate materials.
- The repaired flexural tests provided data on the interaction of the repair material with the concrete substrate. The test interpretation was limited due to the sudden flaw induced failure modes. The final mix flexural repair data was nearly 3/4 of the initial monolithic concrete modulus of rupture and in several failures, a new fracture plane was induced indicating that the total flexural strength available may have been reduced during the initial fracture.
- Direct shear tests gave a shear strength of 575 psi which was near the shear strength of the concrete substrate. The problems with the direct shear test are the lack of standardization and difficulty in fabricating the specimens.
- The single most revealing test for concrete repair systems is the slant shear test. The slant shear or bonding strength for the inorganic epoxy is about 3,500 psi and compares well with commercially available organic repair systems.

CHAPTER 5 - COMPARISON OF ORGANIC AND INORGANIC POLYMERS

5.1 Introduction

This chapter addresses the differences between organic and inorganic polymer systems used for concrete repair. One of the most prominent advantages to using an inorganic system for concrete repair is the lack of deterioration and compatibility with the concrete substrate since it is itself an inorganic substance. The current practice of injecting epoxy into the delaminated layer works to fill the void and provide a small amount of bonding but this solution can only last for a short time and has to be reapplied. The only way to use epoxy as a structural repair by drilling and placing steel rebar across the crack as additional reinforcement (Stratton, Alexander and Nolting, Cracked Structural Concrete Repair Through Epoxy Injection and Rebar Insertion 1978).

One of the specifications for the development of the inorganic polymer is that it should be compatible with concrete, that is, it should allow the transfer of stresses across the repaired plane. One way to measure the compatibility of the repair material is by using the modulus of elasticity. The modulus of the aluminosilicate has already been tested and is given as 1,400 ksi (Foden 1999). The modulus of a normal weight concrete is between 3,000 and 4,500 ksi. In contrast, the modulus of a commonly used structural epoxy is about 0.53 ksi (SealBoss 2012). However, the modulus of elasticity does not directly demonstrate that internal stresses will be effectively transferred across the repaired zone. Consider a low and high modulus composite. As the high modulus component is strained, more stresses are incurred while for the same stress in the low modulus component, the energy of the stresses are absorbed in the strain movement even though the lower modulus part may have a higher yield point. Therefore, the incompatibility of the composite leads to behavior as a single component – that of the higher modulus constituent.

The compatibility of the concrete and inorganic system along with the comparison of the organic epoxy is given in this chapter. The test methods shown here are an ASTM method (slant shear) used for direct comparison and two other proprietary methods designed to replicate the internal stresses found in the delaminated layer of the concrete bridge deck.

5.2 Slant Shear Compatibility

The slant shear test method is described fully in Chapter 4. Basically, two halves of a cylinder are bonded to each other using either the inorganic or organic epoxy. The repair plane is slanted at a 30° angle to allow the two halves to slide past each other when under a compressive load. The stresses induced on this angle are shear stresses and using the ultimate load at failure, the shear or slant shear strength is calculated. This test is a popular test for determining bond strength of epoxies intended for use as a concrete repair material. In Chapter 4, as an expansion on the knowledge of the mechanical properties of the inorganic material, slant shear strength was determined. In this chapter the slant shear strength for both the inorganic repair material and for a commercially available 2-part organic epoxy are shown and compared.

In a head-to-head comparison of the two alternatives, the average organic slant shear strength was about 3,497 psi. This corresponds to the published technical data for the SealBoss 4040 LV Epoxy Resin at 4,000 psi (SealBoss 2012). Recall that the average inorganic polymer strength was 3,975 psi. While the slant shear results from both repair methods are similar and does not conclude that the organic and inorganic repair materials are compatible with concrete, it does demonstrate that the inorganic material performs just as well as an organic epoxy that is commonly used in current structural repair applications. Some of the results from the slant shear tests are shown in Figure 5-1.

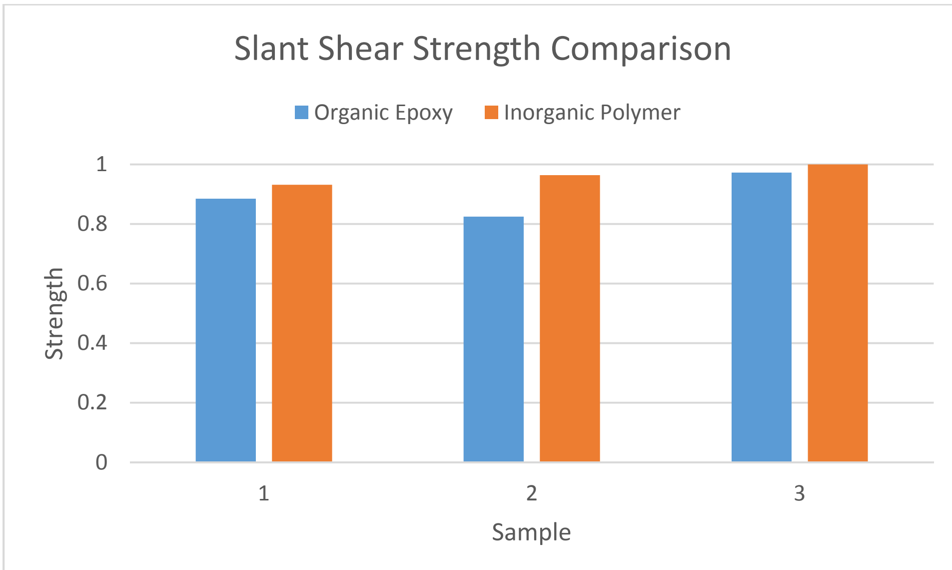

Figure 5-1: Slant Shear Results

5.3 Compatibility Tests

In order to test the idea of compatibility with concrete, the theory behind the test should be developed. The idea begins with the most common defect in concrete – cracks. Delaminations or internal cracks often occur in bridge decks due to corrosion in the reinforcing bars causing tensile stresses to the concrete and flexural loading conditions inducing shear stresses along the top mat of reinforcement. Several theories exist to explain the mechanism with which delaminations form in a concrete bridge deck. An overview of the bridge deck design and behavior is necessary to understand why the full-scale beams were designed. A typical bridge consists of vertical supports spanned by horizontal beams. The bridge deck then rests on the beams which are spaced anywhere from 2 feet to 10 feet apart. The bridge deck is usually 8 inches to 12 inches thick but can be greater if required. Typically the deck features 2 layers of reinforcement called mats and consists of 2 sets of bars oriented perpendicular to each other for transverse and longitudinal flexural loads near the outer edge of the concrete as shown in Figure 5-2.

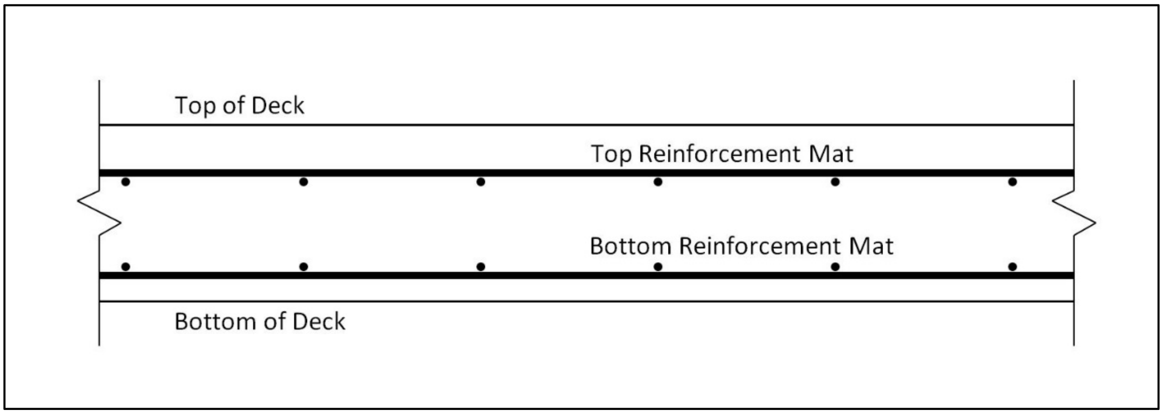

Figure 5-2: Typical Reinforcement Placement in Bridge Deck

When concrete is loaded in flexure, small flexural cracks form as a result of the transfer of tensile forces from the concrete to the steel reinforcement. In addition, when loads are applied to the superstructure, the opposing tensile and compression stresses from the ensuing flexural forces provide shear loads at or near the neutral axis (see Figure 5-3). Since the strength of concrete and steel are different, the neutral axis is not located at the mid-point as would be the case in a homogenous material but rather is located at approximately 1/5 the thickness of the deck. This location often corresponds to the depth of one of the two reinforcing mats described above. Most concrete decks are cast continuously across the supporting girders and therefore the compression and tensile inducing shear zones of the deck alternate with respect to the girder spacing. The zones located at the top surface of the bridge deck are where the maximum stresses can occur –

“compressive” shear stresses near the deck supports and “tensile” shear stresses at the midsection.

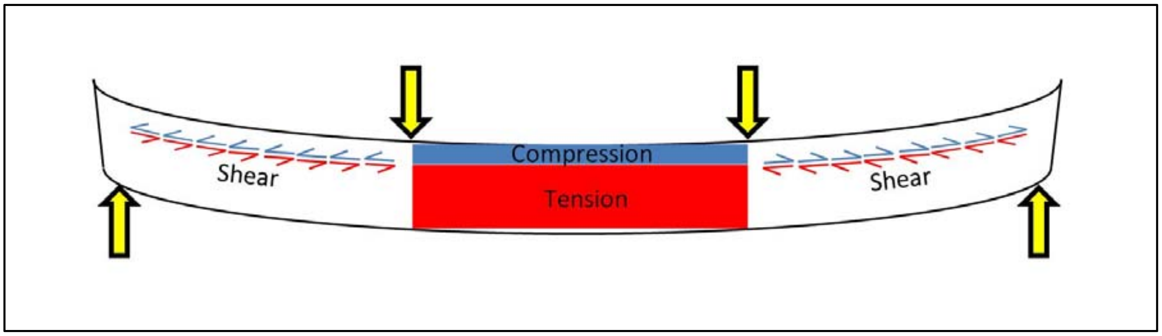

Figure 5-3: Internal Stress Distribution in Third-Point Bending

Another force contributing to bridge deck delaminations are those caused by expansion of the steel reinforcement due to corrosion. Water has been known to infiltrate the steel reinforcement by way of the flexural cracks that form during service loads. When water, oxygen and steel combine, the oxidized product forms known commonly as rust. This form of iron is known to be less dense than the parent materials thereby exerting tensile stresses in the confining concrete around the bar.

Therefore, the main stresses acting on the concrete to form delaminations, spalls, and eventually potholes, are tensile forces from corroding steel reinforcement and/or shear forces due to the neutral axis plane of the opposing compressive and tensile stresses inherent in flexural loading. This theory is also what was used to design a test set-up for determining compatibility with concrete. A beam was designed with notches at either end at the compressive reinforcement (top mat) layer (see Figure 5-4). Then blocks were cast to repair the notches to the size of a rectangular beam.

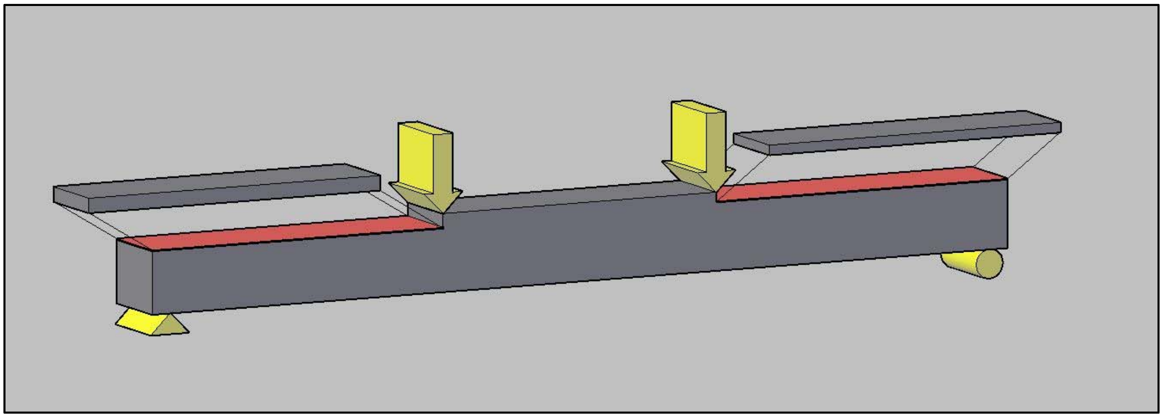

Figure 5-4: Diagram of Compatibility Beam

5.4 Prototype Beam Tests

In order to test the theory, small-scale samples were created first. This would save time and materials if the theory proved incorrect. The small-scale samples were made by cutting 4 inch square by 14 inch flexural samples to size using a tile saw. The dimensions were scaled from the proposed full-scale samples with the length fixed at 14 inches. Four prototype beams could be cut from one 4 inch square flexural beam. The concrete in the flexural samples had a compressive strength of 5,500 psi (see Chapter 4). The dimensions for the width and depth were 1-1/8 inch. The notches were 5/16 inch and 1/4 inch for the approximate neutral axis. Length of the notch was set at L/3 and was equal to 4-3/4 inches including the 1 inch overhang at the end as shown in Figure 5-5. Since the beams were created from existing concrete without internal tensile reinforcement, the beams were strengthened using carbon fibers after the notches were repaired with the carbon fibers as shown in Figure 5-6. Two tows of 35k Zoltec Panex fibers were adherred to the bottom of the beams using a 2-part epoxy. The ultimate service load was calculated to be 109.7 lb with a failure occurring by debonding of the carbon fibers.

Figure 5-5: Prototype Beams

The beams were notched and then repaired using the two types of repair compounds. The first was the inorganic Mix 4A that was the designated final mix. The second repair compound was a commercially available 2-part structural epoxy manufactured and sold by SealBoss, 4040 LV Epoxy Resin. The SealBoss resin boasts low viscosity, high modulus and non-shrinkage properties. The reported viscosity, given in the product data sheet, is about 280 cps and cures in approximately 24 hours (SealBoss 2012).

Figure 5-6: Completed Prototype Beams

The concrete plates that were attached to the beams featured the same dimensions as the notches and were cut from the same concrete as the beam. After the repaired beams were allowed to cure at room temperature for at least one week they were tested on the 10 kip MTS Sintech 10/GL compression machine as shown in Figure 5-7. The loads and deflections were recorded and used to create Figure 5-8.

Figure 5-7: Prototype Beam Test

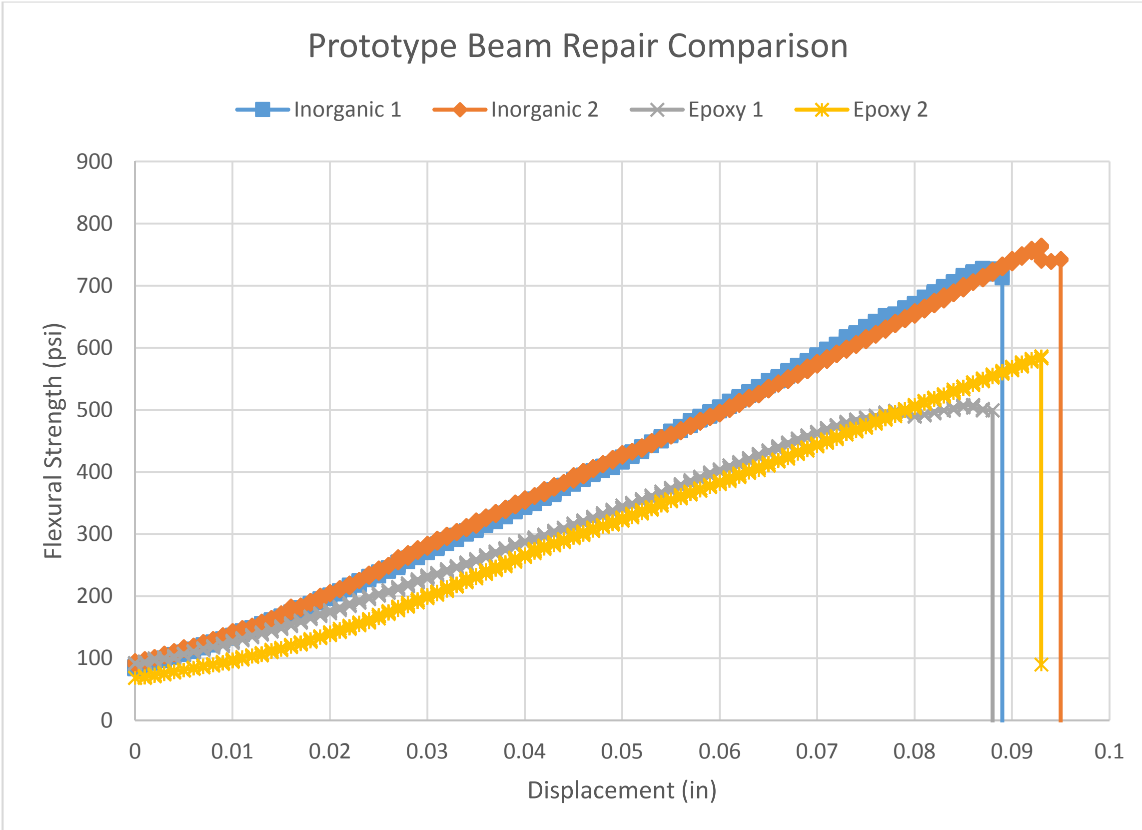

Figure 5-8: Prototype Beam Results

Several things are noticed by observation of the loading graph. First the stiffness is greater in the inorganic repaired beam and second, the load capacities are higher in the same beams. Both of these outcomes were predicted in theory. Recall that if the repair material was compatible with concrete, then it would behave as a single homogeneous beam and offer the same stiffnesses and load capacity. If the repair material could not transfer stresses across the repaired plane, the strongest the beam would act would be in the smallest dimension (the weakest limit on the beam). Hence, the lower values for the beams repaired with the organic epoxy. The beams deflected more with less load acting as a beam that could not rely on the compressive strength of the notched block repair.

The beams all failed at a similar strain and all failed due to debonding of the carbon fibers as predicted. The beams repaired with the inorganic material failed at an average of 747 psi and the beams repaired with the epoxy failed at an average of 547 psi. The average deflections were 0.09125 inches.

Another interesting observation is the fracture location of the beams. Both inorganic repair beams fracture locations occurred in the middle third of the beam as most third-point loading flexural tests usually do. The epoxy repaired beams fracture location occurred at the load point or outside of the middle third of the span as shown below in Figure 5-9. (Recall that the notches were added outside of the middle third of the span on either side).

Figure 5-9: Prototype Failures; Inorganic (left), Organic (right)

While this test procedure showed that it could be used to demonstrate compatibility with concrete by acting as a homogeneous material or as one that was notched, it could not account for the complex stresses that occur in full scale tests. As was mentioned earlier, this test was designed to show that full scale tests could be used in a similar manner. Since the prototype tests were successful, the full-scale compatibility tests could commence without significant loss of material and time.

5.5 Full-Scale Compatibility Tests

The full scale compatibility tests were designed to test the compatibility of a repair material with the concrete substrate. It was hypothesized that if the repair material were completely compatible with concrete, internal stresses would be able to be transferred across the repair plane and distributed over the entire cross-sectional area of the concrete. When concrete is used in flexural applications, tensile reinforcement is required due to the low tensile capacity of the concrete. This is because concrete works the most efficiently in compression. In a homogeneous material, where tensile and compression forces are similar, the neutral axis is always located at the middle of the beam. In concrete, steel reinforcement is added to provide the missing tensile reinforcement. Since the capacities of each material are different, the equivalent area in the concrete is greater to counteract the tensile forces in the steel in order to balance out the flexural internal stresses. However, the effective area of the concrete is only a quarter to a fifth of the total cross-sectional area of the beam. When defects occur in this compression zone, the internal stresses must concentrate around the defect and reduce the load capacity of the concrete. If a repair material is used, it should be able to bond the concrete together so that the entire load resisting area can be utilized.

Consider a slender beam that is composed of several smaller cross-sections that are not mechanically or chemically fastened to one another. If the compression zone of the concrete is removed, the stresses must redistribute to the concrete area closer to the tensile fibers reducing the moment capacity of the beam.

It is this theory that is tested by the full scale beam tests. The dimensions of the beam were chosen to accommodate current equipment at the Rutgers Civil Engineering Lab where a 600 kip beam testing machine is located. The machine is optimized for 96 inch length beams which is a common bridge girder spacing. The depth of the beam, 8 inches, was chosen as a common bridge deck thickness and the width was kept at 8 inches to give a depth to width ratio of 1. In addition, the thickness satisfies target neutral axis calculations by placing the axis between 1-1/2 to 2 inches (approximately 1/5 to 1/4 the depth of the beam). This explains the choice of the notch depth at 1-1/2 inches on one side and 2 inches on the other – so that the full range of the neutral axis can be affected and maximum shear can be applied to the repair. Elevation dimensions are shown in Figure 5-10.

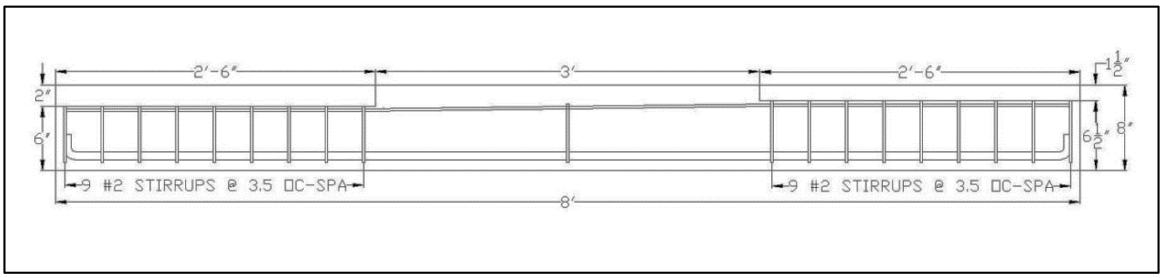

Figure 5-10: Full-Scale Beam Elevation Dimensions

As for tensile reinforcement, four #6 bars were used to create an over-reinforced design as shown in Figure 5-11. That insures that the beam will reach maximum shear in the neutral axis. In an over-reinforced beam, the ultimate failure occurs in the compression zone. The maximum load of the beam was found to be 19.17 kip at each load point (third point bending) for a total of 38.34 kip. However, since the beam is not to be tested destructively and to represent normal bridge loading condition which include respective factors of safety of the inherent error in the load and material resistance, the beam is only loaded to approximately 60% of the ultimate load corresponding to two point loads of 11.5 kip spaced at one-third the length of the beam or 23.0 kip total. This load also satisfies the cracking load which is found to be 1.61 kip, meaning that the reinforcement will be loaded during the test. Minimum shear reinforcement in the critical areas of the beam are also included and consist of #2 stirrups spaced at d/2 = 3-1/2 inches over the outside one-third of the span. The concrete shear resistance is sufficient in the center third of the beam simplifying the design and construction of the beam. Minimum concrete cover of 3/4 inch is supplied in all directions around the reinforcing steel.

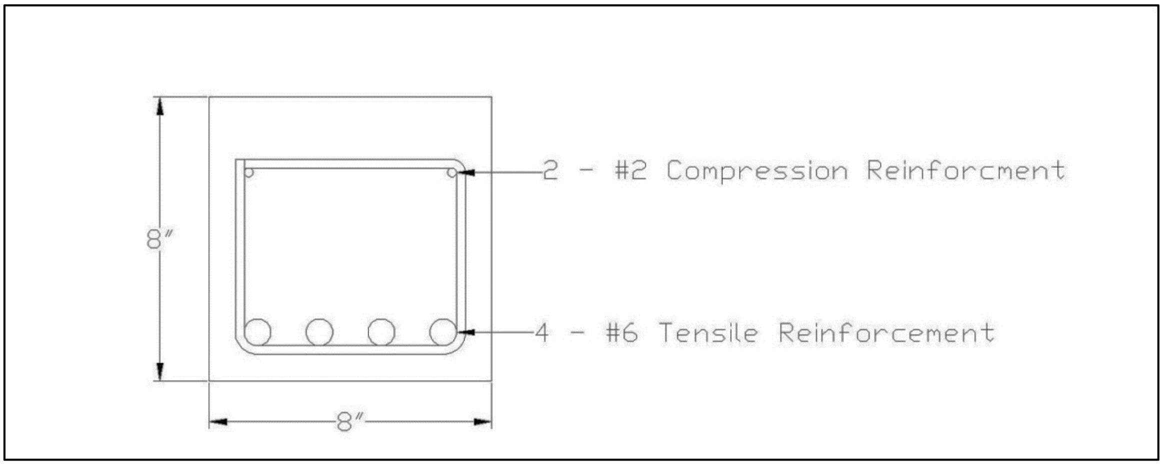

Figure 5-11: Full-Scale Beam Cross-Section Dimensions

For this test, four different types of beams are used; two beams for control, one repaired with the inorganic repair material, and one repaired with a commercially available structural epoxy rated at 4,000 psi bond strength (see Figure 5-12). The inorganic repair mix used is Mix E1, which is the suggested mix for repairing concrete defects based on the mix design testing outlined in Chapter 3. The structural epoxy is manufactured by SealBoss and is the 4040 LV Epoxy Resin. The two control beams are a full-sized 8 inch square beam without notches and a notched unrepaired beam to give the expected upper and lower bounds on the load-deflection curve.

The differences between the prototype beams and the full-scale beams are that the repair blocks are not full length, the tensile reinforcement in the full-scale beams is steel and the compressive strength of the concrete is lower at 4,600 psi. The reason for the sectional repair blocks is that given the deflections of the reinforced concrete beam, full length blocks might cause complex stresses on the blocks that are difficult to account for. By dividing the blocks into sections, pure shear stress along the repair can be applied. The reason for the steel reinforcement should be obvious as traditional concrete bridge decks utilize steel as the tensile reinforcement. The lower compressive strength was specified for the full scale tests to simulate typical field conditions.

Figure 5-12: Notched Full-Scale Beams

The repair was prepared by wrapping half of the horizontal repair plane with tape to prevent the repair material from leaking out. The inorganic repair material was prepared as usual by mixing the liquid and powder components in a mixer for 60 seconds, resting for 120 seconds and finishing with 60 more seconds of mixing. The aluminosilicate epoxy was applied by pouring the mix in the dam created by the tape and lowering each block section into place. The blocks were pressed firmly into the repair material. Excess amounts of material were not allowed to drain so as to reduce the amount of voids. Some of the blocks were taller than the middle compressive zone of the concrete beam, but did not affect the overall strength of the beam since the strength is limited by the smallest moment arm in the pure flexural zone of the loading arrangement. As each block was placed into position, the vertical face mating with the beam or a adjacent block was coated with repair material and pressed together. Once all blocks were in place, the vertical crack was sealed with tape and aluminosilicate mix was poured over the crack to completely fill all the voids.

A similar procedure was followed for the 2-part epoxy system. Tape was wrapped around the beam to prevent leaking and draining of the epoxy. The specifications for the epoxy system required two parts resin to one part hardener. Then the hand mixed material was poured into the dam. The vertical faces of the block and adjoining beam or block was coated and the surfaced pressed together to force out air bubbles and close voids. After all blocks were in place, the vertical cracks were sealed and the remaining voids filled with epoxy.

Once the two beams were repaired, they were allowed to cure for a minimum of 7 days before the tape was removed. The cracks were inspected for voids and none were reported.

5.5.1 Instrumentation

The data collection system captured the loads and deflection at the midpoint and at each load point to create a load-deflection profile for each beam (see Figure 5-13). This presented the effective stiffness of each beam and allowed easy comparison. In addition to the loads and deflection, vertical lines were drawn on the side surfaces of the repaired beams crossing over the repair plane to monitor movement. Initially, the use of crack monitoring equipment was specified but the dimensions of the notches would not allow installation of the gauges.

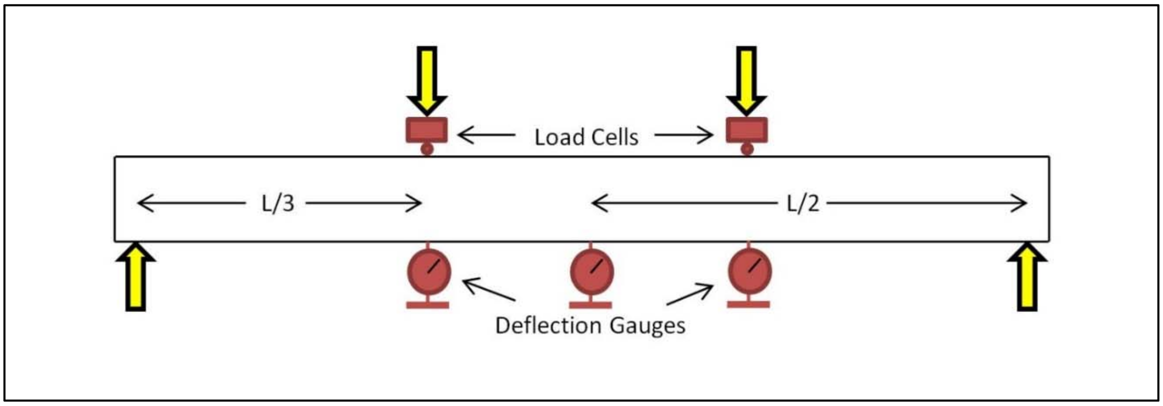

Figure 5-13: Instrumentation Set-Up

The test specimen was preloaded to seat the support and load equipment and zero the gauges. Then the beams were loaded to 60% of failure at a static loading rate (between 15 and 20 lbs per second) totaling of about 15 minutes for the entire test. Once the maximum load is reached, pictures of the crack lines were taken and then the beam unloaded and the entire test repeated two more times for a total of three loading cycles to provide a complete stiffness profile of the beam.

The system used to gather the load and deflection data were a series of sensors that were connected to a computer using USB ports. Two load cells were located under each load and three deflection gauges were positioned at the midpoint for ultimate deflection and under each load to allow for computation of a deflection curve. The data was collected by a proprietary software package developed by Loadstar Sensors called SensorView. The software logged the data collected into a .csv file for importing into any spreadsheet program for further analysis. The data collection rate was set at 1 second intervals.

The hardware used for data collection included the two RSB1 resistive load cells, calibrated to 10 kips in compression and three DISP displacement sensors with a 1 inch range. These were connected to five DI-1000U digital load cell interfaces to convert the millivolt output to a USB format. The USB cables were connected to a powered 7-port USB hub and then to the computer via USB (see Figure 5-14). The signals were processed by the SensorView software and output to the data file. A real-time graph displayed the load and deflection data as a function of time.

Figure 5-14: Full-Scale Beam Test Instrumentation

5.5.2 Results

The full scale tests behaved similar to the prototype tests. The repaired inorganic aluminosilicate beams showed similar stiffnesses to the solid beam. The repaired organic epoxy beam behaved just like the notched beam that had not been repaired.

The curvature (shown in Figure 5-15) shows that the notched and epoxy repaired beams had internal hinges at the load points. The solid and aluminosilicate repaired beams had an even curvature across the span.

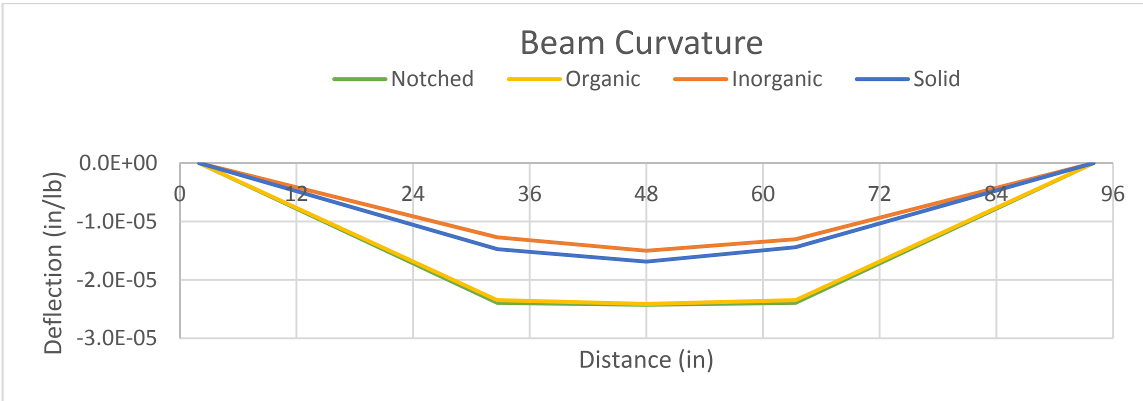

Figure 5-15: Full-Scale Beam Curvature Comparison

The load/deflection graphs yielded a similar trend (Figure 5-16). Both the notched and epoxy repaired beams demonstrated lower stiffnesses with increased deflection over the same loading. The inorganic repaired and solid beams exhibited higher stiffnesses. A model of a solid beam was also generated using the cracked moment of inertia. The inorganic repaired and solid beams closely matched to the model with slight deviations due to imperfections in the cast beams.

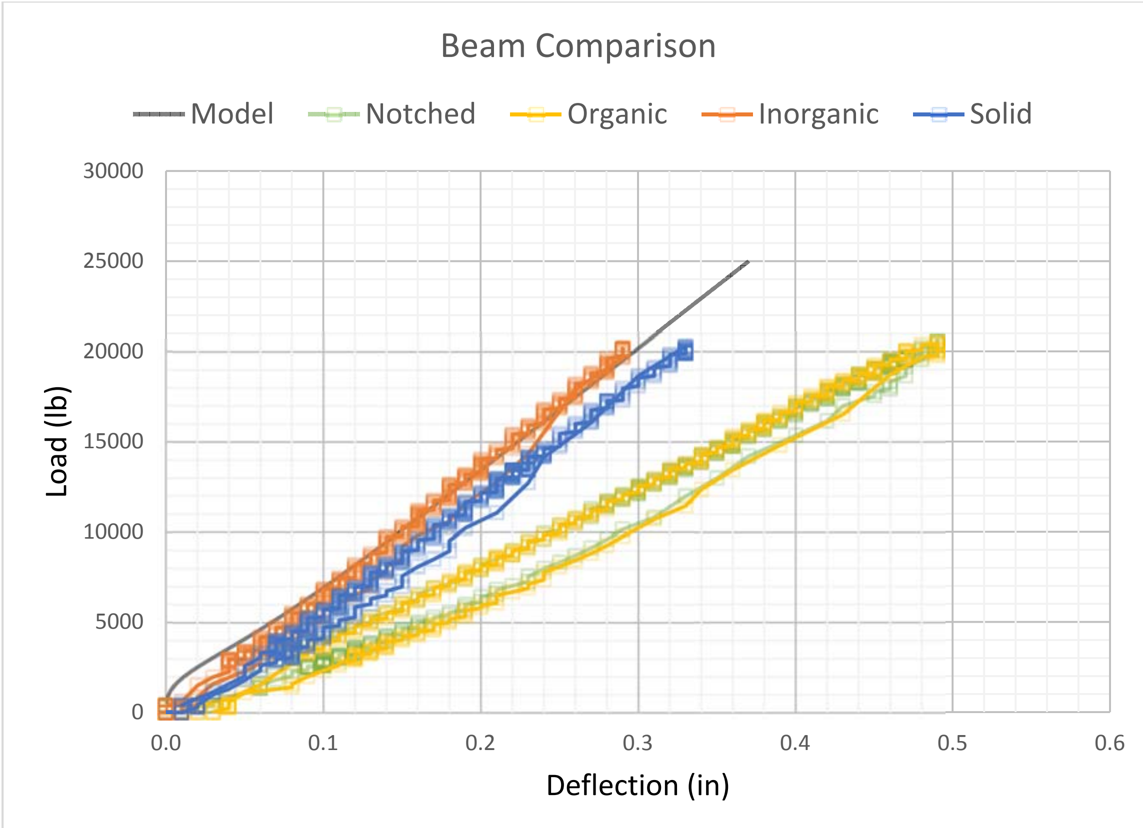

Figure 5-16: Full-Scale Beam Comparison

Both of these results clearly show that the epoxy repaired beam did not benefit by the repair. The beam had the same load and deflection reaction as the beam that was completely notched without repair of any type. The beam repaired with the inorganic polymer showed the same stiffness as the calculated model and slightly higher stiffness than the actual solid unnotched beam. Of course, this is due to imperfections in the beam but the point is still poignantly made, that the inorganic epoxy allows the internal forces to transfer across the repair plane and include the compression block in the resolution of the moment arm in the flexural strength of the beam. The pictures in Figure 5-17 below also illustrate the shifting of the blocks with respect to the beam. The flexibility of the organic epoxy is evident in the offset of the detection lines across the horizontal crack.

The inorganic repaired beam does not have any apparent movement and indicates that the repair of the concrete using the inorganic epoxy will be able to provide stress transfer and concrete compatibility for the structural element. This will allow the repaired component greater resistance against additional delamination cracking and prolong the life of the structure.

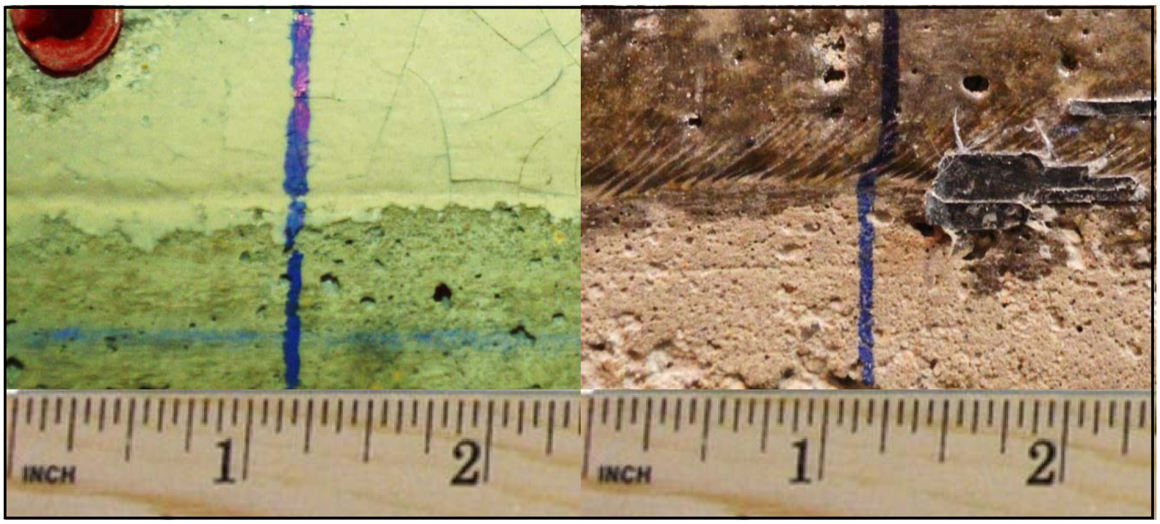

Figure 5-17: Shear Movement Comparison; Inorganic (left), Organic (right)

In addition to the overwhelming evidence of the incompatibility of the epoxy system and the concrete, both the notched and epoxy repaired beams featured shear cracking in the outside third of the beam. This indicated that the minimum shear reinforcement of half the distance from the extreme compression fiber to the centroid of the tensile reinforcement was too large. In essence, the actual extreme compression fiber was not the top of the block in the case of the epoxy repaired beam, but the top of the notch as seen in Figure 5-18.

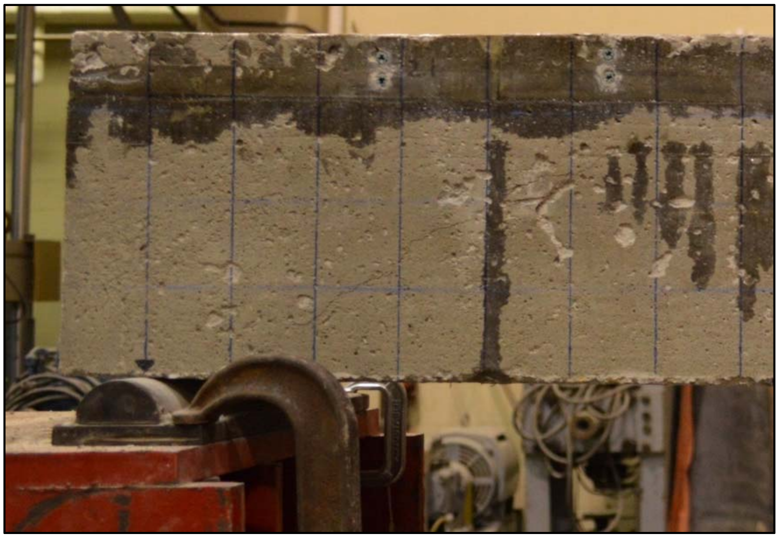

Figure 5-18: Shear Crack in Epoxy Repaired Beam

5.6 Summary

The following remarks are made with respect to the comparison of inorganic aluminosilicate and organic epoxy systems:

- Slant shear tests showed that the inorganic polymer performed slightly better than organic epoxy systems in head-to-head comparisons. Using the universally accepted testing method for concrete bonding materials, the inorganic system had the minimum required specifications needed for use in concrete repair schemes.
- The prototype tests indicated that the organic repair systems were not able to provide the same strength resistance of the inorganic repaired beams. These tests could not show the range of repair that each system offered since control beams were not used.
- The prototype beams showed the feasibility of full-scale beams for use as effective tests of compatibility because of their success on the small scale.

The full-scale beams demonstrated the compatibility of the repair system in the following ways:

- Using a control for either extreme of results, the full-scale tests provided real data on the effectiveness of the repair material.
- The inorganic repaired beams featured higher stiffness, no detectible shear slippage along the repair interface, no failure cracking and loading behavior similar to both the calculated model and the solid unnotched beam.
- The organic repaired system featured lower stiffness, shear slippage along the repair plane, shear cracking near the reaction supports indicating decreased depth from the extreme compression fiber to the centroid of the tensile reinforcement, and loading behavior similar to the notched control beam.

The conclusion is that Mix E4 is compatible with concrete by sharing in the internal stress distribution mechanism and allowing the beam to behave as a homogeneous cross-section through the shear and compression zones.

CHAPTER 6 - DURABILITY

6.1 Introduction

As in all construction materials, durability plays an important role because it is connected to the time and ultimately the cost associated with the use of the material. Durability is often an effective way to compare alternative materials. In addition, some structures are exposed to accelerated deterioration due to the freezing and thawing cycles of the region and the exposure to wetting and drying environments. The structures most often affected by all these components are bridge decks. Bridge decks freeze more often than the roads because of their exposure to air on all four sides. Since bridges are outdoor structures, they are also exposed to wet and drying cycles.

Since the object of this study is to identify a bridge deck delamination repair material that can provide greater durability than the current alternatives, namely organic epoxy systems, a detailed durability study is required. The durability of the inorganic matrix is studied in two parts, freeze/thaw and wet/dry conditions. While the inorganic polysialate has been subjected to durability testing before, the testing rubric is different. In a test documented by Ronald Garon in 2000 at Rutgers University the wet/dry, freeze/thaw and other durability conditions on fiber reinforced concrete samples and coated concrete samples were investigated using a variation of the aluminosilicate epoxy designed for those purposes (Foden 1999). The testing metric was the dynamic modulus and flexural strength tests. While the dynamic modulus test for applicable to testing whether a coating can preserve the integrity of the underlying concrete, it is unable to directly test the strength of the bond during the specific durability tests. Similarly, the flexural test can provide data on whether the integrity of the inorganic matrix used to adhere the carbon fibers to reinforce concrete beams, but cannot test the effectiveness of the matrix in a bonding condition.

In order to test the durability of the bond strength, the same durability conditions are followed but utilizes a more applicable test. The assessment used in this study is ASTM D4541 Standard Test Method for Pull-Off Strength of Coatings Using Portable Adhesion Testers and ASTM D6944 Standard Practice for Resistance of Cured Coatings to Thermal Cycling (ASTM D4541 2009) and (ASTM D6944 2009). The American Society for Standards and Materials (ASTM) does not have a formal method for the durability of concrete coatings in wet/dry conditions so the procedure followed for the test was adapted from the test performed by Dr. Garon.

For both types of durability tests, the inorganic repair material was applied to concrete prisms and subjected to the specific durability test. The types of inorganic matrices applied were chosen to find whether the use of a nano-activator increased durability. The testing metric for all durability tests was the adhesion test. In addition, the effect of curing and the speed of the mixer was tested through the use of the adhesion tests. This was done to see if these variables had any effect on the durability of the material. The objective of this chapter is to provide an overview of the test materials, test procedure and the results from the durability tests themselves.

6.2 Test Materials

The types of mixes and processing variables determined the number of samples required for the tests. A total of four mix designs were tested. The processing variables tested are whether the speed of the mixer has any effect on the durability of the repair material as well as the curing conditions of the mix after it has been applied to the concrete substrate. These variables require then a total of 16 samples plus a control for a final total of 17 for each test. Therefore 34 samples are required for both durability tests.

The four mixes used in this are the 5^{th} iteration series, E Mixes. The variables tested are nano-aluminosilicate powders and different silica-alumina ratios. These are done since research had shown that the reduction of the ratio increases durability though at a possible strength loss. The mixes are summarized in Table 6-1.

E Mixes Design Summary		
	S/A Ratio	Nano AS
E1	62	No
E2	27	No
E3	18	No
E4	27	Yes

Table 6-1: Durability Mix Summary

One of the processing variables tested were whether the mixer speed has any effect on the durability of the repair material. The two mixing speeds tested were 29,000 rpm and 3,000 rpm. The other testing variable is to find whether the newly formulated mix with the zinc oxide activator requires higher temperatures to cure properly and remain durable against freeze/thaw and wetting cycles. So half of the samples were cured at 120°F and the other half were cured at room temperature. In addition to the coated prisms, a non-coated control sample was also included.

In order to use the adhesion test, the test surfaces must be flat. Also the substrate must be sufficiently rigid to resist the pull-out forces of the adhesion testing machine. For these reasons, 3 inch square by 11 inch concrete specimens were used. The coatings were applied to the two long sides reducing the damage that could be caused to the top and bottom during moving the samples from the different test chambers.

The prisms were mixed and cast in the Rutgers University civil engineering laboratory. Formwork was created to cast 60 specimens at one time. The formwork was constructed out of #2 SPF 3/4 inch material and was fastened together in such a manner as to allow the non-destructive removal of the formwork so that the formwork could be reused. Prior to casting the formwork was coated with a commercially available form release agent to aid in removal of the formwork.

The target compressive strength for the concrete prisms was 4,000 psi which corresponded to a water-to-cement ratio of 0.464. The 28-day compressive strength was found to be 4,700 psi. The concrete mix was a normal strength concrete and featured no admixtures. The cement percentage was 17.39%, the water was 8.07%, the fine aggregates were 29.5% and the 3/8 inch coarse aggregates were 45.03%.

Once the concrete prisms had cured for a minimum of 28-days they were coated with one coat of the inorganic repair material. The coatings were mixed starting with the liquid component first and adding the dry parts second. The mix sequence included 60 seconds of mixing followed by a 120 second rest period and a final 60 seconds of mixing. The mix was applied to the concrete using a foam brush and spatula. Table 6-2 below summarizes the designation for each mix design with respect to the type of mixing and curing. Additional details such as setup and specifications of the mixers and curing conditions are given in Chapter 3.

Mix Number (i.e. E1, E2, E3, or E4)		
	29000 RPM	3000 RPM
70°F Curing	A	C
120° Curing	B	D

Table 6-2: Mix Notation

6.3 Adhesion Testing

The previous durability tests on the inorganic material focused on the protective coating formulation and utilized equipment that could find the modulus of the coated concrete in order to determine its resistance to the durability cycles. Since this application of the coating is not for concrete protection but rather as a repair material which depends on the bond strength as a measure of its suitability, the adhesion pull-out test provides a direct method to evaluate the bond strength in tension of the coating to the concrete substrate before, during and after the durability test cycles are performed.

Figure 6-1: Adhesion Test Set-Up

DeFelsko Corporation manufactures the adhesion testing apparatus used in this test. The PosiTest AT-M Manual Adhesion Tester conforms to the ASTM D7234 Test Method for Pull-Off Adhesion Strength of Coatings on Concrete using Portable Adhesion Testers (ASTM D7234 2012). The ASTM procedure is performed by scoring the coating to the surface of the concrete using a coring element with an inside diameter equal to the outside diameter of the loading dolly. The size of the loading dolly is based on the expected strength of the coating. Once the coating is scored, the dolly is secured to the center of the scored surface of the coating with an adhesive. When the adhesive cures, a testing actuator is attached to the loading dolly that can be aligned to the apply tension perpendicular to the test surface. Force is applied to the test dolly in a uniformly increasing manner and recorded until the plug of material detaches (see Figure 6-1). The remaining surface represents the failure plane and the type of failure is categorized to indicate the type and location of the failure. The pull-off strength is computed based on the maximum indicated load, the instrument calibration data and the surface area of the failed plug. While every effort is made to synchronize conditions before and during the test, variations in the substrate, coating, and adhesive may result in different results in the same specimen. For this reason, ASTM recommends at least three tests performed in the same area to draw data from. In this test, four tests were performed at each time.

Figure 6-2: Coring the Specimens

For these tests, the scoring was made using a drill press and diamond coring bit with a 5/8 inch outside diameter as shown in Figure 6-2 (slightly larger than the diameter of the dolly). The drill press was outfitted with a laser crosshair to align the coring bit with the dimple on the dolly representing the center. From preliminary testing, it was determined that a 14 mm (0.55 inch) dolly would satisfy the pressure range required by the project specifications. The test specimens were scoured with an abrasive pad prior to adhesion of the dollies to decrease the risk of adhesion failures. Only the long sides of the specimens were used for adhesion testing because of irregularities in the top and bottom surfaces. The dollies were adhered using manufacturer supplied and recommended 2-part epoxy and were required to cure for a minimum of 24 hours. Once the epoxy had cured, testing was performed at a rate of 15 – 20 psi per second until failure. The ultimate adhesion strength was recorded and the failure plane noted. Also, the failure holes were marked on the specimen: a number for the number of the test and a letter corresponding to one of the four holes. If the failure plane included any irregularities such as voids or epoxy failures, it was excluded from the results. For the freeze/thaw durability testing, data was collected every fifth cycle. For the wetting tests, data was collected on the sixth cycles.

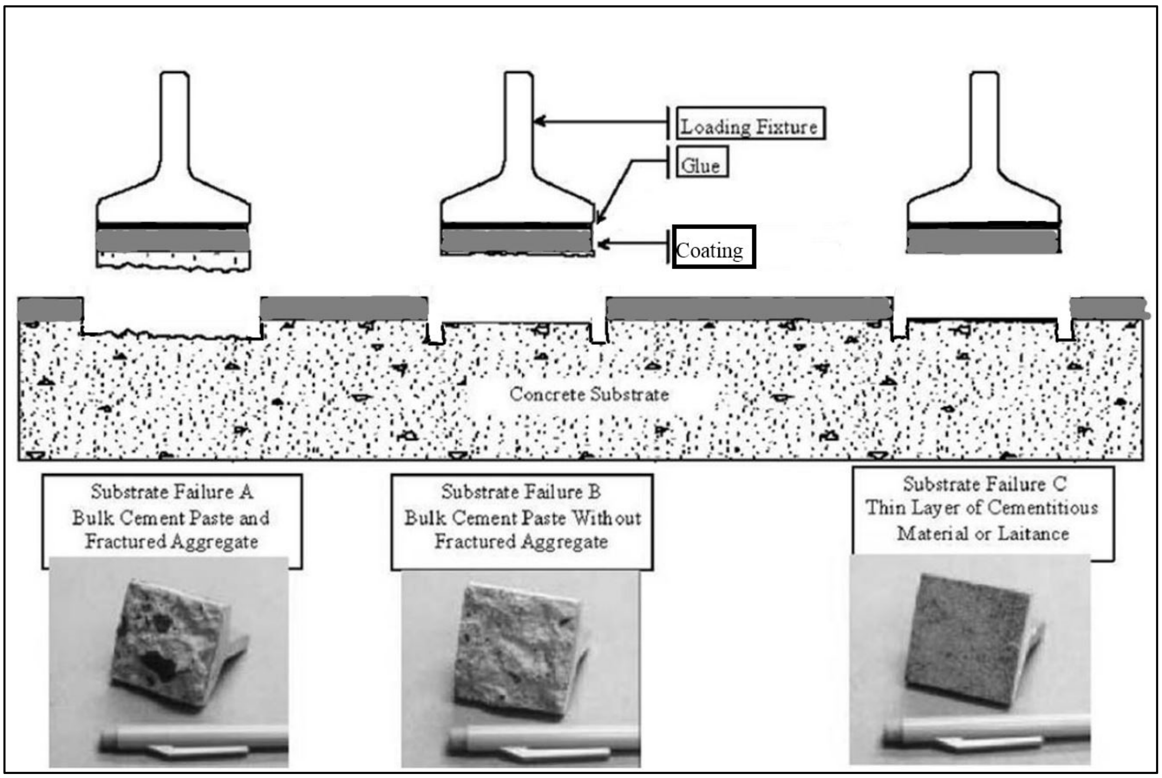

Figure 6-3: Failure Modes A through C

The failure modes are shown in the preceding (Figure 6-3) and following diagrams (Figure 6-4). Failure A refers to a failure in the concrete between the cement and aggregate. Failure B shows another concrete failure in the cement only. Failure C is a failure that includes the surface layer of the concrete. Failure D is a failure that occurs at the interface between the coating and concrete. Failure E is a failure in which the failure plane is within the coating itself. Failure F is a failure that occurs at the adhesive level. It can be a failure in which the adhesive does not adhere to the coating or dolly or fails between the two extremes, i.e. adhesive is remaining on both the dolly and the coating.

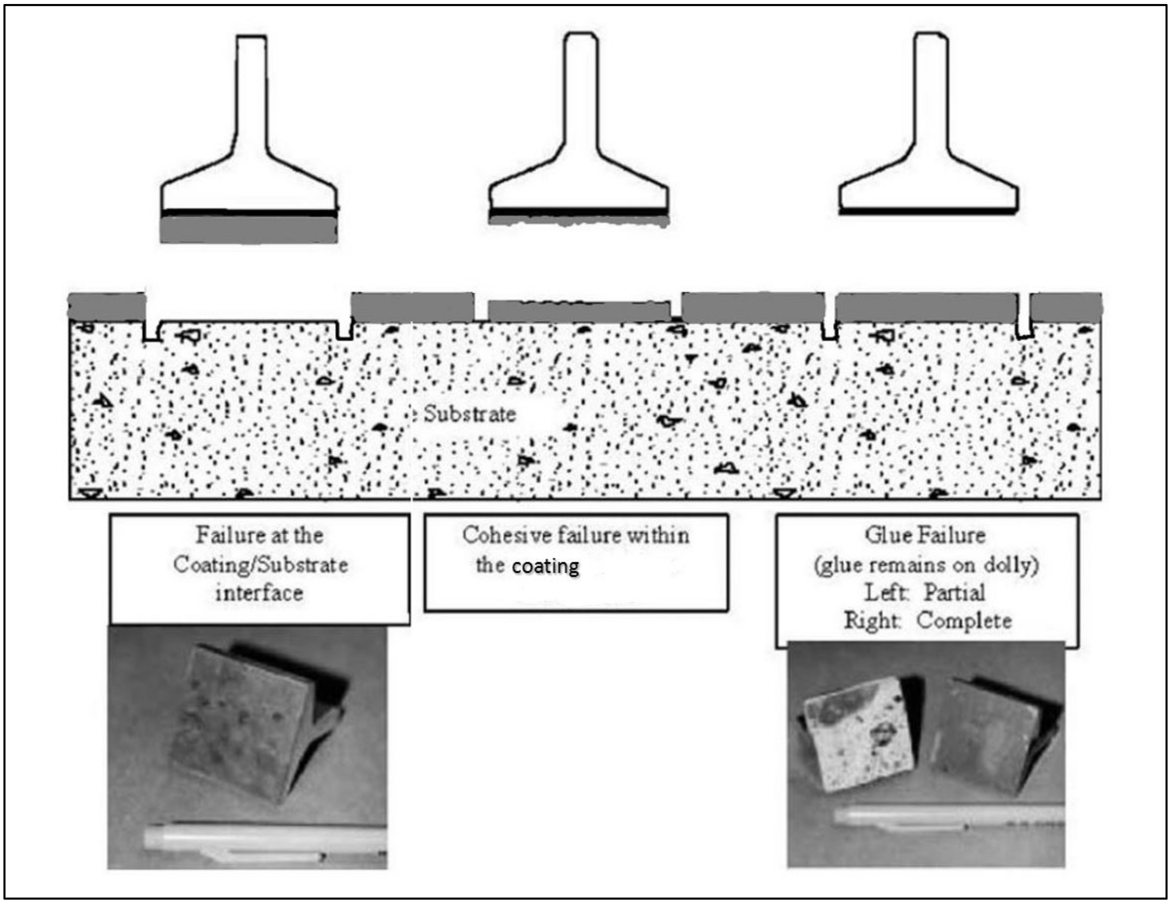

Figure 6-4: Failure Modes D through F

6.4 Freeze/Thaw Test Set-up

ASTM D6944 Method B was used for the determination of freeze/thaw durability of the inorganic coating/repair material. Since an apparatus with the capability to heat and refrigerate in the same unit was unavailable, a custom heat chamber and commercially available chest freezer were used. Independent wireless thermometer units were used to monitor the interior temperature of each chamber to verify specified temperature conditions. The samples were arranged on removable and stackable plastic crates in the chest freezer to minimize contact and the specimens were situated only on the untested top or bottom surfaces to avoid marring the surface. The chest freezer thermostat was set at 5°F. In the heat chamber, the specimens were placed on stainless steel racks with only the bottom or top resting on the shelves to avoid marring the testing surfaces. The heater in the heat chamber was set to maintain a constant 120°F.

Adhesion tests were performed at the end of every five cycles. One cycle consisted of heating at 120°F for 8 hours and cooling at 5°F for 16 hours. At the end of the five cycles, the specimens were allowed to acclimate to room temperature for 24 hours for adhesion of the pull-off test dollies. Then the specimens were allowed to cure for an additional 24 hours before performing the adhesion test. Thus, five tests were accomplished per week and the tests were performed for six weeks for a total of 30 tests as per the minimum required in the ASTM standard. In addition, by the end of the 30 tests, there was not any repair material left on the sides of the specimens for any additional tests even if they were desired.

6.5 Wetting Test Set-up

Since the procedure for wetting tests are not outlined in an ASTM standard, the procedure followed was adapted from similar tests that had been performed previously. The benefit of isolating the wetting tests from the freeze/thaw tests is to determine the singular effects from each of the two variables.

Figure 6-5: Wetting Test Set-Up

The basic test set-up from previous research includes two tanks: one for holding the specimens and the water and the other for holding the water when the specimens are drying (as shown in Figure 6-5). A fan was set up over the specimen tank to dry the specimens during the drying cycle. Two pumps were installed on each tank to pump the water from each tank into the other. The pumps and fan were all controlled by digital programmable timers for automation of the cycling.

The adhesion test was scheduled to take place after six cycles of wetting and drying. Each cycle was three hours long, that is, three hours of immersion in water and three hours drying by air flow. In this manner, two tests were conducted per week with 30 tests performed after two and a half weeks. Finally, since the process is automatic, the system was allowed to run for a total of 138 cycles corresponding to nearly three months of data. A schematic of the test set-up is shown below in Figure 6-6.

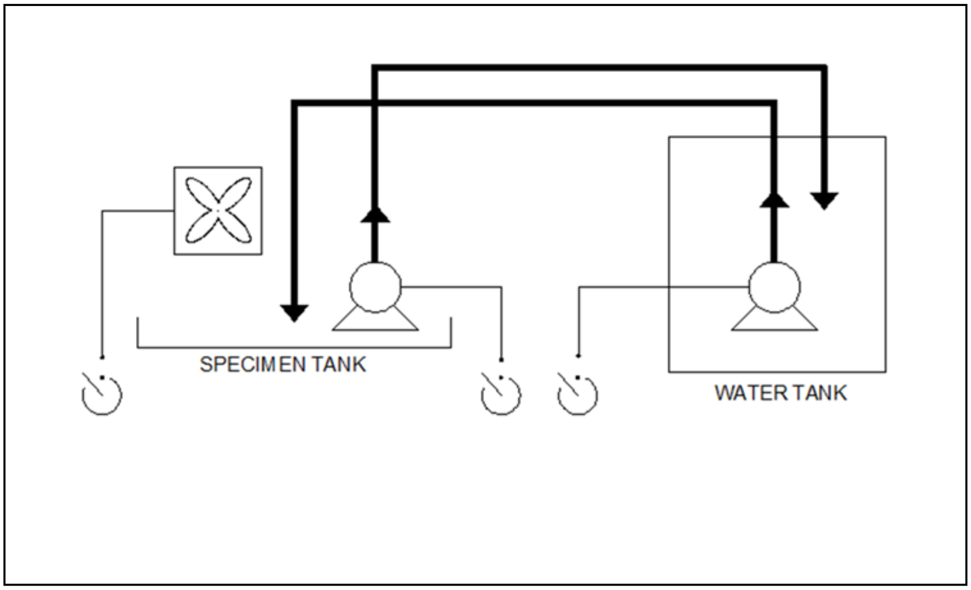

Figure 6-6: Wetting Test Set-Up Schematic

6.6 Freeze/Thaw Durability Results

For each specimen, the average adhesion strength was computed omitting epoxy failures. Graphs comparing each specimen to the control are shown at the end of this section. The control specimen, 404, increased in strength by about 8% over the 30 cycles.

Mix E1 specimen was designed for high strength and nominal durability resistance. Mix E1 coated specimens 451, 446, 427, and 405. All four specimens experienced coating failures throughout. 451 displayed an increase of about 18% over the course of the testing although this was attributed to the extremely low initial strength values obtained in the beginning of the cycling, Specimen 446 showed a decrease in strength of 11%, Specimen 427 exhibited a 10% increase in adhesive strength throughout the course of the testing though it also was associated with a low initial value and Specimen 405 decreased 10% in strength over the course of the testing.

Mix E2 was designed for moderate strength and moderate durability resistance with the decrease in the silica/alumina ratio and consisted of specimens 449, 448, 458, and 457. Specimen 449 experienced an increase in adhesive strength of 19% throughout the testing although this can be attributed to low strength values at the start of the testing, Specimen 448 displayed a 2% increase at the end of the cycling, Specimen 458 had a 20% decrease by the end of the cycling, and Specimen 457 had a 35% decrease at the end of the testing.

Mix E3 was designed for lower strength and higher durability resistance and consisted of specimens 454, 436, 437, and 406. All four specimens experienced a large percentage of coating failures throughout the testing. Specimen 454 demonstrated a decrease in strength of 2% at the end of the testing, Specimen 436 showed a decrease of 25% at the end of the testing, Specimen 437 had a 16% decrease after 30 cycles, and Specimen 406 had a decrease in strength of 14% finishing after 30 cycles.

Mix E4 was designed for moderate strength and moderate durability resistance like Mix E2 yet using nano-materials and consisted of specimens 416, 411, 412, and 424. Specimen 416 exhibited a decrease in adhesive strength of 26% throughout the course of the testing, Specimen 411 displayed a decrease in adhesive strength of 3% throughout the course of the testing, Specimen 412 experienced an increase in strength of 26% at the end of the cycling, and Specimen 424 demonstrated an increase in strength over the course of the cycling of 12%.

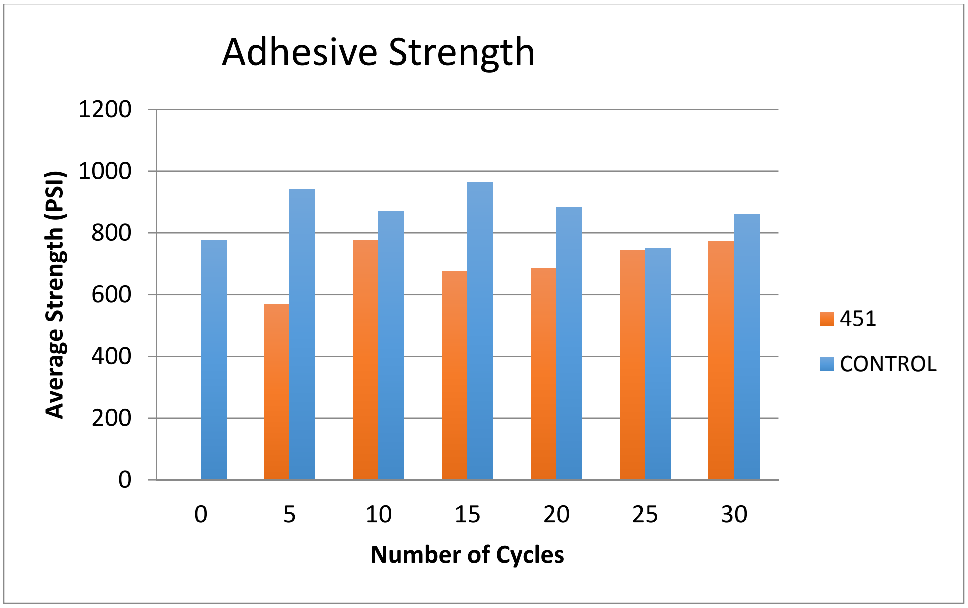

Figure 6-7: Beam 451 Results

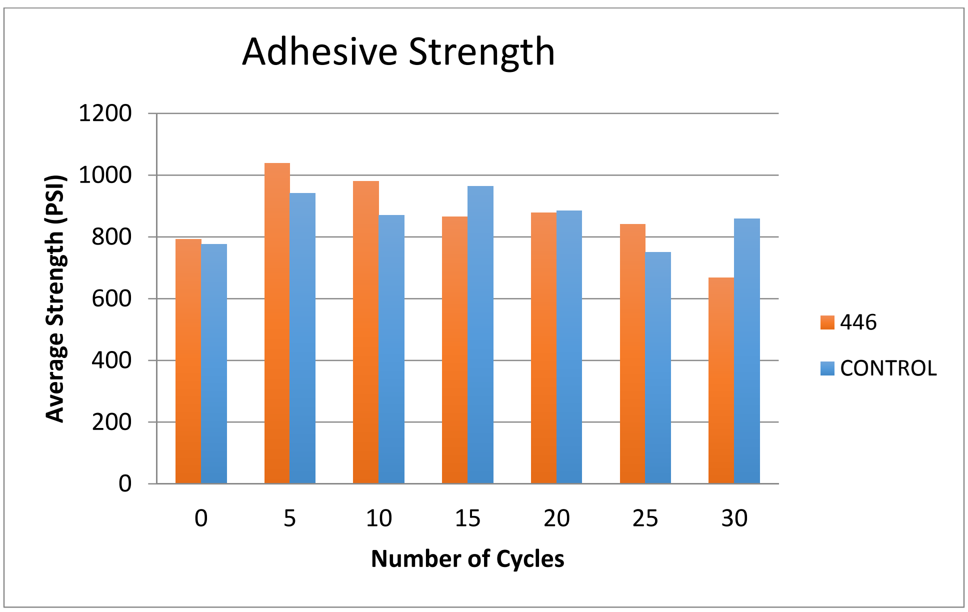

Figure 6-8: Beam 446 Results

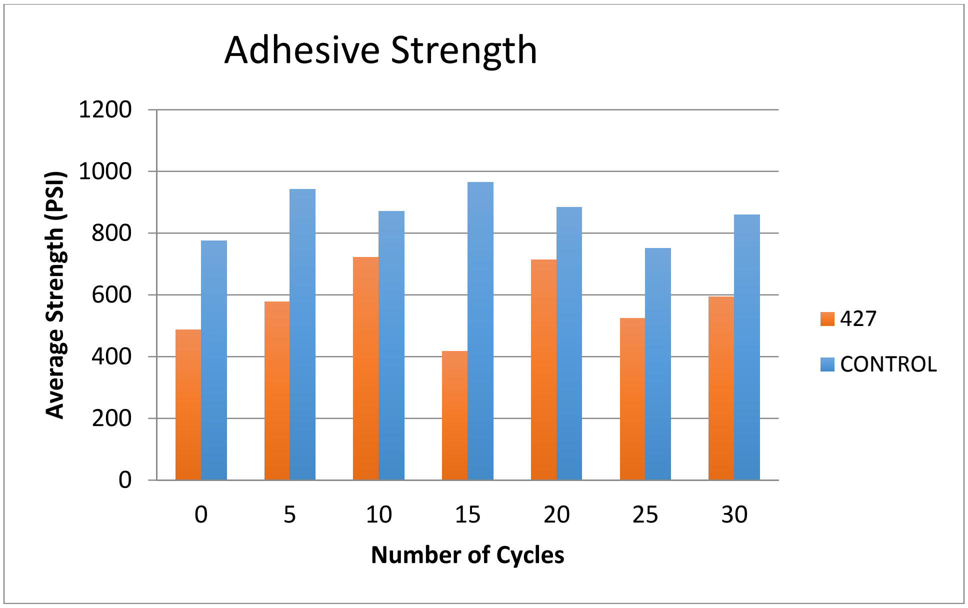

Figure 6-9: Beam 427 Results

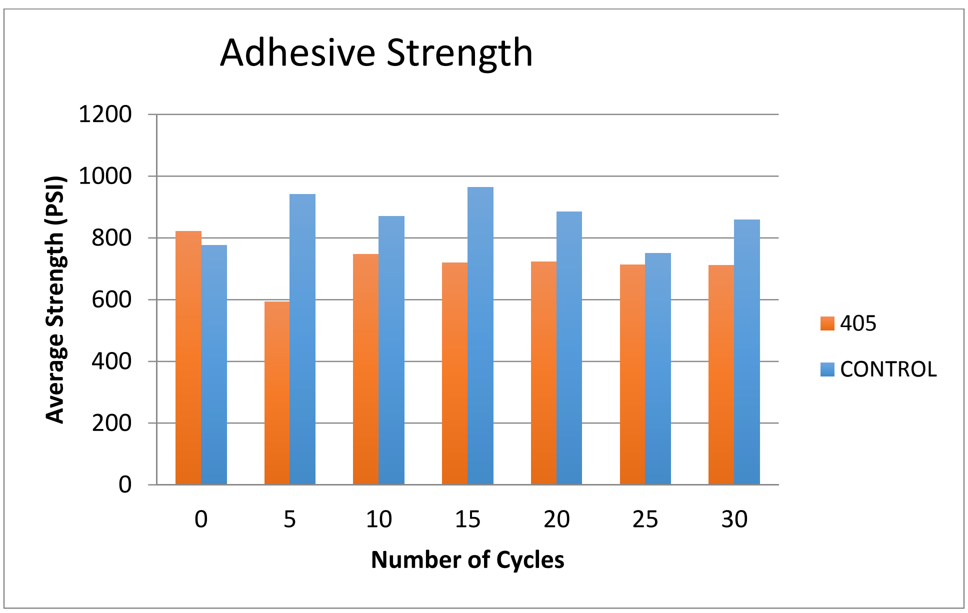

Figure 6-10: Beam 405 Results

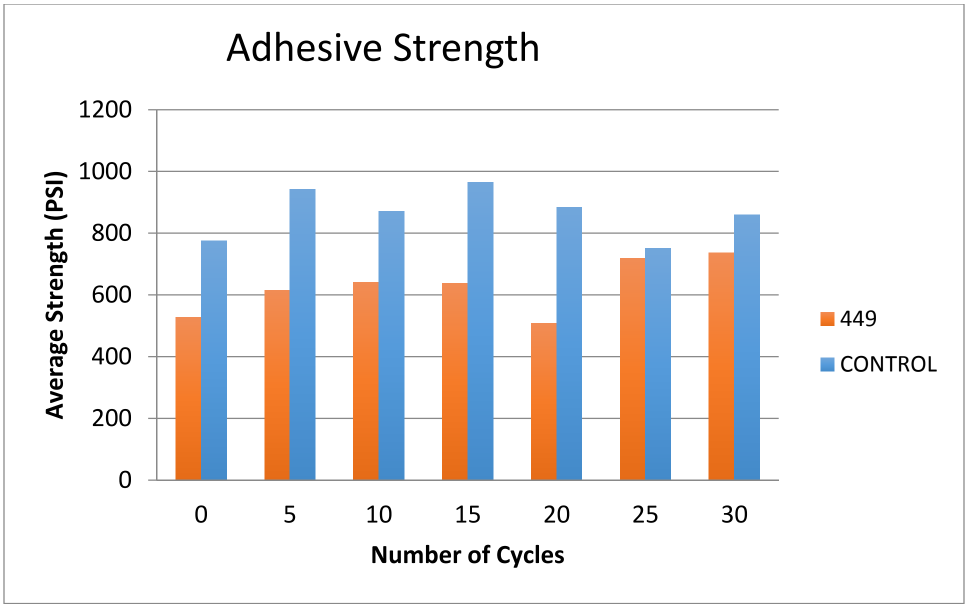

Figure 6-11: Beam 449 Results

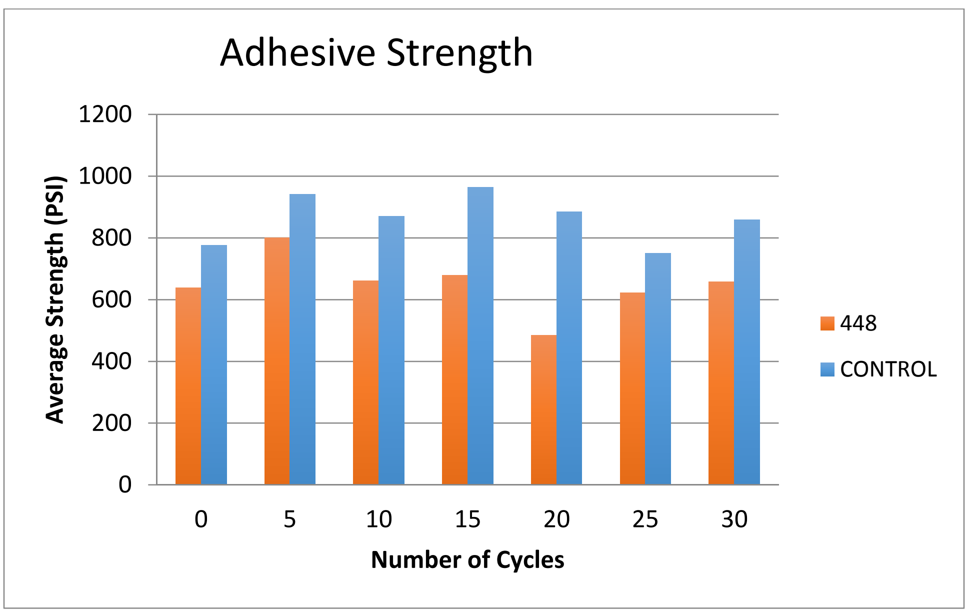

Figure 6-12: Beam 448 Results

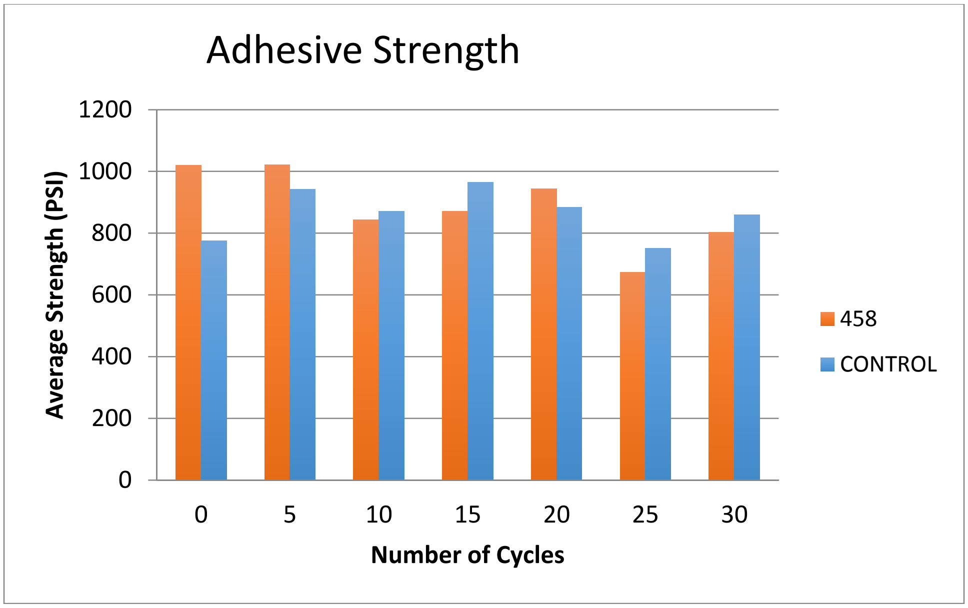

Figure 6-13: Beam 458 Results

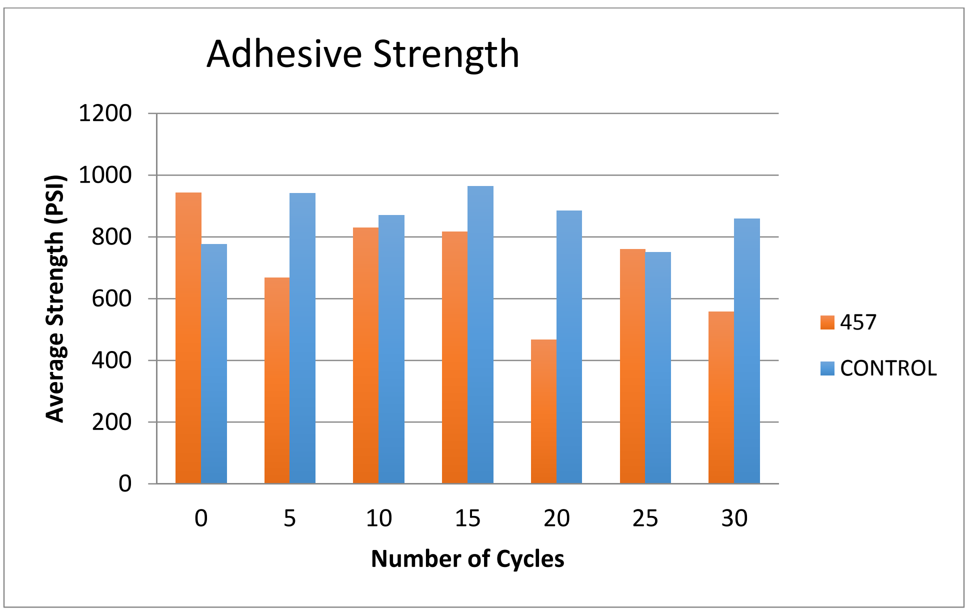

Figure 6-14: Beam 457 Results

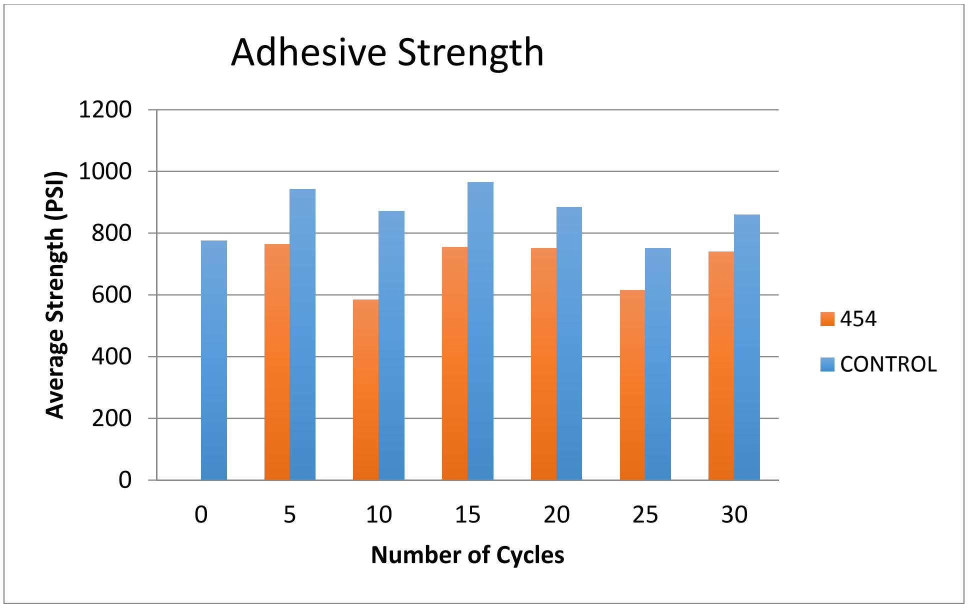

Figure 6-15: Beam 454 Results

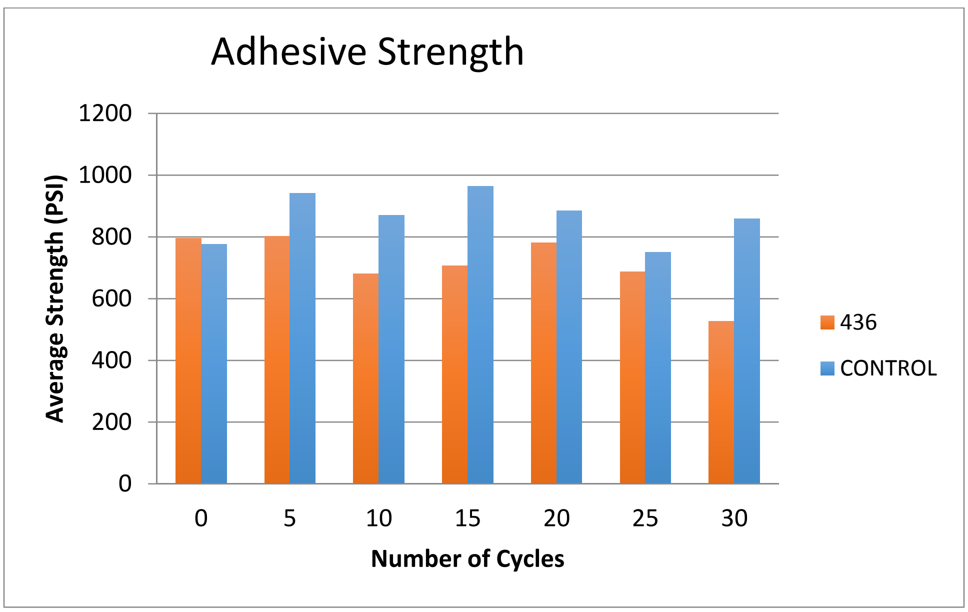

Figure 6-16: Beam 436 Results

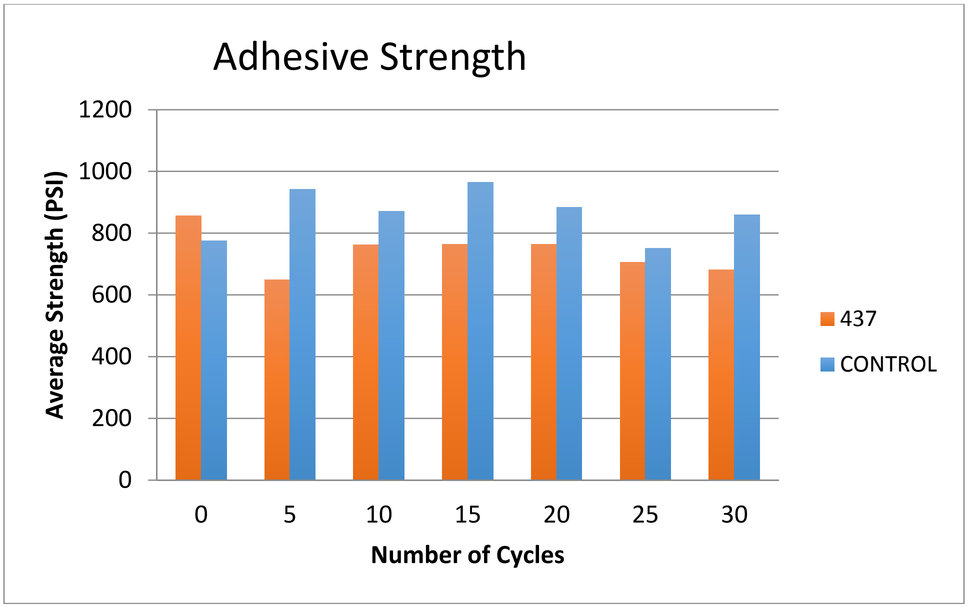

Figure 6-17: Beam 437 Results

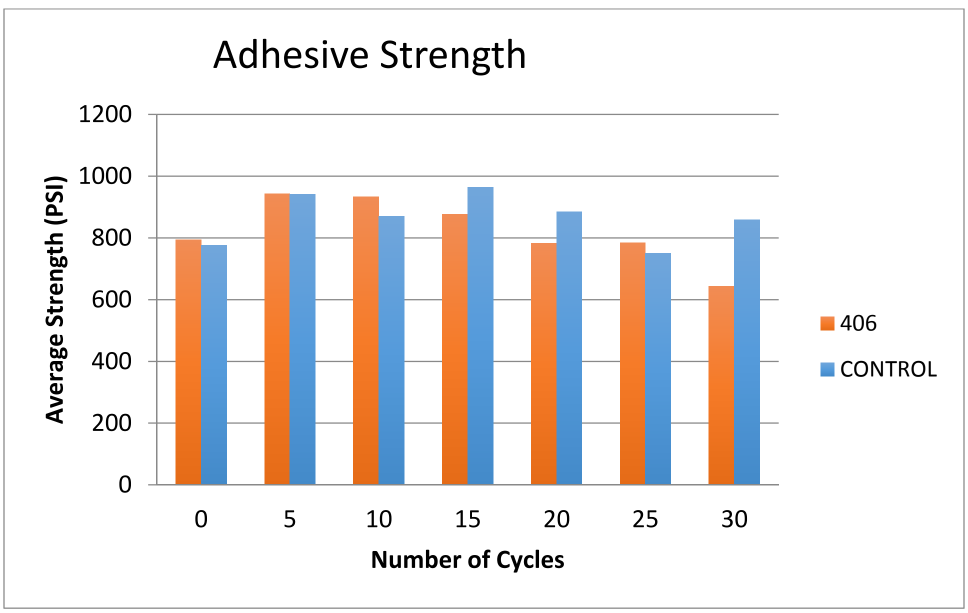

Figure 6-18: Beam 406 Results

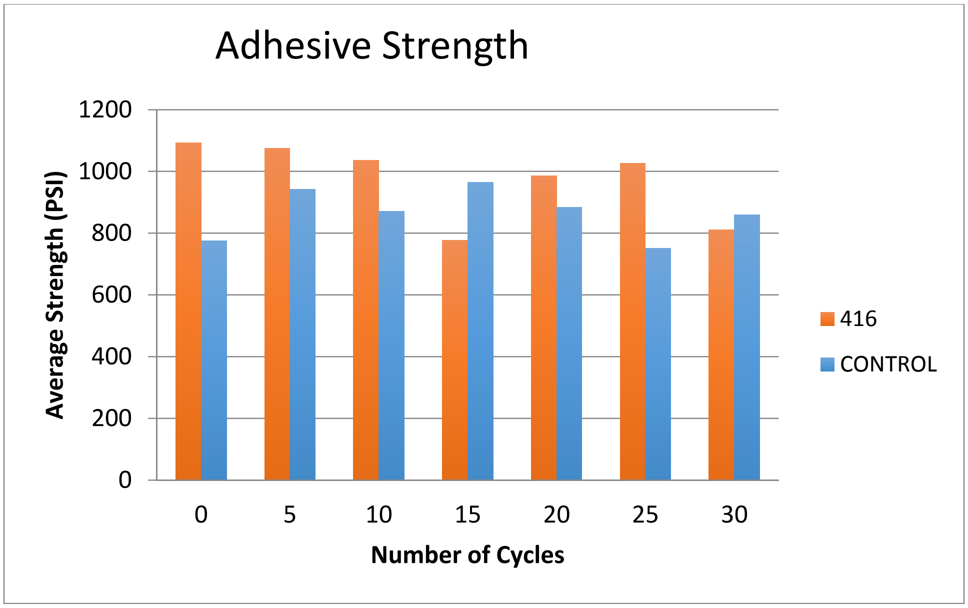

Figure 6-19: Beam 416 Results

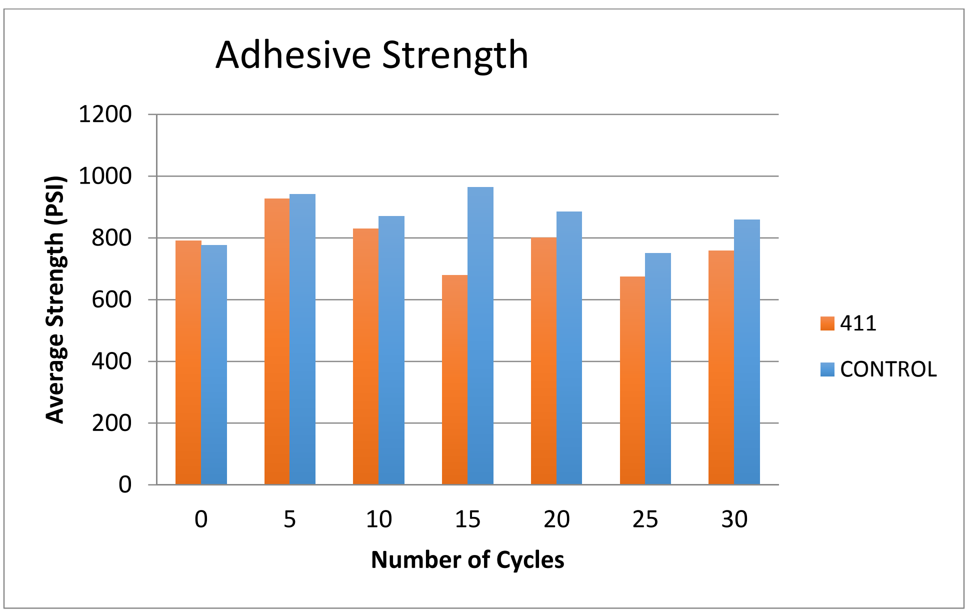

Figure 6-20: Beam 411 Results

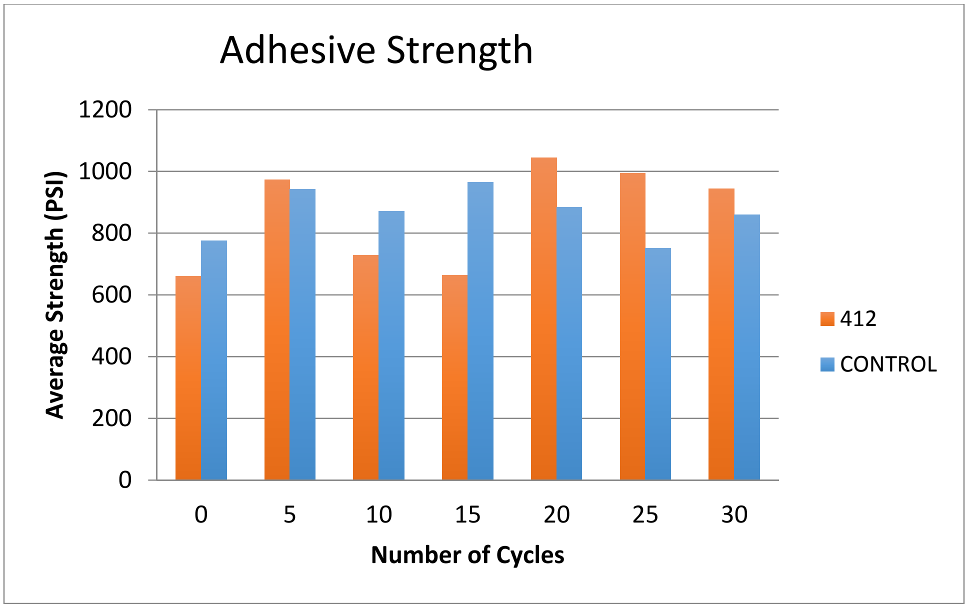

Figure 6-21: Beam 412 Results

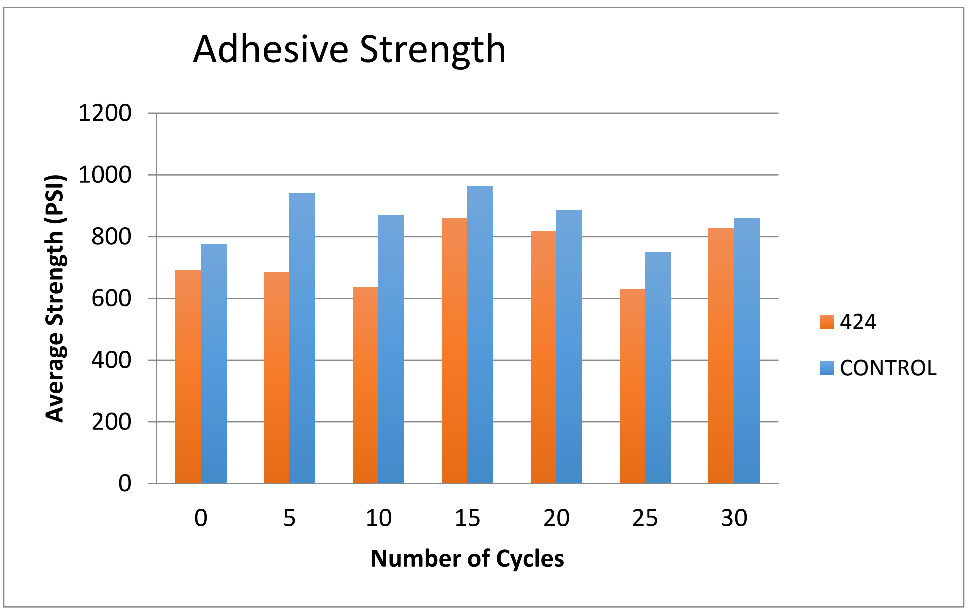

Figure 6-22: Beam 424 Results

6.7 Freeze/Thaw Results Interpretation

The freeze/thaw data analysis proved difficult for many reasons. First, it is known that the aluminosilicate cures better while exposed to curing temperatures up to 150°F and while the initial 7 day curing specifications called for room temperature curing for half of the specimens, they were exposed to higher temperatures during the thermal cycling. This explains the initial and overall gains for the room temperature cured mixes (Ex.A and Ex.C, where x is the mix number). Most of the specimens then experienced some form of gradual decline in adhesive strength after this initial spike. Surprisingly, the curing in the heat chamber gave an overall decrease in strength over the cycles but this is due to the fact that the initial values were higher.

Another reason for real lack in trending data is that the tests may have required a longer exposure period. While the minimum ASTM specifications were followed, more cycles may have yielded greater trends. The specimens did not have any more room for any additional testing because they were designed for the minimum 30 cycles of testing.

The results demonstrated that the mixes made using the high shear mixer resulted in a substantial amount of coating failures. This was likely due to the fact that the high rotational speed of the mixer heated the mix to such high temperatures that much of the liquid evaporated instead of reacting with the other ingredients. The same results were observed for the curing process with those that were cured at higher temperatures may have been forced to cure faster than the mixture had a chance to react. It was noticed that the use of the 29,000 rpm mixer as well as the 120°F curing gave a higher percentage of cracks in the appearance of the coating.

The results show that Mix E4, which was designed for moderate strength and moderate durability resistance using nano-aluminosilicate materials, gave the best overall results of any of the other mixes followed closely by Mix E1. These nano-particles, which are orders of magnitude smaller in size than micro-materials, create a less permeable barrier layer to protect itself (Woo, et al. 2008). The adhesive strength is also increased by having more particles in contact with the concrete substrate. Mix E1 is recommended, however, due to the similarities in results as well as having less costly materials.

6.8 Wetting Durability Results

Adhesion tests were performed on the sixteen coated samples and the control every six cycles up to thirty-six cycles and a break before the last test was performed at 138 cycles. Graphs are shown with a comparison of each sample and the control. Overall, the control, Specimen 413, exhibited a decrease of 12% after the testing.

As mentioned above, Mix E1 was designed for high strength but low durability resistance and consisted of specimens 459, 426, 408, and 402. All four specimens displayed decreases in adhesive strength over the testing period. Specimen 459 experienced a decrease in strength of 23%, Specimen 426 finished after 138 cycles with 32% strength, Specimen 408 had a decline of 11%, and Specimen 402 had a decrease in strength of about 34%.

Mix E2 was designed for moderate strength and moderate durability resistance and consisted of specimens 425, 407, 410, and 432. Specimen 425 had a decrease in strength of about 22%, Specimen 407 experienced a decrease in strength of about 20%, and Specimen 432 finished after 138 cycles with a decrease of 16%. Specimen 410 had epoxy failures in over 70% of the tests throughout the cycling and was not evaluated for this report.

Mix E3 was designed for high durability resistance and low strength and consisted of specimens 423, 455, 422, and 430. All four specimens were subject to epoxy related failures in 88% of the tests. None of the data was reported.

Mix E4 was designed for moderate strength and moderate durability resistance using nano-materials and consisted of specimens 453, 456, 414, and 439. Specimen 453 had a decrease of 45%, Specimen 456 had a decrease in strength of about 25%, Specimen 414 experienced a decrease in strength of 42%, and Specimen 439 exhibited an increase in strength of 31% although this can partially be attributed to the low initial strength and mostly epoxy related failures.

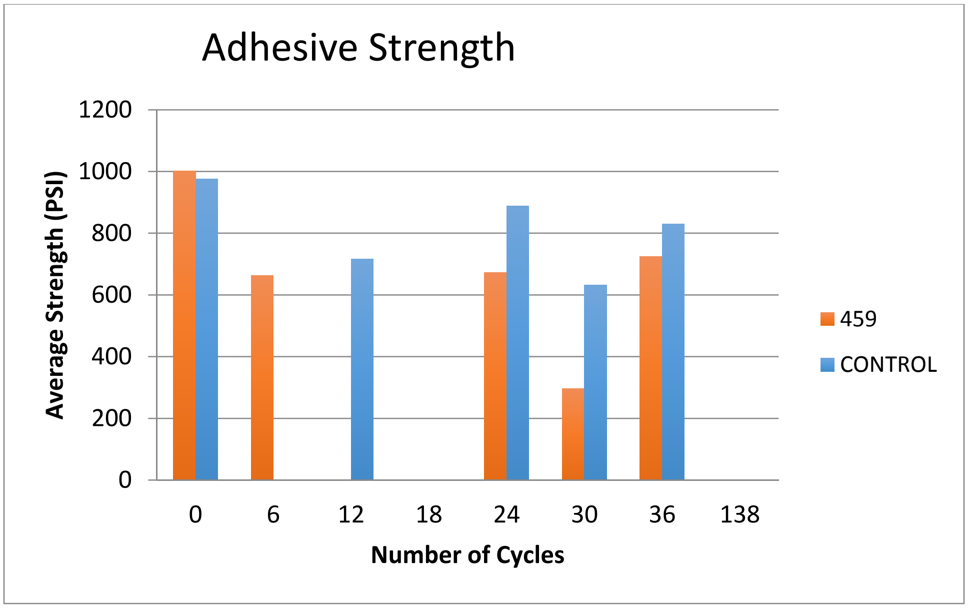

Figure 6-23: Beam 459 Results

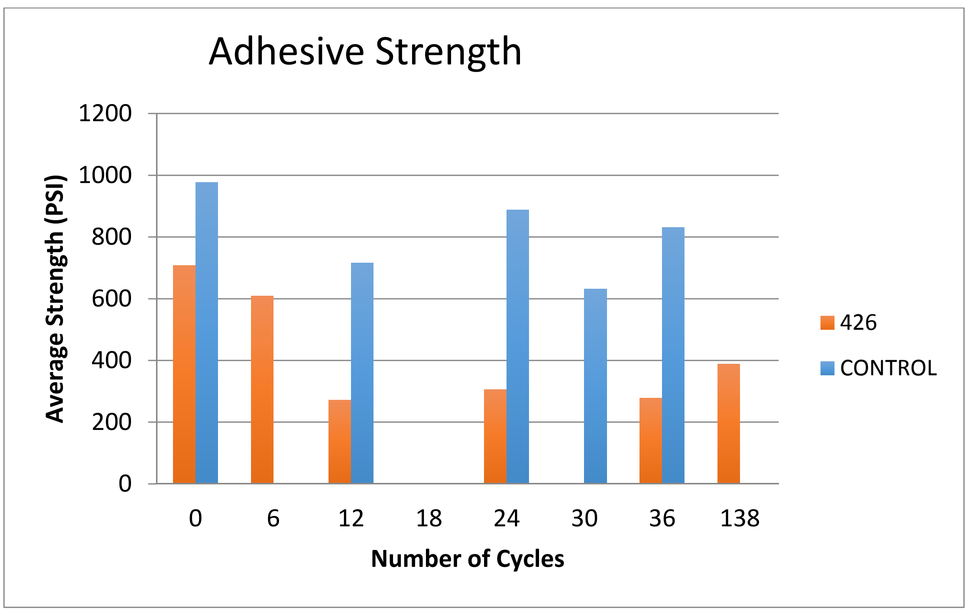

Figure 6-24: Beam 426 Results

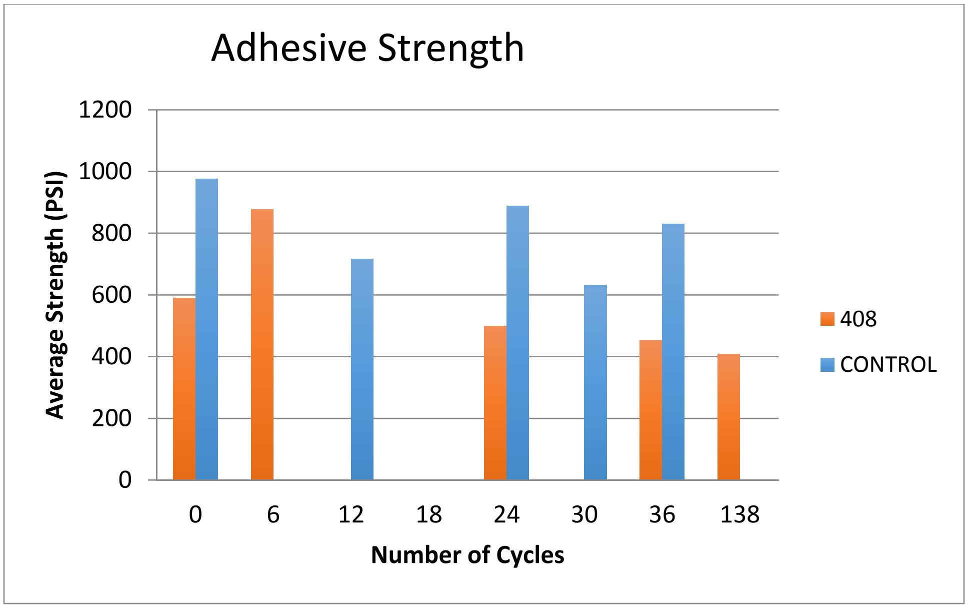

Figure 6-25: Beam 408 Results

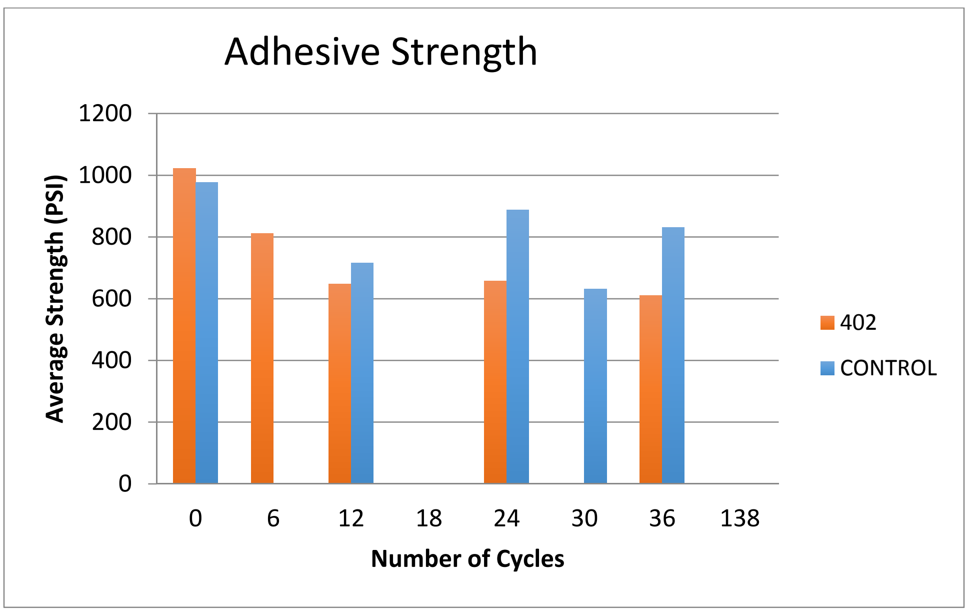

Figure 6-26: Beam 402 Results

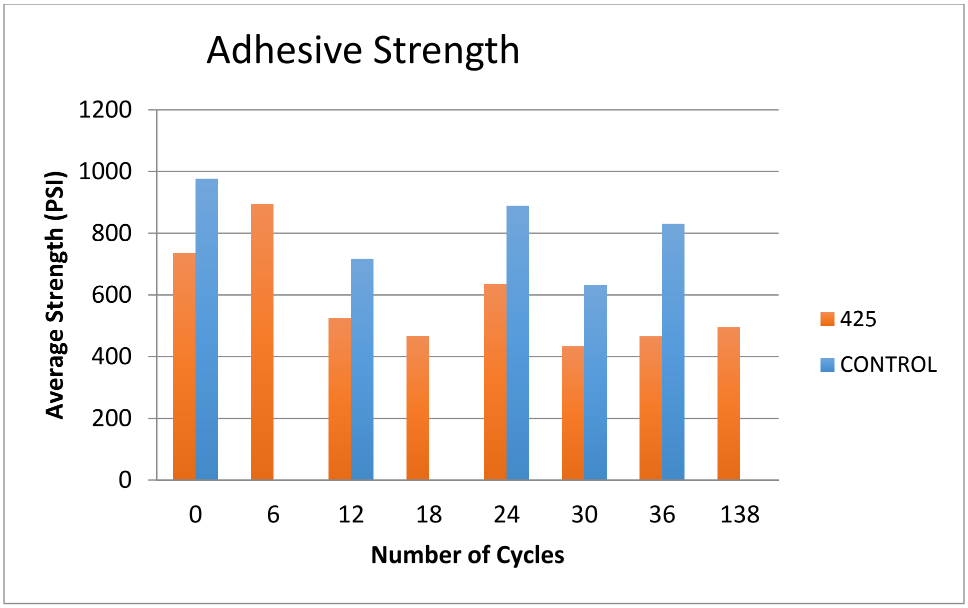

Figure 6-27: Beam 425 Results

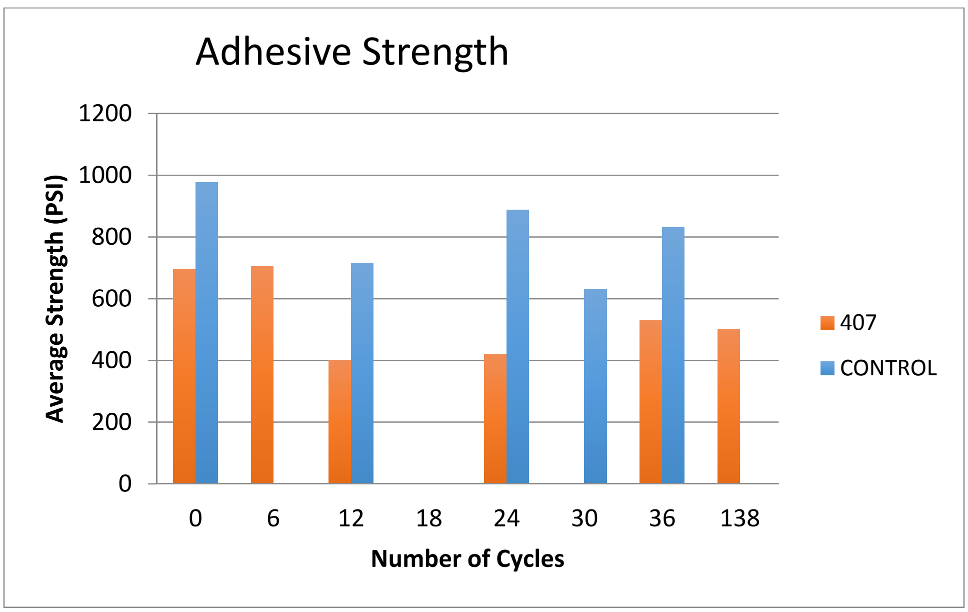

Figure 6-28: Beam 407 Results

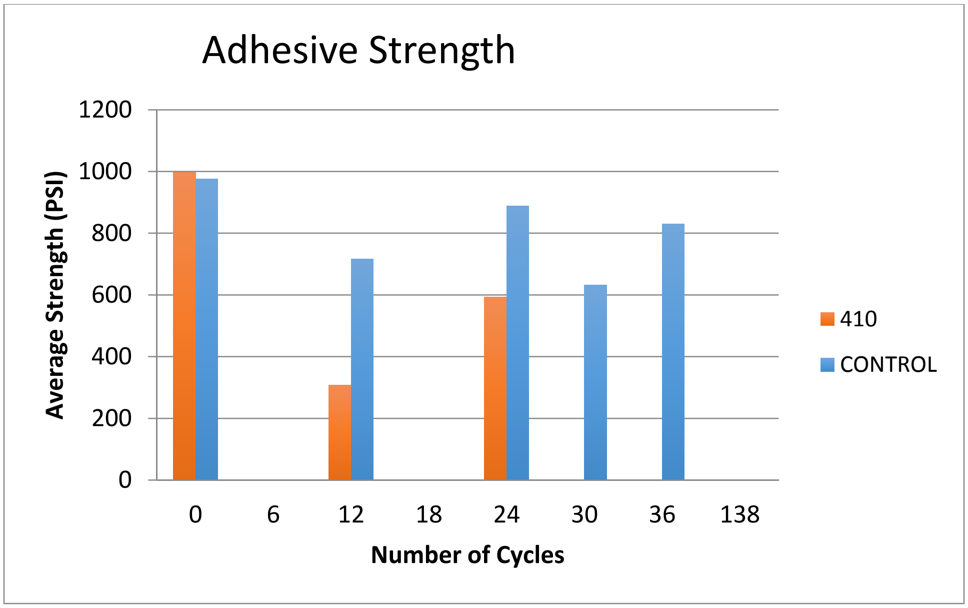

Figure 6-29: Beam 410 Results

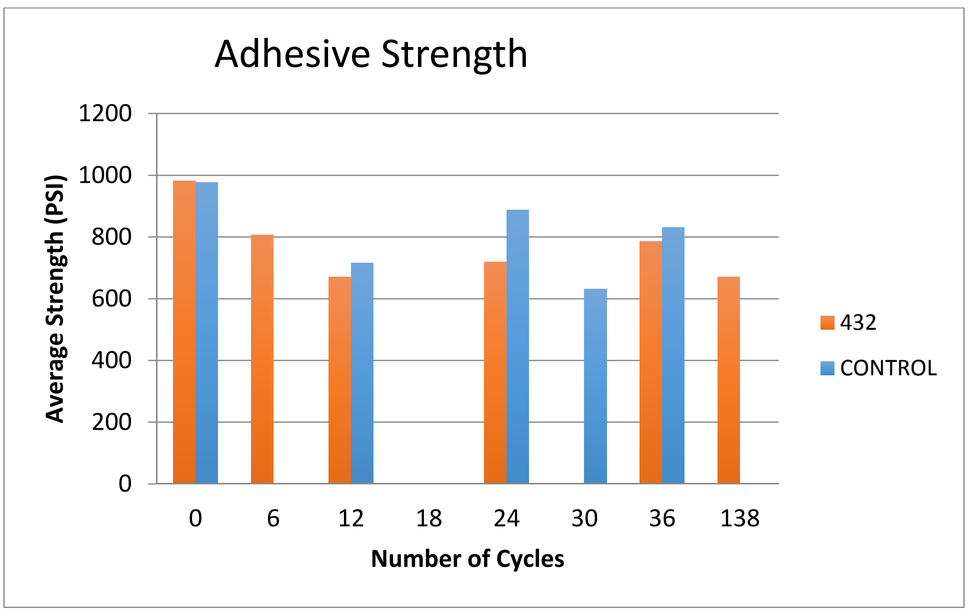

Figure 6-30: Beam 432 Results

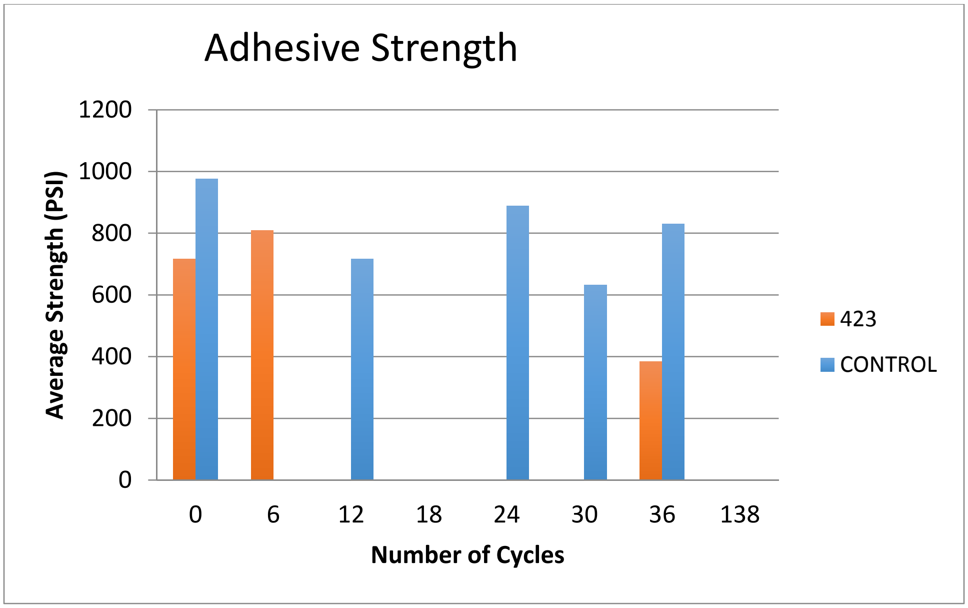

Figure 6-31: Beam 423 Results

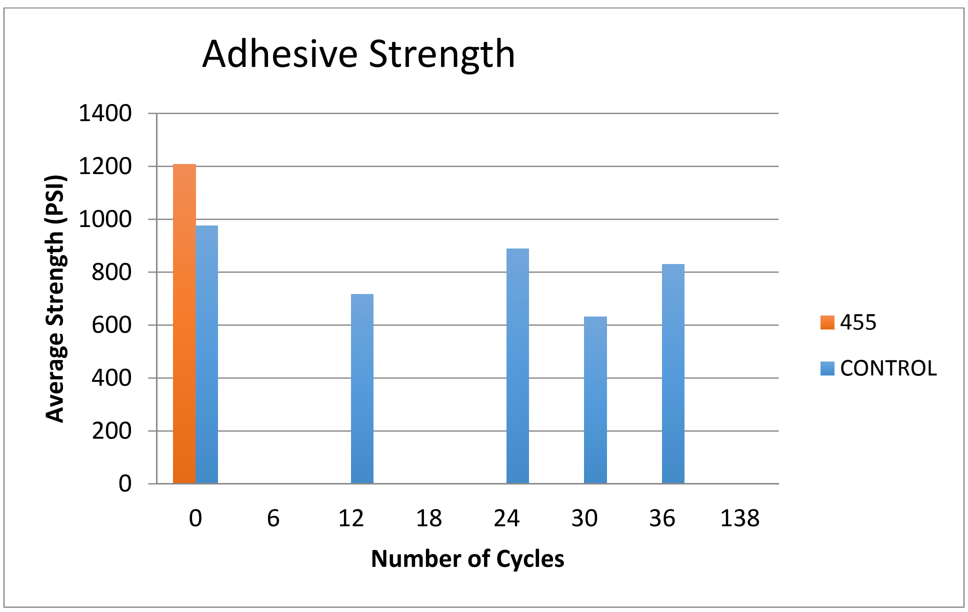

Figure 6-32: Beam 455 Results

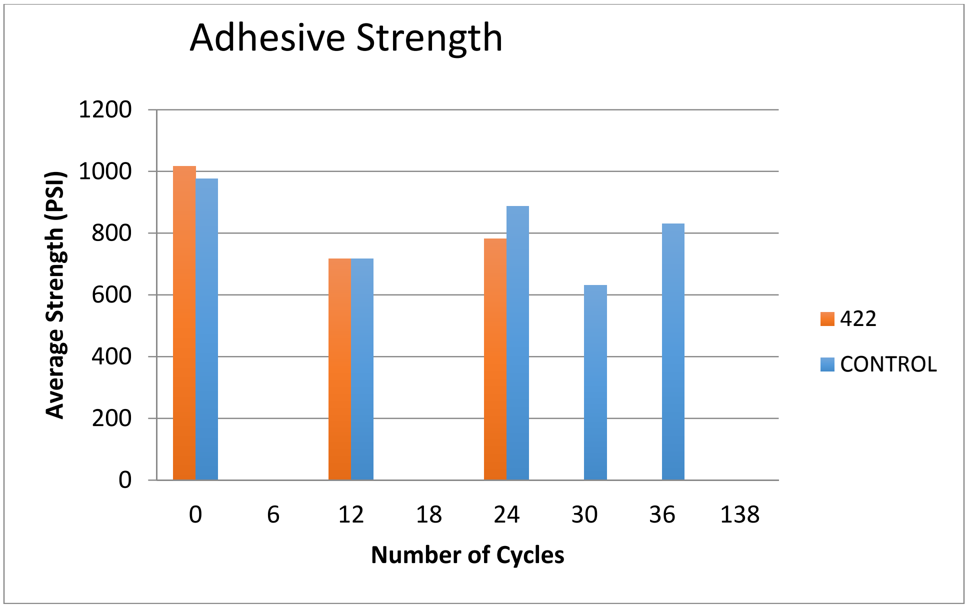

Figure 6-33: Beam 422 Results

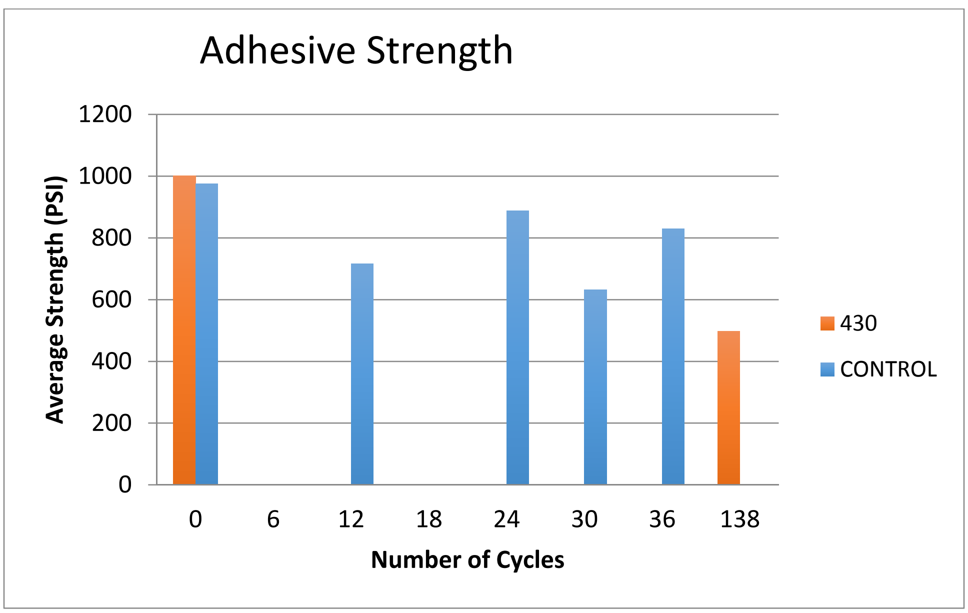

Figure 6-34: Beam 430 Results

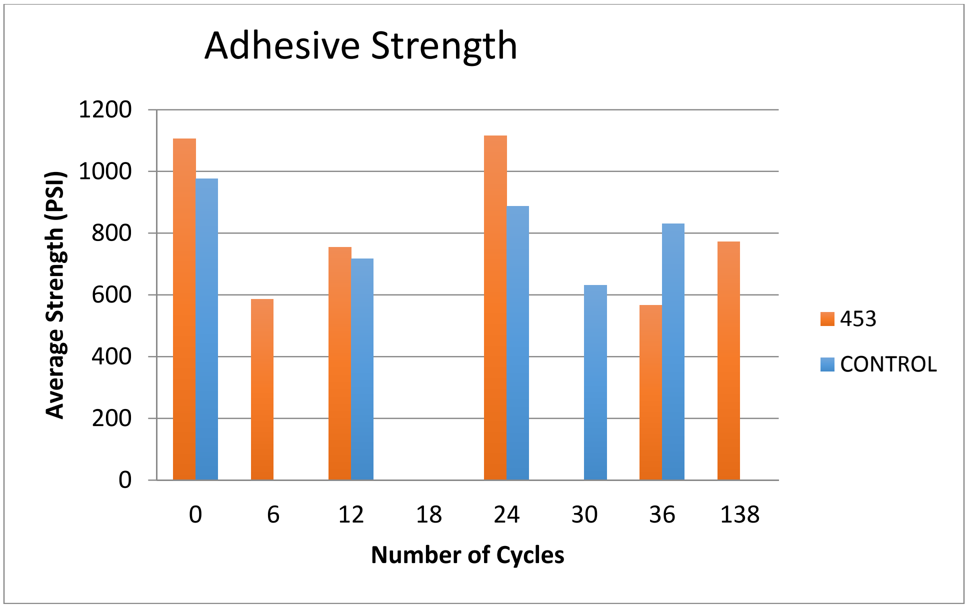

Figure 6-35: Beam 453 Results

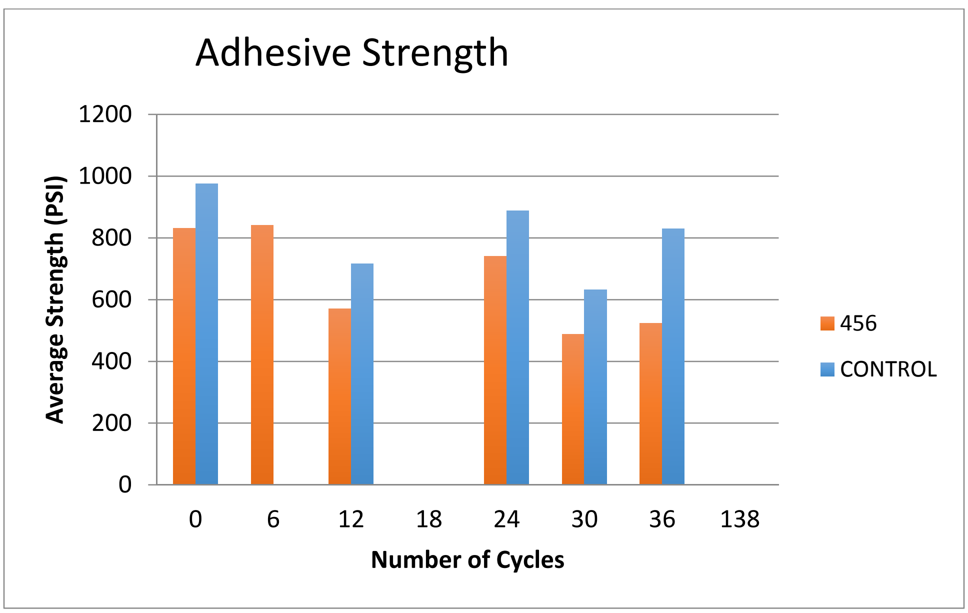

Figure 6-36: Beam 456 Results

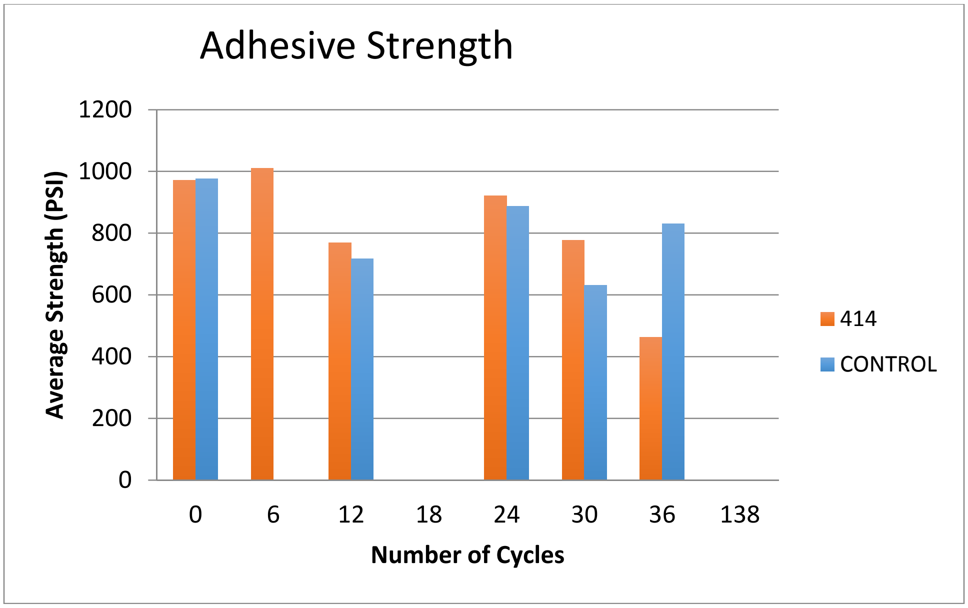

Figure 6-37: Beam 414 Results

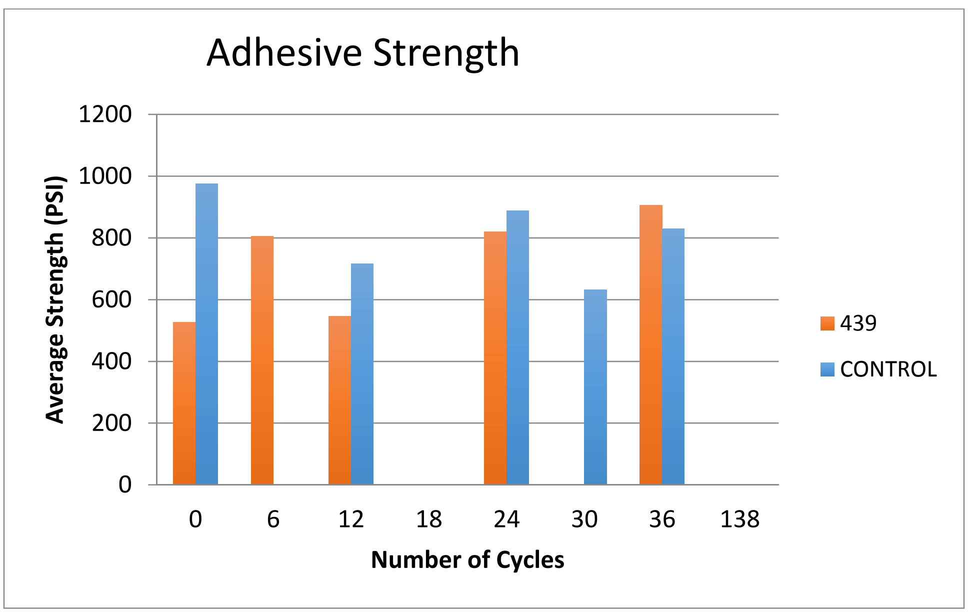

Figure 6-38: Beam 439 Results

6.9 Wetting Test Interpretation

Wetting durability took a toll on the repair material and provided valuable data about the behavior of the aluminosilicate material. The experiment also proved difficult for the adhesion test as well with over 18% of the samples succumbing to epoxy related failures. This was attributed to the presence of water vapor which may have weakened the organic polymer bond. It is proposed that the drying period, especially before attaching the dollies, be lengthened to allow the specimen to completely dry. Tests should be performed to determine the percent saturated that might affect the epoxy bond. In the ASTM specifications for adhesion testing of coatings, epoxy related failures are to be omitted from the data as they are considered equipment and procedure related failures and not representative of the coating or substrate. This led to the omission of all of Mix E3 data and one of the data points from Mix E2.

It was noticed that while the use of the nano-aluminosilicates in the thermal tests seemed to have slight edge over the other mixes, the nano-particle mixes (Mix E4) did not fare well in the wetting tests. Nano-particles may form a barrier against water infiltration but this mechanism may also prevent the escape of water during equilibrium and cause stresses to form in the substrate and coating interface.

While all tests performed badly, the end adhesion strength still met with the minimum specifications for a delamination repair material. The mix design that had the least degradation was Mix E1. The data was also inconclusive with regard to the effect of mixing speed and curing temperature on the durability which corresponded with the strength tests portion of the mix design.

6.10 Summary

The following conclusions are drawn from the durability testing:

Freeze/Thaw cycling:

- The thermal tests were not a significant source of conclusive data possibly due to the relatively short length of the total cycles. Greater results may occur from combining the wetting tests with the thermal cycling or by increasing the test cycles.
- While Mix E4 slightly outperformed Mix E1, Mix E1 was recommended for the final design due to its inexpensive material costs and universal availability of ingredients.
- The use of the 29,000 rpm mixer in conjunction with the 120°F curing temperature resulted in substantially more coating related failures than the 3,000 rpm mixer and the room temperature cured coatings.

Wet/Dry cycling:

- Wetting tests provided valuable information on the effects of environmental conditions on the inorganic coating. However, as the specimens became more water-logged, the time for drying should be increased in order to provide better adhesion for the test dolly. Many tests featured epoxy related failures which excluded the use of that data.
- Though not by a very high margin, Mix E1 performed slightly better than the rest of the mixes and was recommended for the final mix
- The data was inconclusive regarding the type of mixer and the curing temperature for wet/dry testing.

CHAPTER 7 - HIGH TEMPERATURE APPLICATIONS

7.1 Introduction

Since one of the original applications for the aluminosilicate polymer was as a fire resistant material and coating, an investigation of the ability of the coating to operate in that capacity is given. While the specifications for a delamination repair material do not indicate that fire resistance is a requirement, fire/heat resistance data is important for two reasons: to give additional knowledge about the durability of the material and because the inorganic matrix can be used in other bonding scenarios which may be susceptible to fire damage.

On Friday, July 28, 2006 at about 3 pm, a tanker truck carrying an estimated 7,600 gallons of diesel fuel overturned on the Bill Williams River Bridge between Parker and Lake Havasu City in Arizona. The fire damage to the prestressed concrete girders and concrete deck reduced the long-term inventory ratings by about 30% and the operating ratings just over 20% of the original design (Davis, Tremel and Pedrego 2008). If the bridge had been coated, repaired or strengthened with the inorganic aluminosilicate composite, the rating reduction may have been less.

The strength of reinforced concrete beams is a function of the compressive strength of the beam and the tensile strength of the reinforcing bars. In cases where the service loads of a beam are to be increased, a cost effective and efficient method of increasing the load capacity of the beam is found by bonding carbon fibers to the tensile face of the beam. In addition, beams can be repaired in the same manner if the integrity of the steel reinforcing layer is in question. The increase in capacity or repair of the beam has been found to be a realistic alternative to replacing the beam and also allows the designer to retain head room or floor space due to the small thickness of the carbon layer (Balaguru, Nanni and Giancaspro 2009).

While the behavior and analyses of carbon FRP repaired concrete structural elements abound, there has not been very much data on how these special structural components behave under extreme events including high temperatures usually associated with fire. Typical repair methods include an externally applied carbon fiber repair system bonded to the concrete with some variation of an organic based polymeric epoxy. This system functions well to transfer the structural stresses from the concrete to the much stronger and protective carbon fibers, but it does not respond well to high temperatures and the FRP layer typically debonds from the concrete tension face in temperatures in excess of 200°F. For this reason, the ACI Guide for the Design and Construction of Externally Bonded FRP Systems for Strengthening Concrete Structures recommends using the unrepaired load capacity for service loads in fire conditions (ACI Committee 440 2002).

Some of the experimental studies that are available regarding the fire behavior of FRP strengthened concrete members do not explore the application of inorganic matrices or the systems are only practical if a protective insulation layer is added to the FRP layer. In the tests performed by Kodur and Ahmed, four rectangular RC beams were strengthened with FRP using an organic epoxy and then tested under both a specific design fire and ASTM E119 standard fire using a 50% nominal capacity two point load. The beams in these tests also featured a vermiculite-based insulation (Kodur and Ahmed 2011). The variations of the mid-span deflections are shown for each beam in Figure 7-1 and show a failure of the insulation and debonding of the FRP layer in Beam 3 at about 30 minutes.

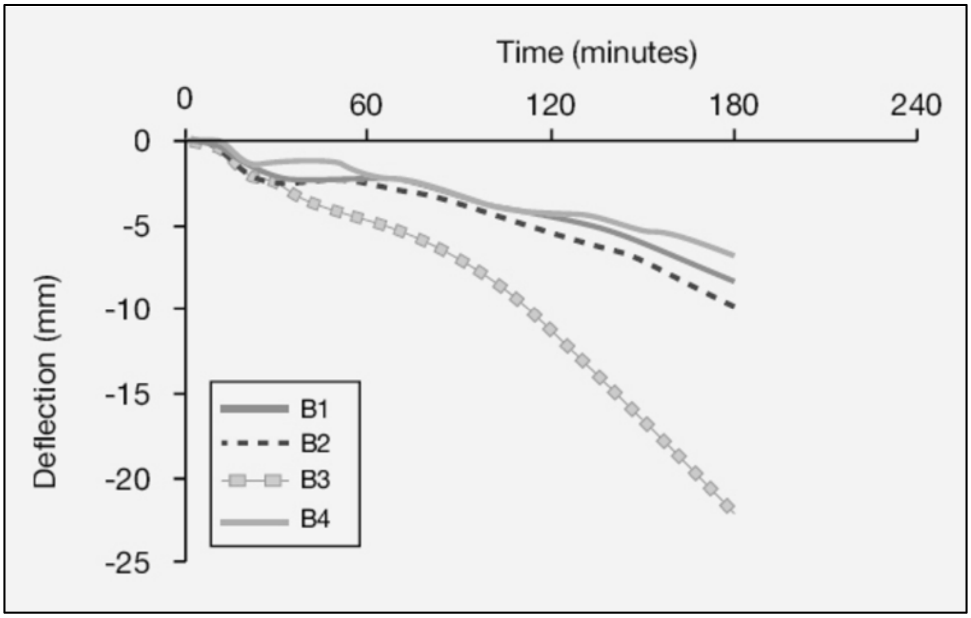

Figure 7-1: Mid-Span Deflections (Kodur and Ahmed 2011)

In tests performed by Green and Williams et al., two T-beams were constructed, reinforced with FRP and organic epoxy and also insulated with a vermiculite-based (VG) insulation. The beams were subjected to ASTM E119 standard fire with successful four-hour rating only due to the insulation layer (Williams, et al. 2005). The conclusions of both of these tests were that an insulation layer is imperative to utilizing the strength of the FRP layer and also discussed the optimal insulation arrangement.

Based on some initial research done in Australia, it seems plausible that if a system is used incorporating an inorganic bonding agent, which is largely unaffected by heat, the carbon fibers will be bonded to the concrete throughout the extreme event (Hashemi and Al-Mahaidi 2008). The theory, set-up, and execution of heat tests performed on several carbon FRP repaired concrete beams are described.

7.2 Initial Tests

Six beams were cast and tested for their stiffness behavior under high temperature conditions. The beams featured carbon fibers in different amounts that were adhered to concrete beams using the inorganic epoxy mentioned in this dissertation. The beams were then tested in third-point loading in flexure with a single heat source applied to the carbon fiber strengthened face. The heat source was capable of up to 955°F and covered the middle 6 inches of the beam (see Figure 7-2). The loads were monitored throughout the test using a USB load cell. Loads were applied statically using a screw jack at either end of the beam to exert 2.5 kips for a total of 5 kips on the beam. Once the load had stabilized after the initial jacking, the heat was applied. During the test on the first beam, the load dropped dramatically during the heat application and it was concluded that the inorganic epoxy had failed. However, upon inspection of the tensile face under the heat source, no damage was found. This trend continued through all beams no matter the type or amount of carbon reinforcement and whether the reinforcement was insulated or not.

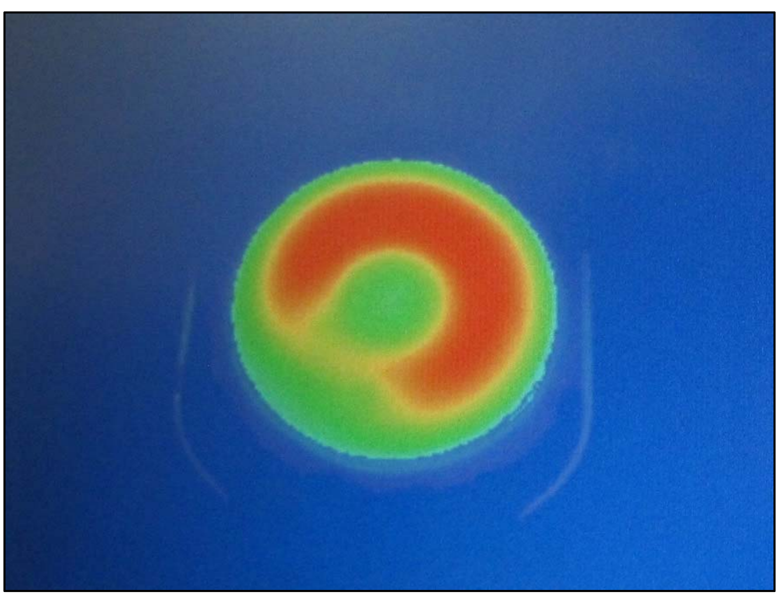

Figure 7-2: Heat Distribution in Initial Heat Source

During the testing of the last beam, however, the load cell data was collected over the period from applying the heat source to removing it and allowing all loads to equalize. Here an important discovery was made: the beam regained almost 100% of the original pre-heated capacity! Since the equipment to simultaneously monitor loads and deflections were not available, a finite element model was generated using classical heat transfer theories to estimate the temperature gradient across the cross-section of the beam. Using this data, virtual work methods were applied to find the deflection of the beam due to the heat differential. Since the beam was statically loaded, meaning that the deflection of the beam could not change due to its being held rigid in the steel load frames, the corresponding load was calculated. This load was presumed to be the “lost” load in the test that was initially thought due to a failure in the adhering properties of the inorganic matrix.

A set of confirmation tests were developed to prove whether the application of the finite element model and virtual work methods were correct in showing that the beam does indeed only change in the load due to the temperature gradient or if the carbon fiber strengthening is compromised. Five of the six original concrete beams were tested which included varying amounts of fiber reinforcement including carbon mats and individual tows and included one unstrengthened control beam. The instrumentation of the confirmation tests included two load cells and three displacement sensors connected to a computer via USB to monitor the loads and deflection. In addition, an infrared camera was used to capture the temperature gradient and store the data digitally for further analysis.

7.3 Confirmation Tests

The second round of tests, referred to as confirmation tests, include a deflection recording setup to log the deflections at the ends and in the center. Thermal imaging is used to record the temperature gradient surrounding the heated area. All tests are performed from zero load to 60% ultimate capacity and a return to the initial temperature after the heat tests to verify thermal stiffness reductions during the heat event in three cycles to provide an unbiased results spectrum. Note that the same beams were used for both tests and therefore the materials, test specimens, and basic procedure apply. The only difference is that full instrumentation is used including infrared camera, two load cells, and three displacement gauges. In addition, a different heat source is used: one that can deliver uniform heat and offer consistent temperatures. The load frame and set-up is the same as well.

7.4 Materials

The target compressive strength for the concrete design was 5000 psi. The standard normal weight mix was designed using ACI 211 by the weight method. Fine aggregates had a fineness modulus of 2.53 and the dry-rodded unit weight (DRUW) of the coarse aggregates was 97.2 lb/ft^3. No air entrainment, water reducers, super-plasticizers or pozzolans were used in the mix. A target water-to-cement (w/c) ratio was set at 0.48 and the target slump was between 3 and 4 inches. At the day of testing the moisture content in the fine aggregates was 2.4% and the coarse aggregates were 2.67%. The total amount of concrete required for the six beams, compression cylinders and waste was found to be 0.53 cubic yards. The beams were cast one at a time due to the size constraints on the mixer. The actual 28-day compressive strength averaged about 7,000 psi. Young's

Modulus tests were also performed with a result close to the expected $57{,}000\sqrt{f'_c} = 4.8$ Msi at 5.3 Msi. The mixture proportions are shown in Table 7-1.

Material	Weight	
Water	317.88	lb/yd^3
Cement	802.08	lb/yd^3
Coarse Aggregate	1312.31	lb/yd^3
Fine Aggregate	1407.73	lb/yd^3

Table 7-1: Heat Beam Concrete Mix Proportions

The fibers were supplied by Zoltek and were the Panex 35 k tow product line which featured a tensile strength of 550 ksi and Young's modulus of 35 Msi. The fibers were bonded to the concrete beam using the inorganic alkali aluminosilicate system.

7.5 <u>Test Specimens</u>

The setup is divided into two separate components: the repaired concrete beams and the test jig. The concrete beams were prepared to for a third-point loading system. This type of system is made of two reaction points and two load points all equidistant from each other. When loaded, the beam undergoes areas of shear and moment stresses at the outer regions and a central pure moment area as shown in Figure 7-3. The pure moment section features tensile stresses on the bottom and compressive stresses on the top. Carbon FRP's are added the extreme tensile fiber of the concrete to strengthen the beam.

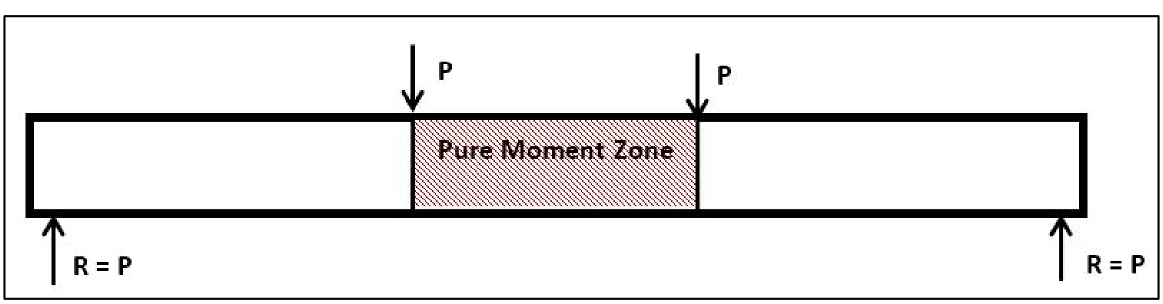

Figure 7-3: Third-Point Bending

The dimensions of the beams are 4 inches wide, 8 inches tall and 96 inches long. Reinforcement was added to satisfy ACI 318 and resulted in two #3 60 ksi flexural bars and #2 80 ksi smooth double-leg stirrups 3 inches on center throughout the shear zones on either end. The stirrups were continued through the moment zone at 7 inches on center. Two #2 80 ksi smooth bars were used as hangars to provide stability to the reinforcement cage. Concrete cover of 3/4 inch was provided for all bars. Refer to Figure 7-4 for the CAD drawings.

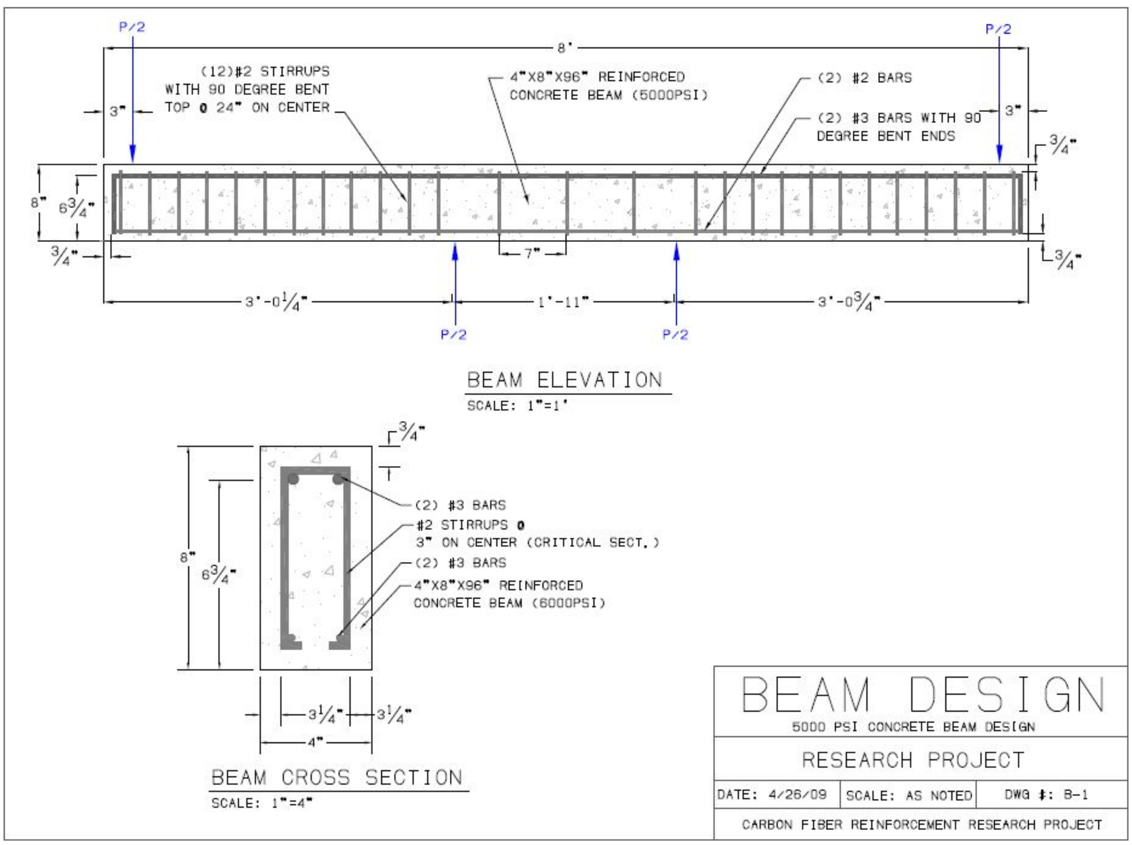

Figure 7-4: Heat Beam Dimensions

As mentioned earlier, target compressive strength was set at 5,000 psi, however the actual compressive strength taken from 6 by 12 inch compressive strength cylinders from the same concrete that the beams were cast at 28 days was about 7,000 psi. When adjusted for the new compressive strength, the experimental moment capacity of the unrepaired beam is 7,210 lb·ft, giving a maximum load of 2,510 lbs. The cracking moment was found to be 2,230 lb·ft and expected to occur at a load of 776 lbs or 388 lbs at each reaction location. The beams were strengthened without any external load resulting in an increased moment capacity. The amount of repair reinforcement was varied from two layers of 0/90 carbon fiber mats to eight carbon tows (4 tows per layer) to sixteen tows. The variation in reinforcement resulted in different stiffnesses and slightly different deflections through a range of 0.22 – 0.25 inches at the target experimental load of 2,500 lbs.

Once the beams had cured for 28 days, the carbon fibers were attached to the tension face of the beam. Since the beams to be loaded in an inverted position, the tension face was on the top side. The fibers were fixed to the top face using the inorganic matrix. The matrix was spread on the surface and then the tows or mats laid into the mixture. Using a ribbed roller, the fibers were worked into the matrix. The mat fibers were the most difficult to penetrate with the matrix due to the density of the fiber placement. Once the fibers were completely saturated with the matrix, the excess was squeegeed off. The single layer was allowed to cure before the next layer was applied.

Figure 7-5: Glass Bead/Cement Polymer Insulation

Though related to the preparation of the samples, the insulation layer was not added until the first beam had been tested (see Figure 7-5). During the first test, it was noticed that the composite layer developed cracks in the matrix. Concern for heat overexposure while the matrix was not fully cured led to the addition of an insulation layer for half of the beams. In addition, the difference in behavior between an insulated and noninsulated beam could be investigated. The insulation layer composition was composed of the original bonding matrix with about 10% insulating material. The layer was formed to a 1/4 inch thickness and applied to the composite layer in the pure moment zone as shown in Figure 7-3. A summary showing the fiber configuration and the insulation layer is shown in Table 7-2.

Beam Number	Fiber Layers	Fiber Configuration	Insulation Layer
0	0	Control	No
1	2	Mat	No
2	2	4 tows per layer	No
3	4	4 tows per layer	No
4	3	4 tows per layer	Yes
6	4	4 tows per layer	Yes

Table 7-2: Heat Beam Design Summary

7.6 <u>Testing Equipment</u>

The test jig consists of two reaction frames at either end of the beam. The load is located at either side of the middle two-thirds of the beam and are formed of two steel reaction cubes. The frames, referred to as the reaction frames, are so named because of the usual location of the reaction is applied at these points. (The beams are positioned upside down to expose the tension face to the heat source.)

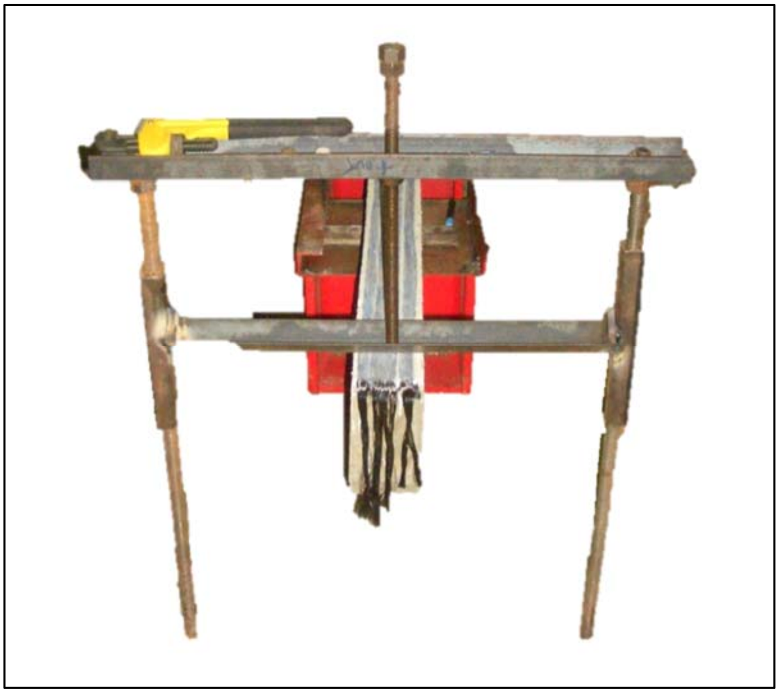

Figure 7-6: Screw Jack Loading Frame

The frames consist of two 3/4 inch all-thread columns forming an upside-down “U” with a 4 inch square tube as the header/beam (Figure 7-6). This header features through holes for the ¾ inch columns to pass through and the header is held in place with a 3/4 inch nut above and below. The ¾ inch columns thread into the connections of the structural reaction floor in the testing laboratory. The load head is comprised of a L2 x 2 x 1/8 inch single angle oriented so the apex is facing downward. The load is applied to the load head using a 3/4 inch all-thread that is threaded to the center of the square tubing header where a nut was welded to the bottom. When the 3/4 inch drive all-thread is rotated, it exerts a force in the inside bottom of the “V” of the single angle, which is in contact with the beam as a screw jack. The load head is held in position laterally and rotationally by 8 inch long sliding pipes welded at either end of the single angle perpendicular to its long axis. Service load of the critical section (limited to 1/100 of an inch deflection), the 4 inch square tube header, is 6 kips which is much greater than the specified load of 2.5 kips.

The reaction cubes are standard lab beam testing equipment. The precise reaction load location is adjusted by moving the reaction plate in the top of the reaction cube.

Heat is applied to the top side (tension face) of the repaired RC beam. The heat was provided by two 1-1/2 inch wide stainless steel strip heaters. The strip heaters are capable of up to 1,200°F temperatures though actual measured temperatures approached 1,400°F. The heater completely straddled the tension face of the beam and was fastened loosely using mending plates and all-thread to keep the heater snug against the surface and avoid movement. Temperature monitoring was provided through the use of a FLIR A325sc infrared digital camera. The resolution of the camera is 320 by 240 pixels and with the use of a 45° lens and an offset of 48 inches equates to 1/8 inch resolution on the side of the beam.

Using USB interface recording equipment, both the temperature and load inputs were logged electronically. A 10 kip load cell was located at each reaction frame to provide feedback on the jacking of each head. Three displacement sensors were used: one at each screw jack/reaction frame and the other in the center. The load and displacement data were logged automatically by a computer acquisition program authored by LoadStar Sensors. The infrared camera data was logged using FLIR's ExaminIR software and used the computer's Ethernet port for the digital data streaming.

7.7 Testing Procedure

Six beams were tested to find the integrity and behavior of the inorganic carbon composite performance in order to provide increased load capacity under extreme high temperature events. The loads, deflections and temperature gradients were recorded.

From this information, the change in deflection and stiffness were determined to find whether the increased deflection under high temperature is due to failure of the inorganic matrix bonding the carbon to the concrete or a function of the decreased stiffness from the temperature gradient expansion and softening. The test setup featured two strip heater heat sources, infrared temperature monitoring and USB connected load cells and dial gauges. The reason for the test with the advanced equipment was to isolate suspected variables from the first test. Recall that in the original tests, the temperature gradient was estimated using heat transfer finite element theory. This was because the load data suggested that the addition of heat decreased the load capacity of the beam. However, the FE model indicated that the decrease in load capacity could be due to decreased stiffness from the temperature gradient. In these tests, the deflections, loads and temperature gradients were all measured simultaneously to distinguish deflections by heat gradient and those by damaged carbon fiber tensile reinforcement.

The beams were loaded into the testing apparatus upside-down to expose the bottom tensile face where the reinforced concrete (RC) beam was strengthened with carbon fiber composite. The reaction frames were located two inches from each end and the load frames were positioned at L/3 corresponding to 30-2/3 inches from each reaction frame. The beam was centered in the testing jig and the load head lowered into position at the reaction location two inches from each end. Initial deflection readings were noted and the data acquisition devices connected to a computer. The screw jacks were engaged to provide approximately 2.5 to 3 kips which is greater than the cracking load of 0.875 kips effectively loading the carbon fiber reinforcement. The jacks were loaded simultaneously to keep all loads and reactions equivalent and were verified by comparing the data on displayed on the computer. Since the jacks were loaded by hand, it was difficult to maintain a consistent loading rate so a standard rotation method was employed. The screws were turned 1/4 turn at a time and then the system allowed to stabilize before continuing. The load cells provided stabilization feedback.

7.8 Initial Test Analysis

The following section outlines the assumptions and calculations made during the initial tests. In order to calculate the deflections and produce a model of the strengthened beam, the cracking moment of the doubly reinforced rectangular beam must be found. When a concrete beam is loaded in flexure, the tensile zone cracks. Once the concrete cracks, the deflections must be found using an effective moment of inertia, I_e, in the calculation of the beam stiffness. The cracking moment is found using the modulus of rupture which then can be used to find the load at which the cracking moment occurs. The equations for cracking moment, M_{cr}, and the resultant cracking load, P_{cr}, are shown for the loading condition featured in Figure 7-7:

$$M_{cr} = \frac{I_g}{h - \bar{y}} \cdot f_r \qquad (7.1)$$

Where I_g is the gross moment of inertia

h is the height of the beam

$\bar{y}$ is the distance to the neutral axis

f_r is the modulus of rupture

$$P_{cr} = \frac{M_{cr}}{k \cdot L} \tag{7.2}$$

Where k is the dividing factor for the span

L is the span

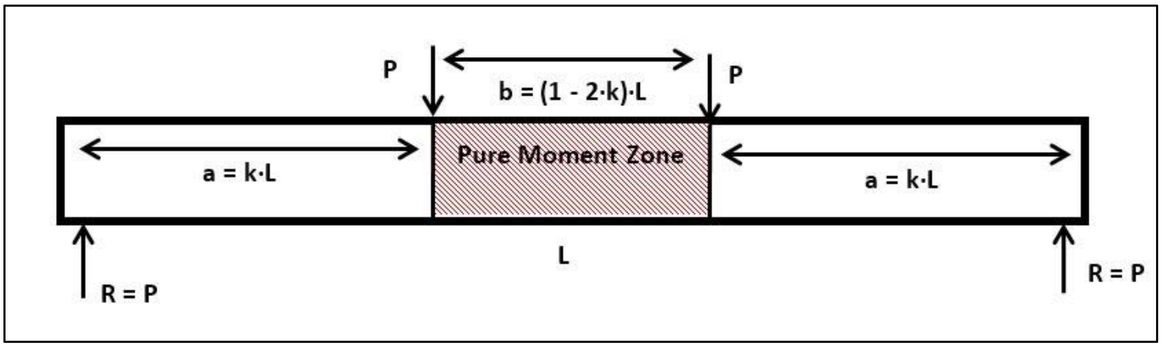

Figure 7-7: Beam Notation

The reason the deflections are so important to find in these tests is to develop the equation for the equivalent loads that are lost to the beam during the heating. Since deflection of the beam is constant due to the static loading, the only way to determine if the loss of load during the test is caused by the temperature gradient is to find the resultant deflection from the change in temperature. Then the deflection can be used to find the load resulting from that deflection. This change in load should match the experimental value. The deflection of the strengthened doubly reinforced concrete beam is given as a function of the cracked moment of inertia, I_{cr}:

$$I_{cr} = \frac{b(kd)^3}{3} + nA_s(d - kd)^2 + (n-1)A_s'(kd - d')^2 + n_f A_f (h - kd)^2 \tag{7.3}$$

Where b is the width of the beam

kd is the depth to the neutral axis

n is the ratio of the steel modulus to the concrete modulus

A_s is the total area of steel tension reinforcement

d is the distance from the extreme compression fiber to the centroid of the tension fiber

A'_s is the total area of the steel compression reinforcement

d' is the distance from the extreme compression fiber to the centroid of the compression steel reinforcement

n_f is the ratio of the fiber modulus to the concrete modulus

A_f is the total area of the fiber reinforcement

Then the effective moment of inertia is found as follows:

$$I_e = I_{cr} + \left(I_g - I_{cr}\right)\left(\frac{M_{cr}}{M}\right)^3 \quad (7.4)$$

Where *M* is the moment at which the deflection is being evaluated

Finally the deflection, δ, is found for the beam:

$$\delta = \frac{P \cdot L^3}{24E_c \cdot I_e} \cdot k(3 - 4k^2) \quad (7.5)$$

Where E_c is the concrete modulus of elasticity

Now the deflection due to a temperature difference is found using the principle of virtual work. A virtual unit load is applied at the point that the displacement is to be found resulting in a virtual internal moment. The deflection, Δ_{Cv}, can be found as follows:

$$1\ lb \cdot \Delta_{C_v} = \int_0^L \frac{m \propto \Delta T_m dx}{c} \tag{7.6}$$

Where m is the internal virtual moment

α is the coefficient of thermal expansion (taken as 5.70 x 10-6/°F for concrete)

ΔT_m is the difference between the average temperature and the temperature at the top or bottom of the beam

c is the mid-point of the beam

Since the temperature was only recorded at the heat source, the temperature gradient is estimated using a finite element model (Holman 2002). The model used is the type where a heat source is applied to one face and all other faces are open to ambient temperatures as shown in Figure 7-8. The numbered circles correspond to the nodes in the model along the cross-section at the mid-point directly under the heat source and at the outer nodes.

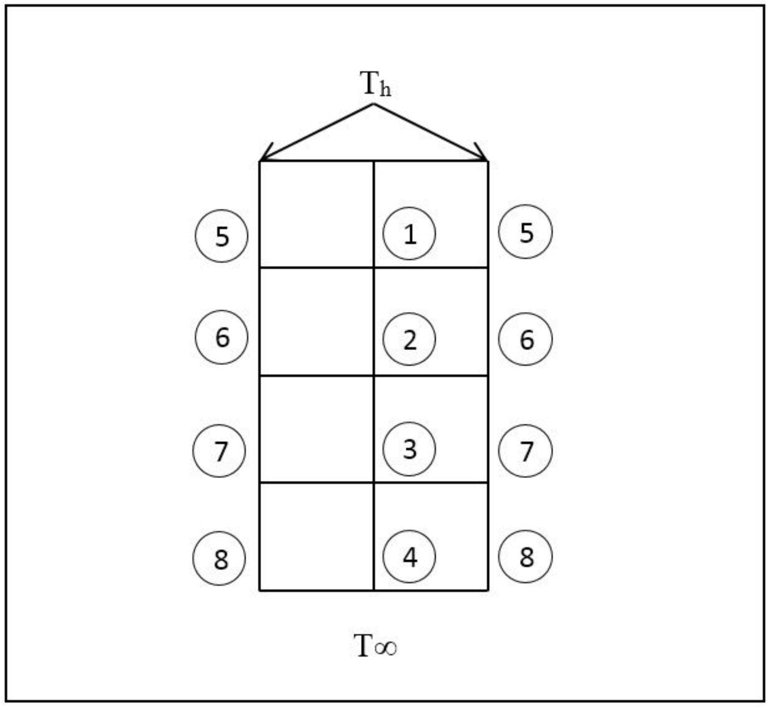

Figure 7-8: Finite Element Node Designation

So for the internal nodes (1 – 3), the equation is:

$$T_{m+1,n} + T_{m-1,n} + T_{m,n+1} + T_{m,n-1} - 4T_{m,n} = 0 \qquad (7.7)$$

And for edge nodes (4 – 7), the equation is:

$$T_{m,n}(A+2) - B \cdot T_{\infty} - \frac{1}{2}\left(2T_{m-1,n} + T_{m,n+1} + T_{m,n-1}\right) = 0 \qquad (7.8)$$

And for the corners (Node 8), the equation is:

$$2T_{m,n}(A+1) - 2B \cdot T_{\infty} - \left(T_{m-1,n} + T_{m,n-1}\right) = 0 \qquad (7.9)$$

Where $B = \frac{h \cdot \Delta x}{k}$, $h = 10\frac{W}{m^2} \cdot$ °C and $k = 1.37\frac{W}{m} \cdot$ °C

These are developed for each node and then all eight equation solved simultaneously to yield the temperature at each point in Celsius. The values are converted to Fahrenheit and the average of bottom temperatures used with the average top temperature to find the equivalent load for the heat gradient.

7.9 Initial Test Results

Once all the data was recorded, graphs were created using time to synchronize the temperature and load values. The temperature data was converted to Fahrenheit. Calculations were made using the updated compressive strength to find each beam's cracking load. Using the peak load, estimates of the stresses in each material were generated and checked to confirm that maximum stresses were not exceeded in the concrete, compression reinforcement, steel tensile reinforcement or the carbon tensile reinforcement. By using the peak temperature for each beam and the thermal conductivity of the concrete, the temperature distribution over the cross-section of the heated portion were estimated using finite element analysis (Holman 2002). This temperature difference was used to find the deflection related to the temperature gradient using the principle of virtual work. Finally, the deflection was used to back-calculate the load that would be "lost" in due to the temperature softening, that is, the decreased stiffness. Also, the load is found to ensure that the maximum load is not exceeded during testing.

The only test where the temperature recording device was unavailable for data logging was the Beam 1 test so an infrared thermometer was used to approximate the temperature of the beam as seen in Figure 7-9. In this graph, the load was increased until about 2,500 pounds and then allowed to stabilize to about 2,400 pounds. The heat was added which triggered a decrease in load related to decreased stiffness. The test was continued until the load stabilized again which occurred after about 500 pounds less from when the heat was applied.

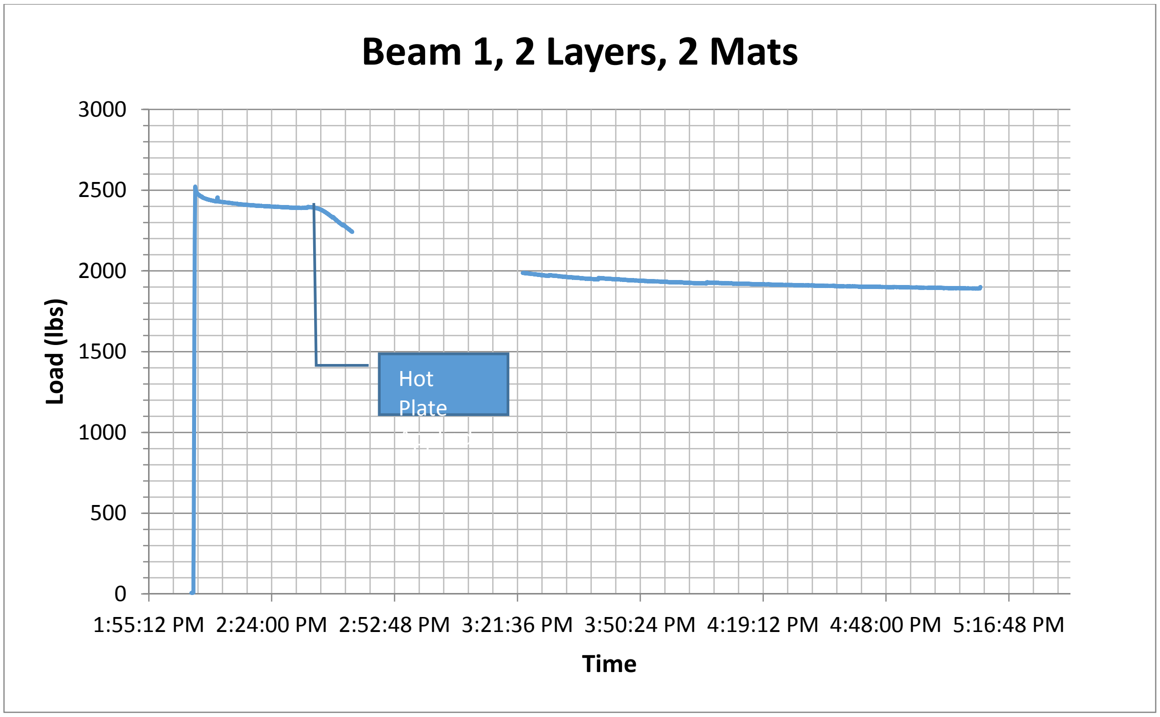

Figure 7-9: Beam 1 Initial Test Results

For the remaining tests, both the load and temperature data were written into the graph simultaneously show the correlation between the two variables. It was observed that the load loss lagged the temperature slightly at the heat source interface. Since the graphs are almost entirely similar for all beams, only Beam 2 graph is shown. It was also noticed that the same behavior occurred whether the beam was insulated or not. In each case, the beam lost about 500 to 600 lbs of load as shown in Figure 7-10.

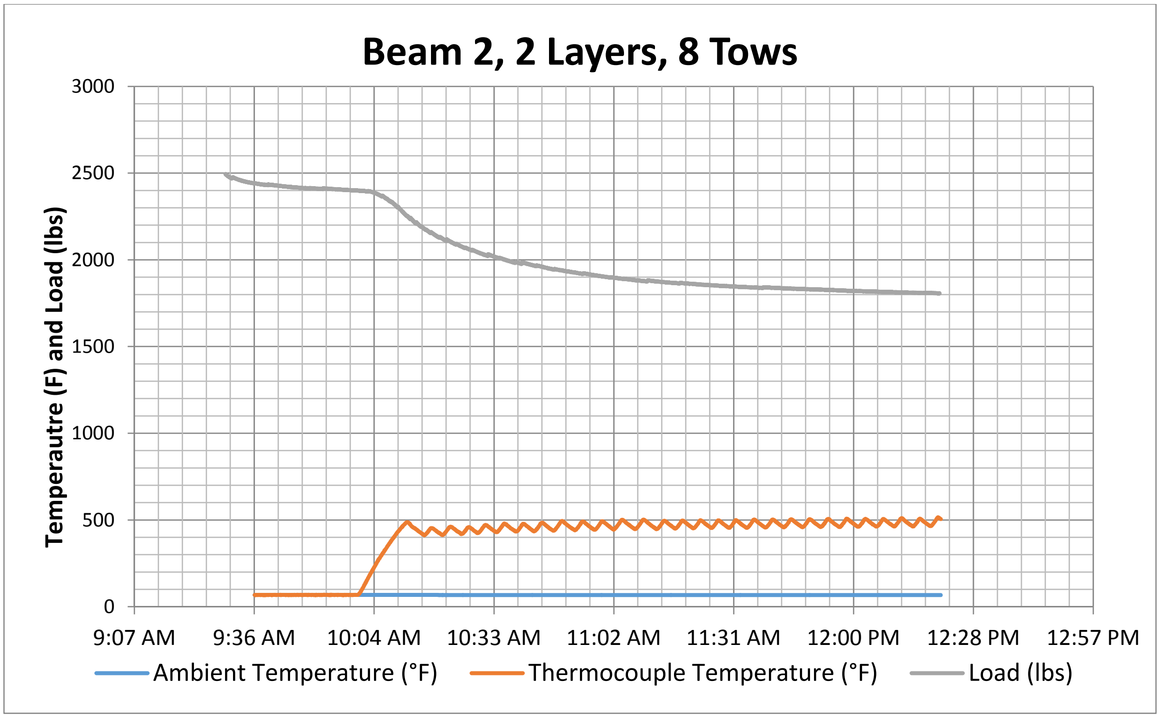

Figure 7-10: Beam 2 Initial Test Results

During the Beam 6 retest (static) the data loggers continued to collect information after the test was completed. In this test, the load dropped about 230 lbs but when the heat dissipated, about 150 lbs of load was recovered. This confirmed the theory that much of the decrease in load is due to decreased stiffness in the beam from the temperature differential across the cross-section (see Figure 7-11). The model developed for this beam showed a loss of load equivalent to 195.6 lbs.

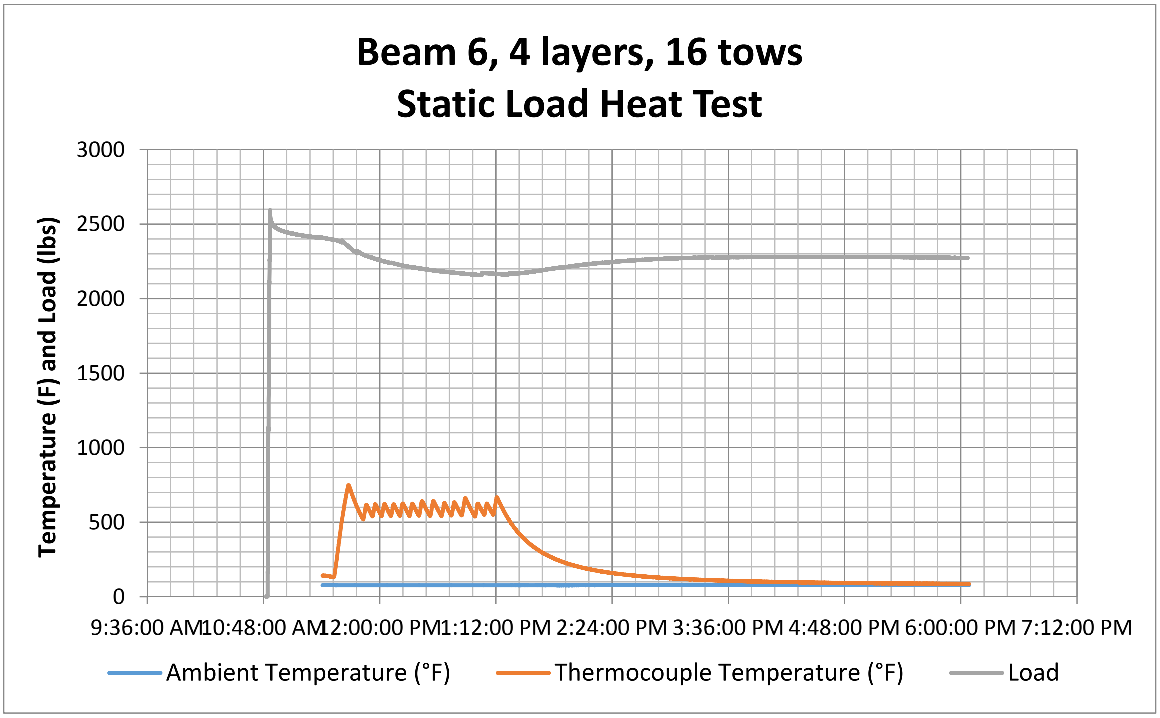

Figure 7-11: Beam 6 Initial Test Results

Similarly for Beam 6 retest (dynamic), the load initially dropped about 200 lbs, but regained almost 150 lbs as the heat was absorbed back into the environment as seen in Figure 7-12. Again, the part of the loss in load capacity that is regained as the beam returns to its initial temperature can easily be explained by the decrease in stiffness due to the temperature gradient. The FE model gives a decrease in load of 178.0 lbs for the beam 6 retest (dynamic).

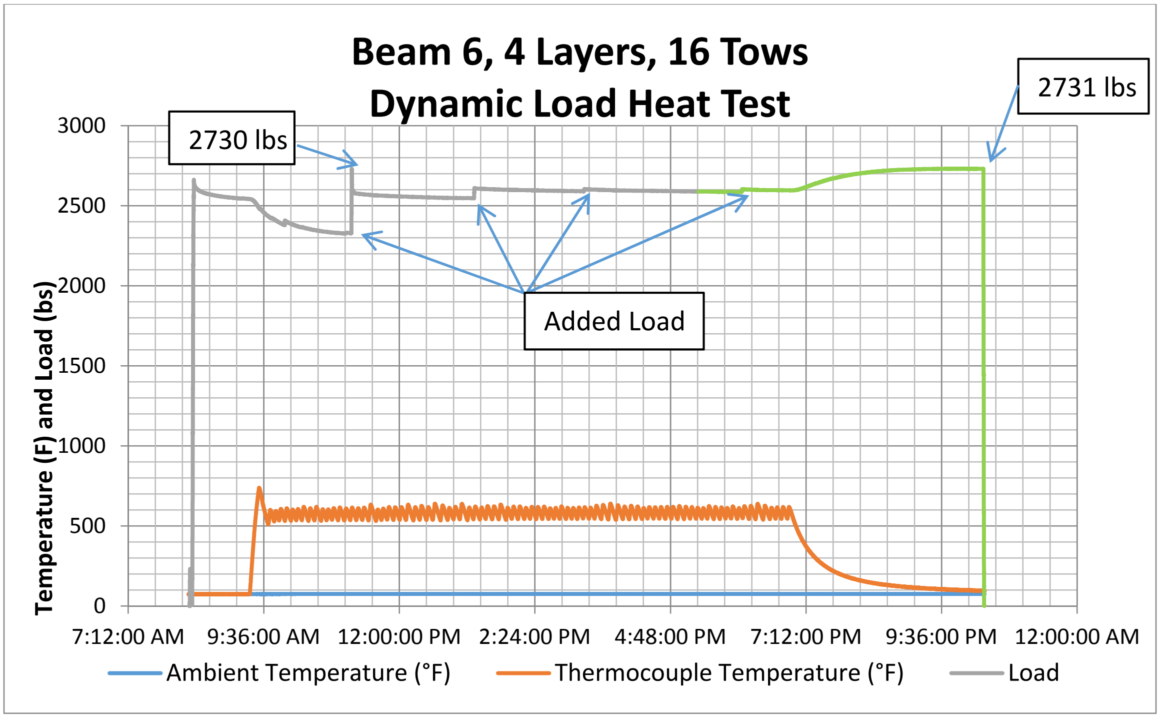

Figure 7-12: Beam 6 Initial Retest Results

The maximum moment (M_n), maximum load (P_n), unheated deflection (δ), deflection due to the temperature gradient (δ_T), and reduction in load due to decreased stiffness (ΔP) are shown in Table 7-3.

Beam	M_n (lb·ft)	P_n (lb)	δ (in)	δ_T (in)	ΔP (lb)
1	16038.54	5578.62	0.268	0.02645	214.44
2	12620.38	4389.70	0.289	0.02524	182.77
3	16168.62	5623.87	0.292	0.02658	220.06
4	14673.00	5103.65	0.282	0.01829	140.86
5	14673.00	5103.65	0.302	0.01761	137.37
6	16168.62	5623.87	0.290	0.01371	112.91
6 Static	16168.62	5623.87	0.276	0.02387	195.58
6 Dynamic	16168.62	5623.87	0.292	0.02152	177.96

Table 7-3: Initial Test Summary

From the information gathered, the inorganic bonding matrix performed well at temperatures well above 500°F. Despite the longitudinal cracks found in the composite layer, the expected loads and deflections corresponded well with the experimental results indicating a successful transfer of stresses between the interface. Even though the load capacity dropped during the heating phase, most of it was shown to be due to a decrease in stiffness by the temperature gradient in the cross section of the beam. Additionally, adding an insulation layer to the FRP did not affect the behavior of the inorganic bond in any noticeable way.

7.10 Confirmation Test Analysis

While the virtual work method of determining deflection due to a temperature gradient was a good start, there were several flaws. One was that neutral axis of the beam is located at the mid-depth of the cross-section. In reinforced concrete beams, the neutral axis is rarely at the mid-depth and this fact causes internal moment inconsistencies if the concrete beam in question is not a balanced failure. The other was that the temperature difference is assumed for the entire span of the beam. To estimate the deflection previously, the area of the virtual work equation was carried out only over the length of the beam where the temperature difference occurred, namely the heat source. However, the heat actually radiates outward and causes differential strain along a distance equal to the height from the heat source. This is because the temperature of the beam at the bottom equalizes with the temperature of the beam at the top at that point. While this may not be the ambient temperature, any strains caused by the increase is also increased at the top and is therefore cancelled out, not causing any curvature or loss of load to the beam. A more accurate way of finding the deflection due to the heat gradient is therefore presented.

The load-deflection responses are computed using elastic-beam theory and the design guidelines presented in the American Concrete Institute Committee 318 Code Provisions (ACI 318 2011). The process involves two steps: first, the flexural rigidity of the beam is compared with experimental results and the second is to use the result to find the deflection caused by the reduction of load due to the differential heating.

The flexural rigidity, or EI, is found in the same manner as in the initial test analysis using the cracked moment of inertia and gross moment of inertia. The deflection is calculated and compared to the experimentally obtained deflection for the same load. This confirms the rigidity of the experimental beams with the model for the second part computations.

The second part of the analysis involves a derivation of the moment area theorem for point source heating. When the top part of the beam is heated, curvature is induced due to differential expansion. The maximum temperatures measured in the top of the beam were around 950°F. Using a coefficient of thermal expansion of 5.70 X 10^{-6}/°F, the strain just underneath the heat source is between 0.003 and 0.0045 in/in for insulated and noninsulated beams respectively. Even though the temperature at the bottom of the beam is greater than the ambient temperature, the increase in temperature is found throughout the beam cross-section resulting in a net strain difference of zero and is therefore omitted. Using the infrared images, the lateral distance from the heat source along the top of the beam to the equivalent temperature at the bottom is found using the height of the beam as a calibration.

Using classical elastic-beam theory, where an internal moment deforms an element of the beam, the angle $d\theta$ is defined. The arc *dx* represents where the elastic curve intersects the neutral axis and the radius of curvature for that arc is given as ρ. In this case the "neutral axis" is defined as the lowest temperature measured directly under the heat source. Therefore, at the top of the beam, the element, which when there is no heat, is equal to a distance *ds*, but when heat is applied the element expands becoming *ds'* and the strain is defined as:

$$\epsilon = \frac{(ds' - ds)}{ds} = \alpha \Delta T \tag{7.10}$$

Since the materials involved are considered homogenous through the use of the ratio of the steel and fiber modulus to the concrete modulus of n and n_f respectively and the expansion behaves in a linear elastic manner, Hooke's law applies. Combining these concepts, gives:

$$\frac{1}{\rho} = \frac{\alpha \Delta T}{h} \tag{7.11}$$

Where h is the distance to the lowest temperature

Graphing this solution for each element *dx* along the beam from the maximum value obtained directly under the heat source produces a third degree parabolic spandrel. This graph is the equivalent of the *M/EI* curves used to find relative slopes and tangents in traditional structural analysis. Thus the moment-area theorems apply where the second theorem is applied to find deflection:

> "Theorem 2: The vertical deviation of the tangent at a point on the elastic curve with respect to the tangent extended from another point equals the "moment" of the area under the *M/EI* diagram between the two points. This moment is

computed about the point on the elastic curve where the deviation is to be determined." – Structural Analysis by R. C. Hibbeler

In this case, the *M/EI* diagram corresponds to the *αΔT/h* diagram. Since the beam is simply supported and symmetrically loaded with an equivalent point load, the compatibility equation to find the deflections is defined as the tangent of one support, *A*, with respect to the other support, *B*, divided in half minus the tangent at the midpoint, *C*, with respect to *B* as follows:

$$\Delta_C = \frac{t_{\frac{A}{B}}}{2} - t_{\frac{C}{B}} \tag{7.12}$$

And

$$t_{A/B} = \bar{x}\int_A^B \frac{\alpha\Delta T}{h}dx \tag{7.13}$$

$$t_{C/B} = \bar{x}\int_C^B \frac{\alpha\Delta T}{h}dx \tag{7.14}$$

The calculated deflections are then used in the deflection equation for a point load to solve for the resultant load that would be exerted in the same direction of the two load points. This accounts for the "loss" or reduction of load during the heat test. If the beam heat source were placed on the other side of the beam and the steel and fiber reinforcement left in the same position, the change in load would be a net gain.

7.11 Confirmation Test Results

The results consist of infrared images, load and deflection graphs and observations. In addition to the infrared images, videos were also recorded. The movies were recorded in Flir's own proprietary file extension and requires the use of the ExaminIR software. Once the file is loaded, all infrared information is displayed as a function of time. Thus, the heat gradient at any point during the test is recorded for additional editing and analysis.

This test was to provide confirmation that the temperature gradient is responsible for the reduction in load and that the carbon fiber strengthening remains intact during the high temperature test. The heat sources, capable of up to 1200°F are applied directly to the inorganic fiber composite layer and the load is monitored for changes. As was mentioned above, a reduction in load was detected in the earlier tests which brought the premature judgment that the carbon fiber layer had failed. However, one test (Beam 6) had the recording equipment continue after the original heat source had been removed and almost all of the load was restored to the beam. This led to the finite element analysis to determine if it was possible to recapture the heat load. The FE analysis proved that it was possible.

The results from calculations and experimental observations are presented in the table below (Table 7-4). The nominal moment, M_n, and resultant load, P_n, capacity are shown along with the deflection at that load, δ. The experimentally determined deflections, δ_{exp}, are shown along with the observed change in load, ΔP, during the heat cycles. The graphs for the loads and deflections of each beam including the control are shown. The calculated change in load, ΔP_{exp}, found using the moment area theorem is shown in the last column. The familiar sawtooth pattern is visible. The bottoms of the saw tooth are due to the addition of heat and the return occurs when the heat is removed. Due to time constraints on the infrared camera rental, absolute equilibrium is not achieved, but the asymptotes are easily interpreted from the graphs.

Beam	M_n (lb·ft)	P_n (lb)	δ (in)	δ_{exp} (in)	ΔP (lb)	ΔP_{exp} (lb)
0	6152.5	2140	0.263	0.250	400	571.08
1	6483.1	2255	0.275	0.290	500	510.18
2	6468.8	2250	0.254	0.260	600	548.55
3	6741.9	2345	0.245	0.280	550	610.60
4	8610.6	2995	0.339	0.320	350	364.46
6	8581.9	2985	0.323	0.300	400	401.31

Table 7-4: Confirmation Test Summary

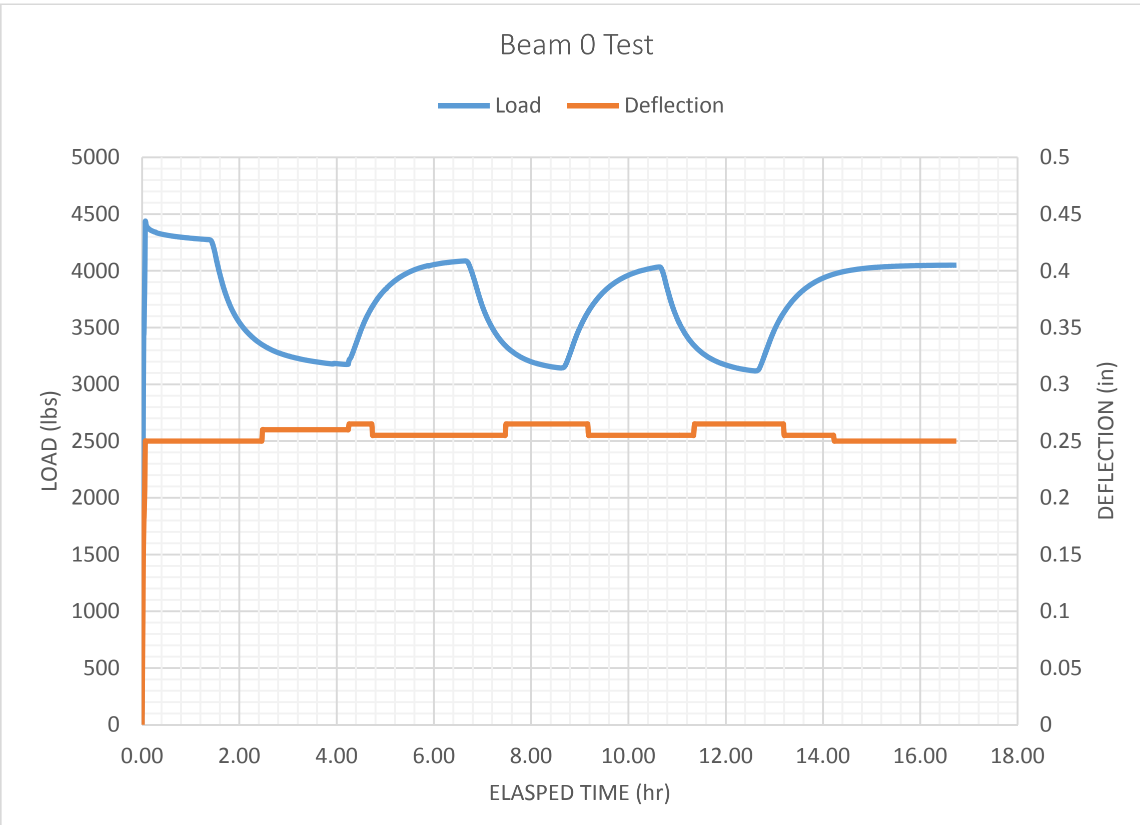

Figure 7-13: Beam 0 Confirmation Test

The first graph of Beam 0 (Figure 7-13) shows the results from the control. Note that at the end of the first cycle, the regained load is about 200 pounds less than the load before heat is added. The end of the second and third cycles result in almost no loss from the first cycle. The center deflection increased slightly during the maximum temperature duration on the beam and then relaxed to the preheat deflection. The loss of load due to the curvature throughout all cycles was about 800 pounds total or 400 pounds for each load cell. This is within about 70% of the calculated load loss at 570 pounds.

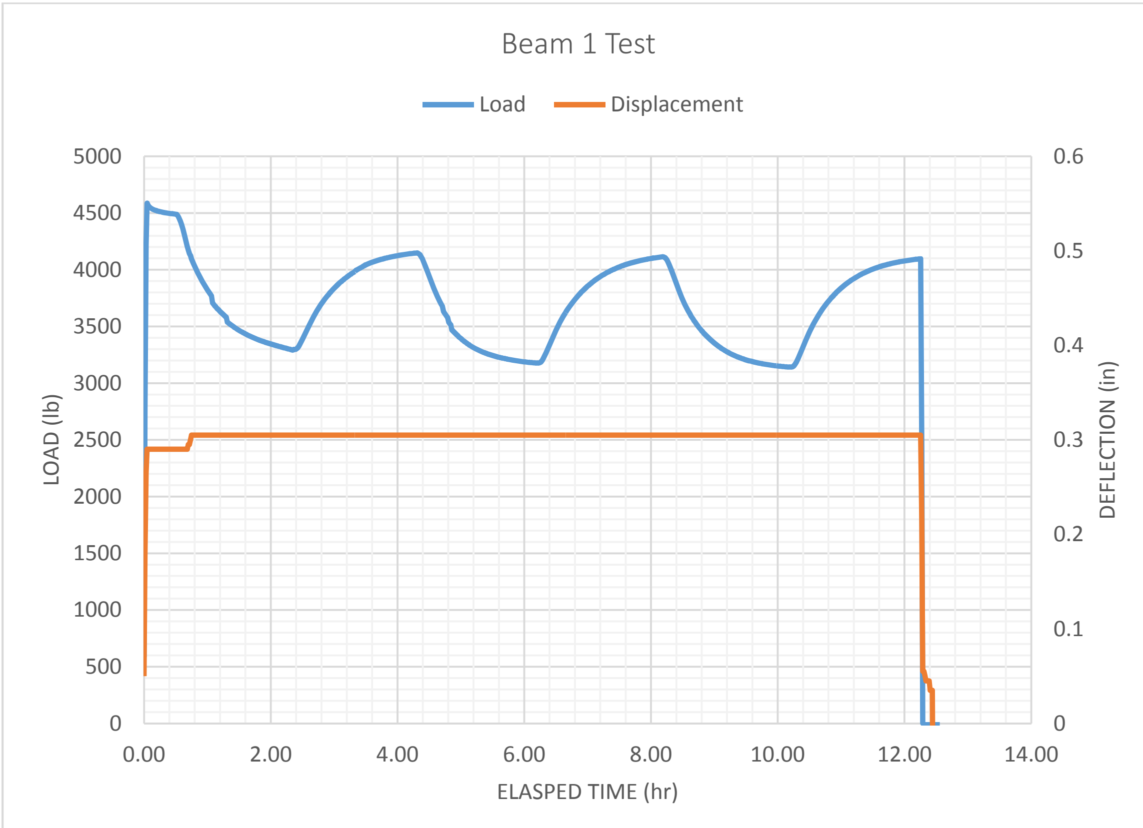

Figure 7-14: Beam 1 Confirmation Test

Figure 7-14 shows the results from Beam 1 which had two mats of carbon fibers. At the end of the first cycle, the regained load is about 400 pounds less than the load before heat is added. Again at the end of the second and third cycles, the net loss is nearly the same. This demonstrates that the beam is retaining its load bearing capacity throughout the heat testing. Deflections also held constant throughout the test also indicating that the beam is unaffected by temperature loadings. The average load loss throughout all the cycles is about 1000 pounds or 500 pound per load cell. The calculated load loss was 510 pounds which was 98% of the observed load loss.

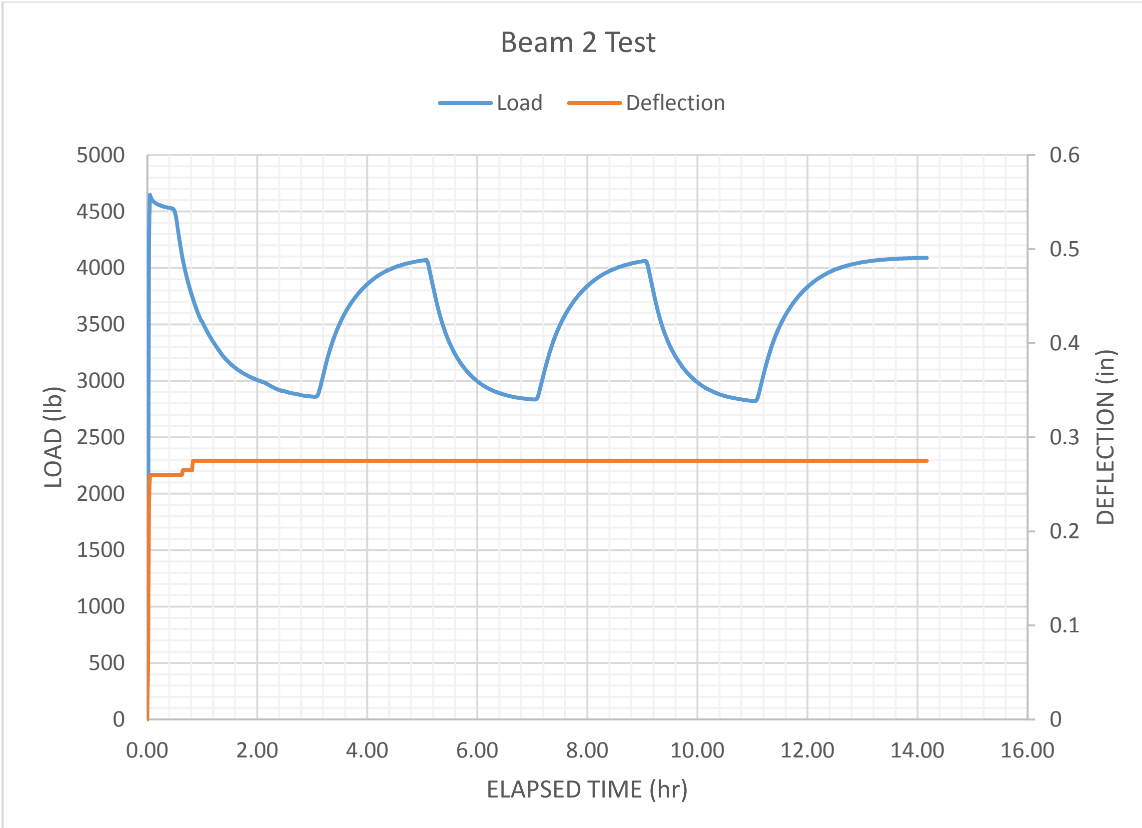

Figure 7-15: Beam 2 Confirmation Test

Beam 2, with 8 tows of fibers, is shown is Figure 7-15. At the end of the first cycle, the regained load is about 400 pounds less than the load before heat is added and the regained load does not differ throughout the remaining two cycles. Deflections remained constant during the test. The average load loss during the addition of heat was about 1,200 pounds or 600 per load cell. The calculated loss was 550 pounds which was 92% of the observed.

Beam 3 (16 tows) results are shown in Figure 7-16. At the end of the first cycle, the regained load is about 600 pounds less than the load before heat is added. The end of the second cycle showed a loss of almost another 200 pounds though the load did not change with the third cycle. The deflections were affected by the heat in the fluctuation. The average load lost due to heat was about 1,100 pounds or 550 pounds per load cell. This was within 90% of the calculated load loss of 610 pounds.

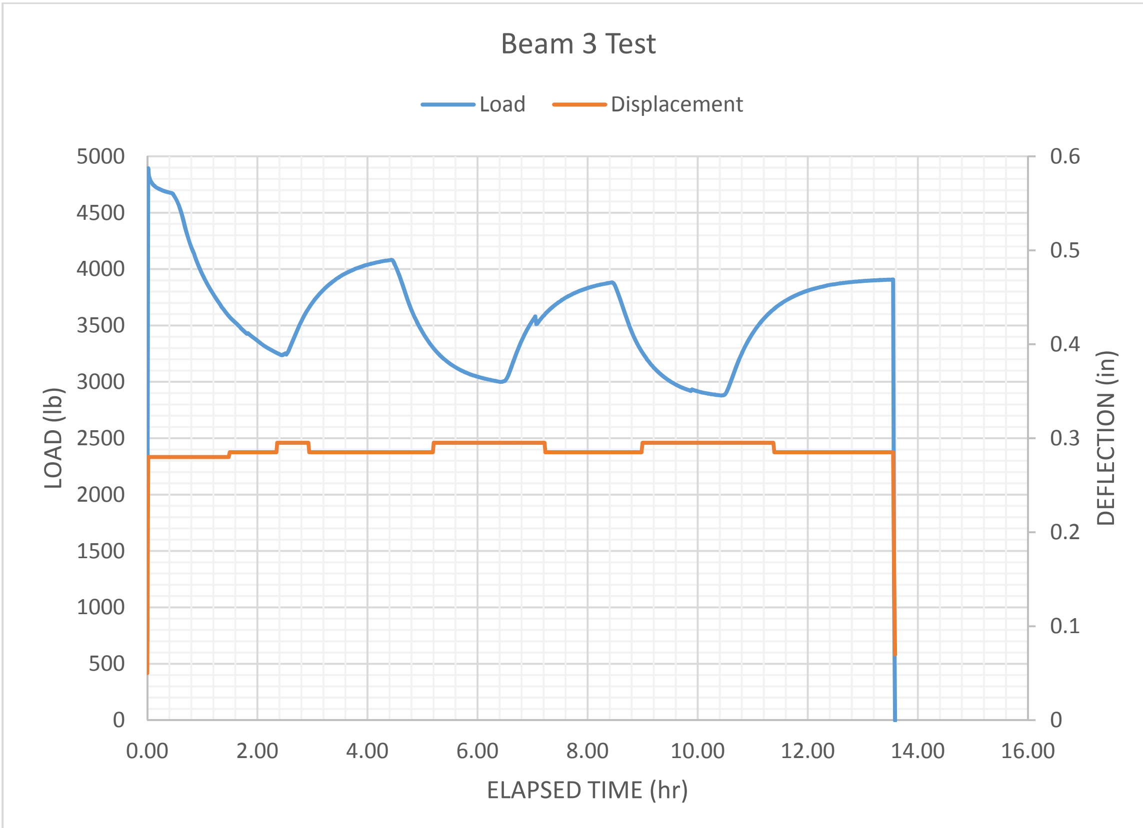

Figure 7-16: Beam 3 Confirmation Test

The graph of the insulated, 12 tow, Beam 4 is shown in Figure 7-17. At the end of the first cycle, the regained load is only about 200 pounds less than the load before heat is added even though the load is about 2,000 pounds greater than the previous four beams. By the end of the third cycle, the total loss is about 100 pounds more but significantly less than the uninsulated beams. The deflection is largely unaffected throughout the test. The total heat loss during the heat cycle averages about 700 pounds or 350 pounds per load cell. The calculated load loss was found to be within 96% at 365 pounds.

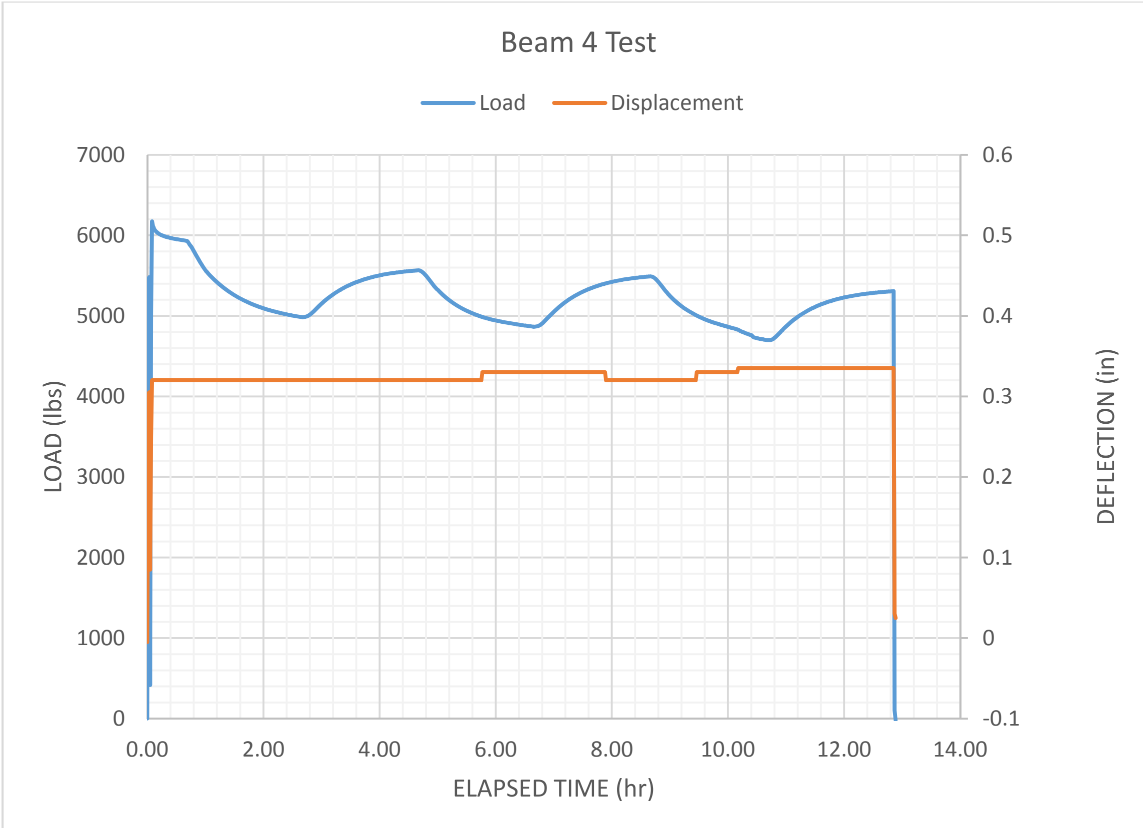

Figure 7-17: Beam 4 Confirmation Test

Figure 7-18 displays the graph for the insulated, 16 tow, Beam 6. At the end of the first cycle, the regained load is about 200 pounds less than the load before heat is added and is largely unchanged through the two successive cycles. Again the initial load is higher to allow for close monitoring of carbon strengthening failure. The center deflection does not change and the average load loss due to heat is again 800 pounds or 400 pounds per load cell. This is within 99% of the calculated load loss of 400 pounds.

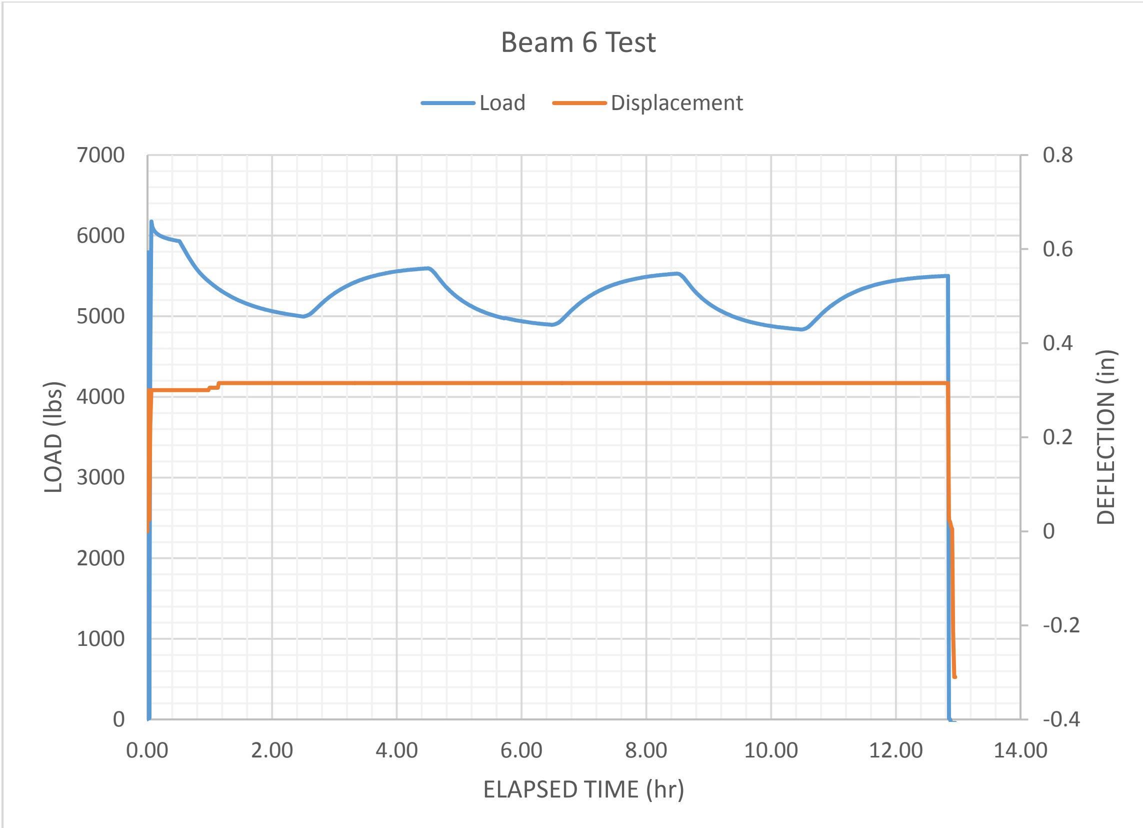

Figure 7-18: Beam 6 Confirmation Test

First, an image of the actual beam is shown to provide perspective (Figure 7-19). The heat elements and the wires are seen on the top of the beam. The strip plates and bolts used to hold the heating elements in place are seen on the side and bottom of the beam. Also shown in this picture is the 3/8 inch layer of glass ball insulation on the top of the beam. The infrared images taken during the heat tests are shown below (see Figure 7-20). Note the distances from the heat source and the distribution of the heat during the test. The maximum temperature noted at the graph is limited to the linear color scale. The noted temperature for the calculation was performed by taking temperature measurements of the heating element and the top surface of the concrete.

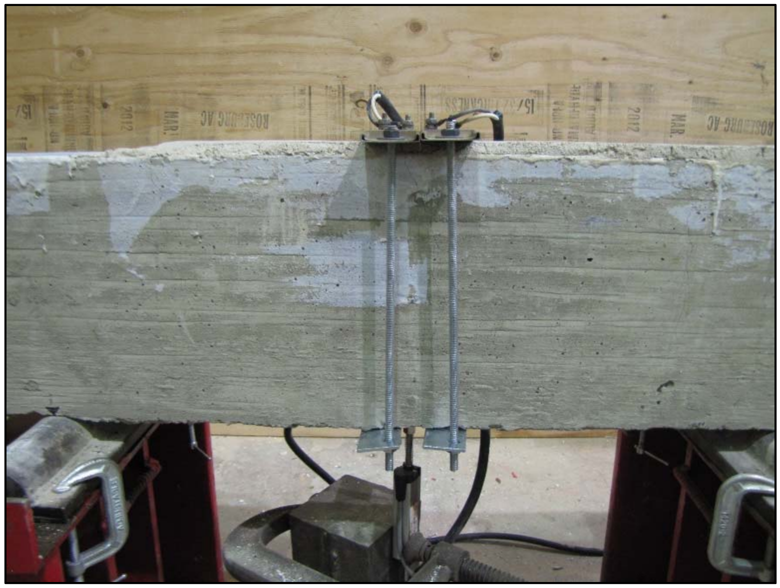

Figure 7-19: Real Light Image

The most interesting observation in the distribution of the temperature is that the last two tests which featured the insulation layer showed that the heat gradient was more flat than all the other tests. This is also reflected in the lower temperatures reported at the bottom of the beam during the tests.

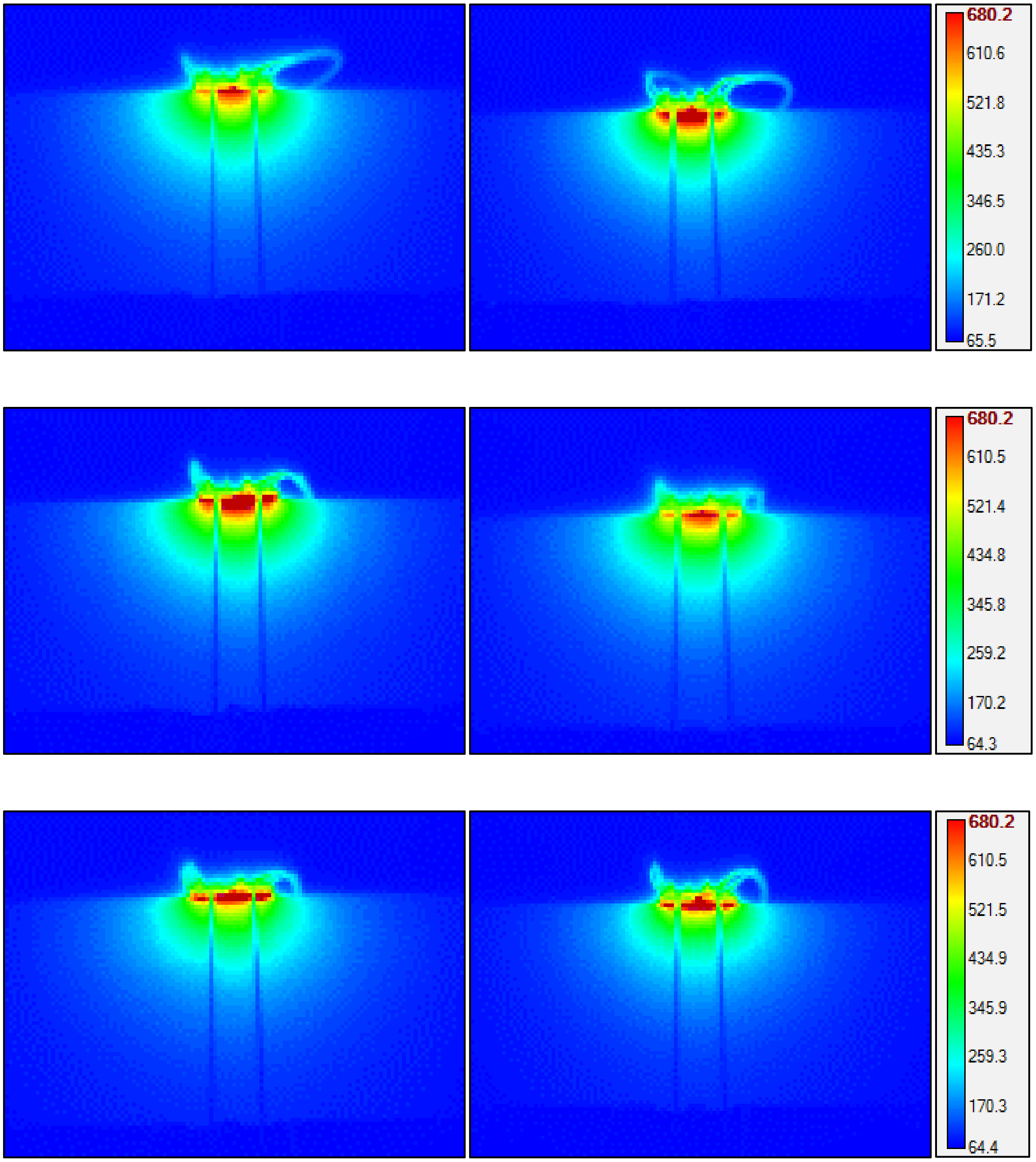

Figure 7-20: Infrared Images; Beam 0 (top left), Beam 1 (top right), Beam 2 (middle left), Beam 3 (middle right), Beam 4 (bottom left), Beam 6 (bottom right)

7.12 Summary

The following observations are made with respect to heat durability of the inorganic matrix carbon fiber composite strengthened concrete beam:

- The inorganic matrix can be used for adhering carbon fibers to the tensile face of the concrete beam in order to provide additional strengthening of the beam. The matrix penetrated the individual and mat fibers to provide a consistent bond.
- The inorganic matrix allows the beam to survive and maintain loading conditions with temperatures exceeding 1,000°F even during cyclical heating events.
- The static loading jig consisting of square tubes and 3/4 inch all-thread was able to apply the load without any lateral loading. The screw jack allowed for loads up to 3,000 pounds per frame without failure or bending in the frame.
- Loads and deflections were successfully logged using USB sensors and a proprietary data acquisition program making calibration and synchronization of the test data easier.
- The findings that the load loss over the heat event was due to differential temperatures causing strain in the heated fibers was significant in the interpretations of the results. It was originally thought that the matrix/fiber layer had failed.
- Moment-area theorem can be used to approximate the deflection and load resulting from the differential heating with close accuracy. The derivation of the equations are shown.
- The actual load loss for Beam 0 was about 400 lbs. and the calculated loss was 571.08 lbs.
- The actual load loss for Beam 1 was about 500 lbs. and the calculated loss was 510.18 lbs.

- The actual load loss for Beam 2 was about 600 lbs. and the calculated loss was 548.55 lbs.
- The actual load loss for Beam 3 was about 550 lbs. and the calculated loss was 610.60 lbs.
- The actual load loss for Beam 4 was about 350 lbs. and the calculated loss was 364.46 lbs.
- The actual load loss for Beam 6 was about 400 lbs. and the calculated loss was 401.31 lbs.
- The infrared camera and data provided a visual method for finding the gradient and temperatures.

CHAPTER 8 - FIELD TRIALS

8.1 Introduction

This last chapter is reserved for the demonstration of the repair of cracks and delaminations in concrete. So far, the following subjects have been covered with respect to creating an inorganic aluminosilicate concrete repair material: a suitable mix design has been identified through an experimental process that has varied ingredients and proportions as well as looked at the influence of heat curing and mixer speed types. The mechanical properties have been tested with respect to repairing concrete samples. Comparison tests have been performed with existing organic epoxy repair systems that included a novel approach to determining concrete compatibility. Finally, the inorganic material has been tested for durability in wetting, freezing and high temperatures.

As mentioned, the repair material was applied to both crack and delamination repair. The chapter is divided into the procedure for both crack repair and delamination rehabilitation. Crack repair was accomplished using large slabs that were saw cut to produce the vertical or surface crack with a known width and depth. The delamination repair featured slabs that were cast with a removable insert of known dimensions. The slabs were located outside at the CAIT laboratory on Rutgers Livingston campus.

8.2 Surface Crack Repair

8.2.1 Specimen Preparation

The specimens for the surface crack repair were 4 feet square by 8 inch thick slabs that were available from another project. The slabs were reinforced with deformed steel bars with 2 inches of cover on top and 3/4 inches of cover on the bottom. The spacing of the bars in both directions in both the top layer and bottom layer were 10 inches. The concrete was batched and delivered by Clayton Block Company from the Edison, New Jersey plant. The concrete compressive strength was specified at 4,000 psi and the 28-day strength was found to be 4,500 psi. The slabs were originally designed for unrelated nondestructive testing so there was not any existing damage to the slabs.

The cracks were dry cut using a diamond coated concrete saw blade. The width of the blade and crack was 0.09 inches. The depth of the cut was limited to the concrete cover of 2 inches over the reinforcing steel. The cuts were made within half of the beam to retain the solid integrity of the other half of the beam (see Figure 8-1). Therefore, the total length of the cut was about 21 inches.

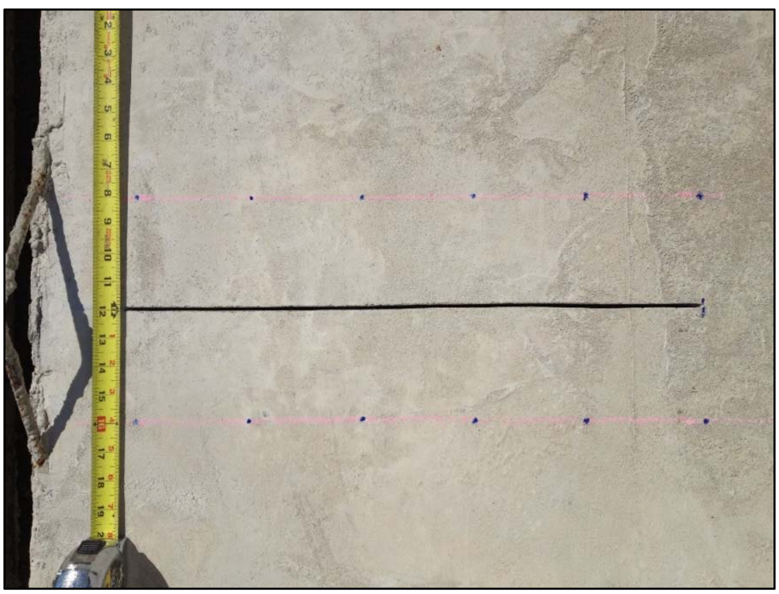

Figure 8-1: Surface Crack Preparation

After the concrete was cut, the void was cleaned using compressed air. Then using cast acrylic and synthetic rubber adhesive, the crack was covered and sealed so that the flow of the repair material could be monitored during the injection process. Holes were drilled in the acrylic to allow the material to pass through and surface mounted injection ports were adhered to the acrylic over the drilled hole. Slide-on zerk fittings were attached to the surface mounted port as shown in Figure 8-2. These were the most successful injection fittings used during the paver testing. The ports were spaced just over 12 inches apart for a total of 2 ports per crack. A total of three cracks were prepared for testing.

Figure 8-2: Surface Mount Port and Slide-On Zerk Fitting

8.2.2 Test Set-up

The test was performed using the SealBoss P3003 injection machine with the slide-on zerk fitting. As mentioned in Chapter 3, the injection machine features a gravity fed positive displacement piston pump with pressures up to 5,000 psi. However, previous tests have shown that pressures between 30 and 50 psi are sufficient and any pressures over this range could result in additional concrete damage. The equipment consisted of the pump, a 12 foot long, 1/4 inch diameter flexible hose and a ball valve operated zerk connection.

8.2.3 Test Results

The inorganic matrix was mixed and poured into the pump hopper (see Figure 8-3). The fitting was attached to the zerk port and the pump was operated at about 1/3 speed. A video of the test was captured. One 300 gram Mix E1 could fill two cracks. The approximate volume of the crack was 3.24 cubic inches and the entire 21 inches was filled in about 50 seconds for a flow rate of one-fifth of a quart per minute (the standard flow rate units for injection systems). The maximum pressure was not exceeded during the test. The crack was filled only using one of the injection ports meaning that the spacing could be set farther apart for crack filling on horizontal surfaces. The testing was done when the temperature was 50°F during the day and around freezing at night. Due to the low temperatures, the inorganic matrix did not cure for three days.

Figure 8-3: Surface Crack Injection Test Set-Up

8.3 Delamination Repair

8.3.1 Specimen Preparation

Rectangular concrete slabs were cast with removable steel inserts. The dimensions of the slabs were 24 inches by 36 inches and 3-1/2 inches thick. The forms were constructed from #2 SPF 2 X 4 material. Earlier tests had shown that metal inserts were more applicable than wood ones since the thickness is smaller, emulating the smaller crack size in delaminated bridge decks. In addition, the steel inserts are easier to remove if they have been thoroughly coated with a release agent. Finally, due to tensile strength of steel compared to wood, the inserts can be much larger in area, simulating actual delamination conditions. The steel inserts were 24 inches long and penetrated 6 inches into the concrete slab from either side on the long side of the slab. The corners of the insert were rounded at a 6 inch radius to aid in the removal of the insert. The inserts were fabricated from 22 gauge steel which corresponds to 0.03 inches thick. The inserts were fastened to the inside of the formwork at a depth of two inches to imitate the typical concrete cover to the steel reinforcement on a bridge deck as shown in Figure 8-4. This is also the first layer which would be susceptible to delaminations due to the corrosion of the steel bars. The slabs were also fitted with steel lifting hooks along the 24 inch dimension to allow for easy transporting of the nearly 300 pound slabs.

Figure 8-4: Artificial Delamination Inserts

Concrete was provided by Accurate Concrete Company of South Amboy, New Jersey. The concrete was mixed onsite using their volumetric mixer which proportions and mixes the concrete in the truck instead of a central batch plant. The specified strength of the concrete was 4,000 psi and the 28-day strength was found to be 3,500 psi.

The initial plan to remove the inserts from the formwork was to use a pry bar to place tension on the attached formwork. In addition, the inserts were to be removed two days after casting the slabs to reduce the reaction time with the steel and to keep concrete cracking to a minimum. However, even after only two days, the pry bar force was not enough to remove the inserts. Two weeks later, a second insert removal system was developed. The tab end of the insert was bent in plane with the rest of the insert and sandwiched between a 2 inch by 1/4 inch flat steel bar and 2 inch by 1/4 inch angle with five bolts spaced evenly along the 24 inches. This was then attached to a chain connected to a forklift. The slab was held in place to a steel post by chains connected through the steel lifting hooks. The forklift was driven forward and the force was great enough to pop the inserts out of the concrete though by this time, the beginning stages of corrosion had already begun rending the inserts unreusable.

Once the steel inserts had been removed, the resulting "crack" represented the cross-section of a delamination in the concrete (Figure 8-5). The cracks were cleaned using a vacuum. Cast acrylic windows were adhered to the concrete over the delamination using a silicone adhesive. This allowed for viewing of the delamination during the repair to inspect the quality of the repair and consistency of the flow.

Figure 8-5: Cross-Section of Artificial Delamination

Injection holes were drilled through the top surface of the slab to the delamination using a DeWalt D25324 1 inch L-Shape SDS Rotary Hammer coupled with the D32300DH Dust Extraction Kit to remove the dust from the hole during drilling to prevent blockage of the delamination plane when the drill penetrates the crack. The initial size of the hole was 1/2 inch. During the first attempt at filling the delamination, the pressure in the piston pump reached nearly 500 psi. The injection hole was inspected for blockage and it was determined that as the large diameter drill bit reached near the delamination, the remaining concrete punched through into the void causing blockage that could not be removed using the drill mounted vacuum. A second more powerful shop vacuum was enlisted to remove the debris to no avail. So a smaller 1/8 inch diameter hole was attempted and resulted in a 50% chance of blockage (Figure 8-6). The holes were spaced 18 inches apart.

Figure 8-6: Drilling Injection Holes using Dust Extraction Equipment

Each delamination was outfitted with two holes: one for injection and the other for air to escape to prevent back pressure. One of the holes was equipped with a surface mounted slide-on zerk injection port if testing with the injection gun was desired. A total of three slabs were prepared.

8.3.2 Test Set-up

This test also featured the SealBoss P3003 Injection Machine used in the paver repair and surface crack repairs. The end of the system was fitted with a 1/8 inch diameter tapered rubber air nozzle as shown in Figure 8-7. The rubber nozzle allowed the fitting to be pressed against the hole in the concrete to form a water-tight seal around the opening during the placement of the repair material. Using downward force applied by hand, typical injection pressures could be resisted. The nozzle was used without an end valve. The test was performed using a 300 gram amount of Mix E1.

Figure 8-7: Delamination Injection Nozzle

8.3.3 Test Results

As mentioned in the Specimen Preparation section, the test required two attempts to be successful. The problem with the first attempt was determined to be blockage in the delaminated layer due to punch out of the concrete from the large diameter drill bit during the production of the injection holes. In order to confirm this theory, the acrylic covers were removed and a thin metal instrument was placed in the crack to confirm the presence of debris around the hole. Since the slabs had been cast nearly three years previous, it was also thought that particles left from the steel inserts may have blocked the voids. The metal instrument confirmed the presence of debris around the injection holes since it could be inserted in the delamination at all other locations.

A scraper was fashioned out of a metal cutting reciprocation saw blade by grinding the thickness to the width of the delamination. This was an attempt to saw the concrete but the steel blade just dulled in contact with the cement. The blade was then cut to just protrude past the edge of the concrete while inserted in the crack and hammered like a chisel against the concrete debris. Using this procedure, enough concrete was broken away from the hole to allow compressed air to pass from the injection hole to the delamination. Once both holes were cleared, the acrylic window was reattached to the concrete over the crack using a synthetic rubber adhesive. This provided a way to confirm the injection path to the delamination in order to demonstrate acceptable flow. This operation was executed on one of the three original samples since the first sample was ruined.

To prove that the larger size hole drilling procedure was the culprit for crack debris, smaller diameter holes were tested in the third sample. New smaller diameter holes were drilled and compressed air was forced into the hole to check for blockage. Once the holes were confirmed as not blocked, injection could commence as shown in Figure 8-8. Evaluation was provided by visual inspection through the plexiglass window and the injection was recorded on video.

Figure 8-8: Performing the Delamination Injection

Both the cleared larger diameter holes and smaller diameter holes were successful. Because the adhesive for the acrylic had not fully cured, injection could not be completely attempted from only one injection hole. The increased pressure caused leaking in the adhesive. So the injection tip was inserted in the second hole to completely fill the void. It is believed however, that a spacing of 18 inches is adequate as long as the hole isn't blocked.

The approximate volume of the void is 11.57 in^3 and was filled in about 73 seconds at about 1/3 power on the pump. This equates to a flow rate of 0.25 quarts per minute. While maximum recommended pressure was not exceeded during the test, the recently adhered acrylic windows detached in isolated locations due to uncured adhesive. Because of the leaking acrylic window, both injection holes were utilized to fill the crack. Nonetheless, a maximum spacing of 18 inches is recommended for delamination filling depending on the width of the crack. The injection was completed during weather that was between 30 and 50°F so the repair material will take longer to cure. Recommended minimum curing temperatures are between 65 to 70°F.

8.4 Summary

Based on the findings discussed in this chapter, the following observations are made:

- The final designed Mix E1 was suitable for surface crack repair and delamination injection due to the low injection pressure requirements and the ability to flow in cracks ranging from 0.03 to 0.09 inches.
- The repair mix also worked in commercially available epoxy injection equipment.
- While the recommended temperatures for injection are required for acceptable curing times, the repair mix was able to be injected in 45 to 50°F temperatures without a significant increase in pressure or viscosity. It is recommended that for low temperature applications, the retarder amount should be reduced to allow the material to set up faster.

With respect to delamination injection, the following remarks are presented:

- Injection holes with smaller diameter holes are recommended. The use of 1/8 inch masonry drill bits are suitable for injection. This type of drill bit is not susceptible to punch-out shear failure at the delamination plane causing blockage of the repair material flow. It was noted that the 1/8 inch bit only worked 50% of the time. Thus the drill should be kept as part of the injection process to redrill holes that are blocked.
- Dust extraction systems are also recommended to be integral with the drill to remove the concrete dust during the drilling.

- The tapered rubber injection tip performed well during the testing for quick and easy access to the injection holes. A mechanically expanding rubber tip with a lock feature could be useful and reduce operator strain though the set-up time may increase. In addition, a shut-off valve could be designed into the tip to reduce loss of the repair material during movement to the next injection hole.
- The specimen preparation involving removable 22 gauge steel inserts worked well to provide a thin layer artificial delamination. The inserts were difficult to remove however and a mechanical operation should be utilized to assist in the removal.

CHAPTER 9 - CONCLUSIONS

The major findings of this dissertation are provided in the following paragraphs. A review of the available state-of-the-art for epoxy injection systems and the development and application of inorganic aluminosilicate material are shown below:

- Preparation for repairing delaminations include vacuum drilling to the depth of the hollow plane. Preparation for crack repair includes mounting the injection ports and sealing the external surface of the crack to exclude leakage during injection.

- Injection systems must include a pump, mixer and injection probe. The specified pump is a positive displacement pump. Recommended mixers are either a brush type or reverse spiral inline mixer. For delamination injection, suggested injection probes should feature a surface seal to eliminate minimum injection depths and to make the process faster for multiple injections. For crack repair, the injection probe should be compatible with the injection ports to form a non-leaking seal during injection.

- Epoxy systems are part of a continuous repair scheme. It is not intended for one-time use but should be evaluated periodically to determine the injection schedule. Most repairs should be re-injected every 3 to 4 years. Organic epoxy systems are susceptible to natural breakdown and experience increased brittleness over time.

- Inorganic epoxy systems are more suitable for concrete repair due to the similarities in chemical make-up, stress distribution and stiffness.

- Many of the basic mechanical properties of the inorganic mixture have already been tested. The use of the inorganic matrix to bond fiber reinforcement to steel and concrete tensile faces to increase strength capacity has been successfully tested. In addition, the use of the inorganic epoxy as a protective coating has been demonstrated by several field projects at Rutgers University.

The tests of this study have provided the following observations:

- The final mix design included nano-aluminosilicates for increased bonding, standard silica/alumina ratios and optimized zinc oxide activator. The recommended mixing speed is 3,000 rpm with the mix curing at room temperature.
- The mix is well suited for use in positive displacement type pumps and flows well into small width cracks ranging from 0.03 to 0.09 inches. In addition, the mixture also is compatible with commercially available injection systems and accessories. Thus typical injection procedures can be followed with little modification.
- Direct shear tests of the inorganic repair material gave a shear strength of 575 psi which was near the shear strength of the concrete substrate. The slant shear or bonding strength for the inorganic epoxy is around 3,500 psi and compares well with commercially available organic repair systems.
- Using a control for either extreme of results, prototype and full-scale beam tests provided real data on the effectiveness of the repair material. The inorganic repaired beams featured higher stiffness, no detectible shear slippage along the repair interface, no failure cracking and loading behavior similar to both the calculated model and the solid unnotched beam. The organic repaired system

featured lower stiffness, shear slippage along the repair plane, shear cracking near the reaction supports indicating decreased depth from the extreme compression fiber to the centroid of the tensile reinforcement, and loading behavior similar to the notched control beam.

- The freeze/thaw durability tests were not a significant source of conclusive data possibly due to the relatively short length of the total cycles. Greater results may occur from combining the wetting tests with the thermal cycling or by increasing the test cycles. The use of the 29000 rpm mixer in conjunction with the 120°F curing temperature resulted in substantially more coating related failures than the 3000 rpm mixer and the room temperature cured coatings.
- Wetting durability tests provided valuable information on the effects of environmental conditions on the inorganic coating. However, as the specimens became more water-logged, the time for drying might have to be increased in order to provide better adhesion for the test dolly. Many tests featured epoxy related failures which were excluded from the final results. The data was inconclusive regarding the optimal type of mixer and the curing temperature.
- The inorganic matrix can be used for adhering carbon fibers to the tensile face of the concrete beam in order to provide additional strengthening of the beam. The matrix penetrated the individual and mat fibers to provide a consistent bond.
- The inorganic matrix allows carbon fiber strengthened beams to survive and maintain loading conditions with temperatures exceeding 1,000°F even during cyclical heating events. The static loading jig consisting of square tubes and 3/4 inch all-thread was able to apply the load without any lateral loading. The screw

jack allowed for loads up to 3,000 pounds per frame without failure or bending in the frame. Loads and deflections were successfully logged using USB sensors and a proprietary data acquisition program making calibration and synchronization of the test data easier. The infrared camera and data provided a visual method for finding the gradient and temperatures.

- Moment-area theorem can be used to approximate the deflection and load resulting from the differential heating with close accuracy. The derivation of the equations are given.
- While the recommended temperatures for injection are required for acceptable curing times, the repair mix was able to be injected in 45 to 50°F temperatures without a significant increase in pressure or viscosity. It is recommended that for low temperature applications, the retarder amount should be reduced to allow the material to set up faster.
- Injection holes with smaller diameter holes are recommended. The use of 1/8 inch masonry drill bits are suitable for injection. This type of drill bit is not susceptible to punch-out shear failure at the delamination plane causing blockage of the repair material flow. It was noted that the 1/8 inch bit only worked 50% of the time. Thus the drill should be kept as part of the injection process to redrill holes that become blocked.

REFERENCES

ACI 318. 2011. *Building Code Requirements for Reinforced Concrete.* Farmington Hills: American Concrete Institute.

ACI Committee 403. 1962. *Guide for Use of Epoxy Compounds with Concrete.* Proceedings, Farmington: American Concrete Insitute.

ACI Committee 440. 2002. *Guide for the Design and Construction of Externally Bonded FRP Systems for Strengthening Concrete Structures.* Guide, Farmington Hills: ACI.

ACI Committee 503 and 548. 2007. *Specification for Crack Repair by Epoxy Injection.* Technical Documents, Farmington: American Concrete Institute.

Amer, Ahmed. 2008. "Effectiveness of Inorganic Concrete Coating Matrices and Their Self Cleaning Properties." *Dissertation.* New Brunswick, New Jersey: Rutgers, The State University of New Jersey, January.

ASTM C496. 2011. "Standard Test Method for Splitting Tensile Strength of Cylindrical Concrete Specimens." American Society for Testing and Materials.

ASTM C666. 2008. "Standard Test Method for Resistance of Concrete to Rapid Freezing and Thawing." American Society for Testing and Materials.

ASTM C672. 2012. "Standard Test Method for Scaling Resistance of Concrete Surfaces Exposed to Deicing Chemicals." American Society for Testing and Materials.

ASTM C882. 2012. "Standard Test Method for Bond Strength of Epoxy-Resin Systems Used With Concrete By Slant Shear." American Society for Testing and Materials.

ASTM D4015. 2007. "Standard Test Methods for Modulus and Damping of Soils by Resonant-Column Method." American Society for Testing and Materials.

ASTM D4541. 2009. "Standard Test Method for Pull-Off Strength of Coatings Using Portable Adhesion Testers." American Society for Testing and Materials.

ASTM D6944. 2009. "Standard Practice for Resistance of Cured Coatings to Thermal Cycling." American Society for Testing and Materials.

ASTM D695. 2010. "Standard Test Method for Compressive Properties of Rigid Plastics." American Society for Tests and Materials.

ASTM D7234. 2012. "Standard Test Method for Pull-Off Adhesion Strength of Coatings on Concrete Using Portable Pull-off Adhesion Testers." American Society for Standards and Materials.

ASTM D790. 2010. "Standard Test Methods for Flexural Properties of Unreinforced and Reinforced Plastics and Electrical Insulating Materials." American Society for Testing and Materials.

Balaguru, Perumalsamy, Antonio Nanni, and James Giancaspro. 2009. *FRP Composites for Reinforced and Prestressed Concrete Structures.* New York: Taylor and Francis.

Brownstein, Jeremy. 2010. "Inorganic Polymer Fiber Composites for Protection of Structures." *Thesis.* New Brunswick, NJ: Rutgers, The State University of New Jersey, May.

Chynoweth, Gary, and Ronald R. Stankie. 2001. *Concrete Repair Guide.* Farmington: American Concrete Institute.

Connor, E. J. 1979. *Bridge Deck Repair Using Injected Epoxy Resin.* Ames: Iowa Department of Transportation.

Darwin, David, Tony C. Liu, Andrew Scanlon, Grant T. Halvorsen, Alfred G. Bishara, and Peter Gergely. 1998. *Causes, Evaluation and Repair of Cracks in Concrete Structures.* Farmington: American Concrete Institute.

Davidovits, J. 1991. "Geopolymers: Inorganic Polymeric New Materials." *Journal of Thermal Analysis* 1633-1656.

Davidovits, J. 1979. "Synthesis of New High-Temperature Geo-Polymers for Reinforced Plastics/Composites." *Annual Pacific Technical Conference and Displays* 151-154.

Davis, Martha, Paul Tremel, and Alex Pedrego. 2008. "Bill Williams River Concrete Bridge Fire Damage Assessment." *Structure Magazine* 30-32.

Deteresa et al, S. J. 1984. "Compressive and Torsional Behavior Kevlar 49 Fibre." *Journal of Materials Science* 57-72.

Epoxy Chemicals, Inc. 2013. "History of Epoxy." *List.* Chicago, Illinois: Epoxy Chemicals, Inc.

Foden, Andrew J. 1999. "Mechanical Properties and Material Characterization of Polysialate Structural Composites." *Dissertation.* New Brunswick, NJ: Rutgers, The State University of New Jersey, January.

Garon, Ronald J. 2000. "Effectiveness of High Strength Composites as Structural and Protective Coatings for Structural Elements." *Dissertation.* New Brunswick, New Jersey: Rutgers, The State University of New Jersey, May.

Hammell, James A. 2000. "The Influence of Matrix Composition and Reinforcement Type on the Properties of Polysialate Composites." *Dissertation.* New Brunswick, New Jersey: Rutgers, The State University of New Jersey, May.

Hashemi, Siavash, and Riadh Al-Mahaidi. 2008. "Cement Based Bonding Material for FRP." *Inorganic-Bonded Fiber Composites Conference.* Madrid: Department of Civil Engineering, Monash University. 267-271.

Holman, J. P. 2002. *Heat Transfer.* New York: McGraw-Hill.

Iowa DOT, Office of Materials. 1998. *Inspection and Acceptance of Epoxy Injection Resins.* Ames: Iowa Department of Transportation.

Keane, Brian F. 2003. *Structural Crack Repair by Epoxy Injection.* Farmington: American Concrete Institute.

Kodur, Venkatesh, and Aqeel Ahmed. 2011. "Behavior of FRP-Strengthened Reinforced Concrete Members Under Fire Conditions." *Fire Protection Engineering* 1-13.

Krauss, Paul D., John M. Scanlon, Margaret A. Hanson, and Wiss, Janney, Elstner Associates, Inc. 1995. *Evaluation of Injection Materials for the Repair of Deep Cracks in Concrete Structures.* Washington, D.C.: US Army Corps of Engineers.

Leivo, Jarkko, Mika Linden, Cilaine V. Teixeria, Janne Puputti, Jessica Rosenholm, Erkki Levanen, and Tapio A. Mantyla. 2006. "Sol-gel Synthesis of a Nanoparticulate Aluminosilicate Precurser for Homogeneous Mullite Ceramics." *Journal of Materials Research* 1279-1285.

Lyon, Richard E., P. N. Balaguru, Andrew Foden, Usman Sorathia, Joseph Davidovits, and Michel Davidovics. 1997. "Fire Resistant Aluminosilicate Composites." *Fire and Materials* 67-73.

Momayez, A., A. A. Ramezanianpour, H. Rajaie, and M. R. Ehsani. 2004. "Bi-Surface Shear Test for Evaluating Bond between Existing and New Concrete." *ACI Materials Journal* 99-106.

Moore, William M. 1972. *Detection of Bridge Deck Deterioration.* College Stateion: Texas Transportation Institute.

Pattengill, M. G., C. F. Crumpton, and G. A. McCaskill. 1969. *Spot Treatment of Hollow Areas by Rebonding with Injected Epoxy Resin.* Study, Topeka: State Highway Commission of Kansas.

Sashco. 2013. *Lexel Support Frequently Asked Questions.* Accessed 3 7, 2013. http://www.sashco.com/hi/lexel-faqs.html.

SealBoss. 2012. *Sealboss 4040 LV Epoxy Resin.* Product Data Sheet, Santa Ana: SealBoss Corporation.

Smoak, W. Glenn. 1996. *Guide to Concrete Repair.* Denver: Bureau of Reclamation.

Stratton, F. W., and B. F. McCollom. 1974. *Repair of Hollow or Softened Areas in Bridge Decks by Rebonding with Injected Epoxy Resin or Other Polymers.* Topeka: State Highway Commission of Kansas.

Stratton, F. Wayne, and Barbara J. Smith. 1988. *Bridge Deck Hollow Plane Repair Using Injected Epoxy.* Topeka: Kansas Department of Transportation.

Stratton, F. Wayne, Roger Alexander, and William Nolting. 1978. *Cracked Structural Concrete Repair Through Epoxy Injection and Rebar Insertion.* Final, Topeka: Kansas Department of Transportation.

Wagh, Arun S., Dileep Singh, and Seung-Young Jeong. 1997. "Chemically Bonded Phosphate Ceramics for Stabilization and Solidification of Mixed Waste." *Journal of Environmental Science and Health* 527-541.

Webster, Ronald P., David W. Fowler, and Donald R. Paul. 1978. *Bridge Deck Impregnation in Texas.* Farmington Hills: American Concrete Institute.

Whiting, John E. 1989. *Bridge Deck Rehabilitation Rebonding A Delaminated P.C.C. Overlay by Epoxy Injection.* Ames: Iowa Department of Transportation.

Williams, B., L. Bisby, V. Kodur, J. Su, and M. Green. 2005. "An Investigation of Fire Performance of FRP-Strengthened RC Beams." *International Symposium on Fire Safety Science.* Beijing: National Research Council Canada. 247-258.

Woo, Ricky S. C., Honggang Zhu, Michael M. K. Chow, Christopher K. Y. Leung, and Jang-Kyo Kim. 2008. "Barrier Performance of Silane-Clay Nanocomposite Coatings on Concrete Structure." *Composites Science and Technology* 2828-2836.

VITA

Matthew J. Klein

Education

Ph.D., Structural Engineering; May 2013; Rutgers, The State University of New Jersey

M.S., Structural Engineering; May 2011; Rutgers, The State University of New Jersey

B.S.E., Civil Engineering; June 2008; Walla Walla University

Experience

Graduate Assistant/Research Engineer, Rutgers University, 2009 to present

Contract Lecturer for NJ DOT, Rutgers University, annually from 2008 to present

Teaching Assistant, Rutgers University, 2008 and 2009

CAD Technician and Network Manager, Ketelsen Construction, Summer 2008

Engineering Intern, Berger ABAM, Summer 2007

Journeyman Carpenter, Good Morning Builders, Summer 2006

Engineering Intern, NC DOT, Summer 2005

Lab Teaching Assistant, Walla Walla University, March 2007 to June 2007 and March 2008 to June 2008

Journeyman Carpenter, Ketelsen Construction and Madison Associated Contractors and Consultants, May 2001 to July 2008

Owner, Fiddlers on the Roof Roofing Construction LLC., May 2002 to December 2003

Salesman, 585 Metal Roofing and Sales, December 1999 to May 2001

Apprentice Carpenter, HLF Inc., Marvin Habegger, Lester Schmucker and John Marks Construction, October 1995 to December 1999

Publications

Balaguru, P., **Klein, M.**, Najm, H., & Venkiteela, G. (2013). Placement/Delivery Evaluation of Nano-composites for Robot Supported Nondestructive Rehabilitation of Concrete Bridge Decks. SPIE (pp. 1-10). San Diego: SPIE.

Balaguru, P., Brownstein, J., & **Klein, M.** (2012). Inorganic Polymer Fiber Composites for Protection of Structures. Trenton: NJDOT.

Balaguru, P., **Klein, M.**, Najm, H., & Venkiteela, G. (2012). Evaluation of Nano/Micro Composites for Nondestructive Repair of Delaminated Structures. SPIE (pp. 1 - 10). San Diego: SPIE.

Balaguru, P., **Klein, M.**, Najm, H., & Venkiteela, G. (2011). Nanoscale Materials for Non-Destructive Repair of Transportation Infrastructures. SPIE (pp. 1 - 7). San Diego: SPIE.